

Development of a new advanced elastoplastic constitutive model that considers soil behavior at small strains. The EPHYSS model

Javier Castellón^{1,2}  | Alberto Ledesma^{1,3} 

¹Universitat Politècnica de Catalunya–BarcelonaTech (UPC), Barcelona, Spain

²Infraes, Barcelona, Spain

³Department of Civil and Environmental Engineering, CIMNE, Barcelona, Spain

Correspondence

Javier Castellón, Universitat Politècnica de Catalunya–BarcelonaTech (UPC), Barcelona, Spain.

Email: javier.castellon.lopez@gmail.com

[Correction added on 13 June 2022, after first online publication: many of the symbols appearing incorrect along with other textual corrections, now corrected.]

Abstract

The Elastoplastic Hysteretic Small Strain (EPHYSS) model is an advanced elastoplastic model as a result from the combination of the Hysteretic Quasi-Hypoelastic (HQH) model that considers strain-induced anisotropy and can reproduce the nonlinear reversible, hysteretic and dependent on recent history soil behavior, and the Cap-Cone Hardening Soil Modified (HS_{MOD}) model that can reproduce soil plastic behavior. EPHYSS model uses state variables that define different short and long-term memory levels which provide it with robustness for the reproduction of soil hysteretic behavior and confers it a great versatility and adaptability to experimental results. It also corrects some inconsistencies of the Hardening Soil with Small Strain Stiffness (HS-SS) model of Plaxis whose effects can have a considerable influence on the numerical simulations of boundary problems. The performance of EPHYSS and a comparison with the HS-SS model is presented in some experimental and numerical tests, and in a boundary value problem of a large excavation in Barcelona.

KEYWORDS

constitutive model, EPHYSS, history, hysteretic, nonlinear, small strain

1 | THE RANGE OF SMALL STRAINS IN GEOTECHNICAL ENGINEERING

Multiple engineering problems, especially those related to works in urban areas, require realistic calculations of soil displacements under serviceability conditions. Generally, in these problems only a small part of the ground is subjected to intermediate or large strains, while most of it is subjected to small or very small strains that, once integrated throughout the area in which they appear, can have an important contribution to soil displacements. Therefore, it is essential to correctly simulate the behavior of the soil in the range of small strains, corresponding to Zones I and II of Jardine.¹ In Zone I, the behavior of the soil is considered linear reversible, while in Zone II it is considered nonlinear reversible, hysteretic and dependent on the recent history. On the other hand, any complete constitutive model must also be able to simulate the behavior of the soil in the range of intermediate and large strains, close to failure, corresponding to Zone III and IV

This is an open access article under the terms of the [Creative Commons Attribution](https://creativecommons.org/licenses/by/4.0/) License, which permits use, distribution and reproduction in any medium, provided the original work is properly cited.

© 2022 John Wiley & Sons Ltd.

of Jardine, in which this behavior is not reversible, either in a linear or nonlinear way, due to the appearance of plastic strains.¹

There are numerous advanced constitutive models capable of simulating the behavior of the soil in the whole strain range,² although the use of many of them is reduced to an academic use. However, some of these advanced models have managed to extend to the professional practice. Among them, stands out the well-known Hardening Soil with Small Strain Stiffness (HS-SS) model, based on the work of Benz,³ implemented in Plaxis and recently in other numerical software.

After analyzing in depth 54 constitutive models that consider the soil behavior in the range of small strains, there have been identified some aspects that can be improved in the elastic part of the HS-SS model in relation to: (1) nonlinear behavior; (2) hysteretic behavior; (3) deviatoric strains reversals effect on the elastic bulk modulus; (4) consideration of the strain induced anisotropy; and (5) correction of some inconsistencies that have been detected.^{2,4-7} All these points have motivated the development of the Elastoplastic Hysteretic Small Strain (EPHYSS) model with the aim of being used in the geotechnical engineering professional practice. The entire code of the EPHYSS model, implemented in the User Defined Soil Model (UDSM) modulus of Plaxis may be consulted in Castellón.⁴

2 | THEORETICAL FRAMEWORK OF THE EPHYSS MODEL

The EPHYSS model has multiple tensorial zones^{8,9} and, therefore, it is an incrementally multilinear model,¹⁰ although its indirect stiffness dependence on deviatoric strain increment when describing soil behavior in the range of small strains allows to consider it, in practice, as an incrementally nonlinear model. Specifically, the EPHYSS model belongs to the subtype of incrementally multilinear models called as advanced models of the elastoplastic type following the classification of Castellón and Ledesma.² Such model results from the combination of the Hysteretic Quasi-Hypoelastic (HQH) model, which aims to reproduce the quasi-static reversible behavior of the soil in the range of small strains (Zones I and II of Jardine), and the Hardening Soil Modified (HS_{MOD}) model, which aims to reproduce the irreversible behavior of the soil in the range of intermediate and large strains (Zones III and IV of Jardine).⁴

The HQH model is a quasi-hypoelastic hysteretic model of the variable moduli type.^{2,11-14} The Hysteretic denomination is due to the capacity of its structure to partially comply the Generalized Masing Rules,^{15,16} while the Quasi-Hypoelastic denomination is due to the use of nonlinear apparent stiffness moduli in its constitutive equation.

The reversible behavior of the soil in the HQH model is conditioned to the closure of the strain cycles, in a similar way to what happens in paraelastic models.² To define the cycles, HQH model requires information about soil state at the extreme points of those cycles, which constitutes the active reversal points. An active reversal point that belongs to a specific cycle has an effect on the soil stiffness while the cycle remains opened. Once the cycle (or larger cycles that contain it) is closed, the active reversal point disappear and it is erased from HQH state variables. It should be added that the EPHYSS model allows reproducing the behavior of the soil along paths that include common strain cycles in quasi-static geotechnical problems, but it cannot reproduce soil dynamic behavior, since it does not consider factors such as the accumulation of irreversible strain after multiple cycles, cyclic hardening/softening or elastoplastic coupling.

The HS_{MOD} model belongs to the models denominated Cap-Cone and has four yield surfaces. This model considers two different isotropic hardening mechanisms: a shear hardening mechanism on the Cone-type surface, which allows to reproduce the plastic strains in hard soils generated by deviatoric loadings, and a compression hardening mechanism on the Cap-type surface, which allows to reproduce the plastic strains generated by oedometric and isotropic loadings. EPHYSS model presents some important limitations that are inherited from the plastic model HS_{MOD} and are described in Section 6. Therefore, it is recommended to not use EPHYSS model for numerical analyses of geotechnical works in which intermediate or large strains play a significant role.

3 | HQH MODEL

3.1 | Strain domains of the model

Two strain domains are considered. Domain 1 corresponds to values $\gamma_{oct}^{\Delta R} \leq \gamma_{ur}^{\alpha}$ and domain 2 corresponds to values $\gamma_{oct}^{\Delta R} > \gamma_{ur}^{\alpha}$, where R refers to the last reversal point that conforms the endpoint of the active strain cycle and α refers to the deviatoric strain rotation angle corresponding to the active degradation curve.

In domain 1 the reversible component of the strain (whose reversibility is conditioned to the closing of the open strain cycles) follows a behavior that is nonlinear with both deviatoric strain and mean stress, and strain-induced anisotropy is also considered, while in domain 2 the reversible component of the strain (whose reversibility is also conditioned to the closing of the open strain cycles) follows a behavior that is both linear with the deviatoric strain and nonlinear with the mean stress.

The model considers the hysteretic behavior in both domains thanks to its ability to reproduce cycles in which shear strain produces a degradation of the elastic shear stiffness (which happens in domain 1) until it reaches a minimum value (which happens in domain 2). It should be clarified that both domains can appear during primary loading, but it is meaningless to talk about hysteretic behavior until a reversal takes place and at least one cycle appears.

In addition to that, the model considers the recent deviatoric strain history in both domains. It has to be understood as recent history those deviatoric strain paths that modify the model state variables which control elastic shear stiffness. Once strain cycles are closed, these state variables are reinitialized and the recent history erased.

In order to reproduce the soil hysteretic behavior (partially complying with the Generalized Masing Rules), as well as to consider the recent deviatoric strain history, the model uses a set of state variables whose formulation will be introduced in Section 3.5. These variables are the following:

○ **Short term state variables:**

- \mathbf{h} and $G_{s,0}^{ap,\alpha,H,ref}$ allow considering the effect on the shear stiffness of deviatoric strain paths from the last reversal point.
- \mathbf{e}^R and $\mathbf{e}^{e,R}$ define the origin of a new strain cycle after a reversal and relativizes the constitutive equation to that origin.

○ **Long term state variables:**

- \mathbf{H}_{MEM} , \mathbf{E}_{MEM} and \mathbf{E}_{MEM}^e allow considering the effect on the shear stiffness of both active strain cycles and their closure.

3.2 | General and incremental constitutive equation in domain 1

The general constitutive equation in domain 1 ($\gamma_{oct}^{\Delta R} \leq \gamma_{ur}^\alpha$) is the following:

$$(-p'\mathbf{1} + \mathbf{s}^{\Delta R}) - \boldsymbol{\sigma}'^{ini} = \mathbf{E}'_s (K'_s, G_s^{ap}) : (-\boldsymbol{\varepsilon}_{oct}^e \mathbf{1} + \mathbf{e}^{e,\Delta R}) \tag{1}$$

$$\mathbf{E}'_s (K'_s, G_s^{ap}) = \left(K'_s - \frac{2}{3} G_s^{ap} \right) \mathbf{1} \otimes \mathbf{1} + 2G_s^{ap} \mathbb{I} \tag{2}$$

The elastic secant bulk modulus K'_s in domain 1 adopts the following expression based on a generalization of the expression of Duncan et al.,¹⁷ which is widely accepted:

$$K'_s = K_s'^{ref} \left(\frac{-p'}{p'_{ref,1}} \right)^{m_1} \tag{3}$$

The apparent secant shear modulus G_s^{ap} adopts the Expression (4) in domain 1, based on the expression of Dos Santos and Correia.¹⁸

$$G_s^{ap} = \frac{G_{s,0}^{ap,\alpha,H}}{1 + a \left(\frac{\gamma_{oct}^H}{\xi \gamma_{0.7}} \right)} \tag{4}$$

$$G_{s,0}^{ap,\alpha,H} = G_{s,0}^{ap,\alpha,H,ref} \left(\frac{-p'}{p'_{ref,2}} \right)^{m_2} \tag{5}$$

$$\gamma_{oct}^H = \sqrt{\frac{4}{3}} \|\mathbf{h}\| \tag{6}$$

For the calculation of G_s^{ap} , the structure of the HQH model allows directly applying the Hashiguchi strategy,¹⁹ which consists of considering a value $\xi = 1$ in primary loading branch and $\xi = 2$ in unloading or reloading branches. However,

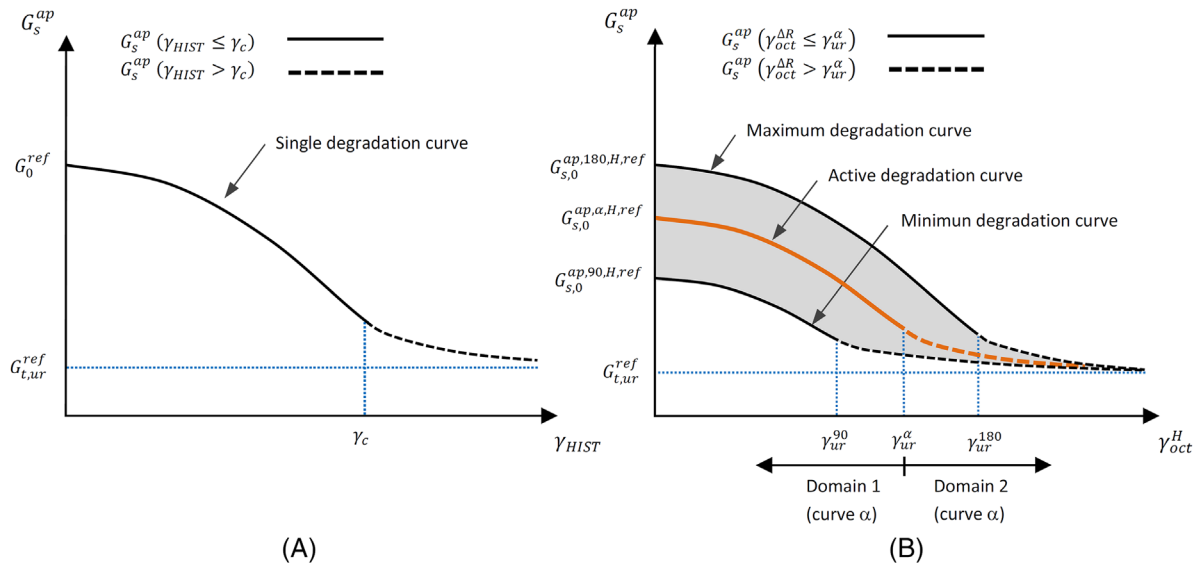


FIGURE 1 (A) Single degradation curve in Small Strain Overlay Model (SSOM), Hardening Soil Small (HS-S) and HS-SS models. (B) Multiple degradation curves that give place to a range of values of G_s^{ap} in the HQH and EPHYSS models

a different strategy is used when HQH is combined with a plastic model. This strategy consists of using a value of $\xi = 2$ in all situations, while other variables that will be added in the plastic part of the EPHYSS model will be the responsible for reproducing the stiffness of the soil during primary loading.

Unlike most models in which the maximum shear modulus remains constant (G_0^{ref}) and gives place to a single degradation curve of G_s^{ap} (Figure 1A), the HQH model considers that the maximum value of the shear modulus corresponding to the active degradation curve α is a state variable $G_{s,0}^{ap,\alpha,H,ref}$ that, as well as \mathbf{h} , depends on the total recent deviatoric strain history, giving place to an area of possible values of G_s^{ap} (Figure 1B), so that the HQH model considers infinite degradation curves of soil shear stiffness as a function of the rotation in the recent deviatoric strain path, which offers great versatility and adaptability to experimental data.

The incremental constitutive equation in domain 1 can be deduced from the Expression (1).

$$\dot{\sigma}' = \mathbf{E}'_s (K'_s, G_s^{ap}) : \dot{\varepsilon}^e + \dot{\mathbf{E}}'_s (K'_s, G_s^{ap}) : (-\varepsilon_{oct}^e \mathbf{1} + \mathbf{e}^{e,\Delta R}) \quad (7)$$

The second term from the Expression (7) allows considering strain-induced anisotropy, and it can be demonstrated that $\dot{\mathbf{E}}'_s (K'_s, G_s^{ap}) = \mathbf{E}'_s (\dot{K}'_s, \dot{G}_s^{ap})$, where \dot{K}'_s and \dot{G}_s^{ap} are given in Expressions (8) and (9), respectively.

$$\dot{K}'_s = \left(\frac{K'_s}{\frac{p'}{3m_1 K'_s} - \varepsilon_{oct}^e} \right) \dot{\varepsilon}_{oct}^e \quad (8)$$

$$\dot{G}_s^{ap} = G_s^{ap} \left(\frac{3m_2 K'_s}{p'} \left(1 + \frac{\varepsilon_{oct}^e}{\frac{p'}{3m_1 K'_s} - \varepsilon_{oct}^e} \right) \dot{\varepsilon}_{oct}^e + \frac{\dot{G}_{s,0}^{ap,\alpha,H,ref}}{G_{s,0}^{ap,\alpha,H,ref}} - \frac{a}{\xi \gamma_{0,7}} \frac{G_s^{ap}}{G_{s,0}^{ap,\alpha,H}} \dot{\gamma}_{oct}^H \right) \quad (9)$$

3.3 | Incremental constitutive equation in domain 2

The incremental constitutive equation in domain 2 ($\gamma_{oct}^{\Delta R} > \gamma_{ur}^\alpha$) is the following:

$$\dot{\sigma}' = \mathbf{E}'_t (K'_t, G_{t,ur}) : \dot{\varepsilon}^e \quad (10)$$

$$\mathbf{E}'_t (K'_t, G_{t,ur}) = \left(K'_t - \frac{2}{3}G_{t,ur} \right) \mathbf{1} \otimes \mathbf{1} + 2G_{t,ur} \mathbb{I} \tag{11}$$

The expression of the elastic tangent bulk modulus K'_s in domain 2 is the following:

$$K'_t = K'_s \left(1 + \frac{\varepsilon_{oct}^e}{\frac{p'}{3m_1 K'_s} - \varepsilon_{oct}^e} \right) \tag{12}$$

Regarding to the (hypo)elastic tangent shear modulus G_t in domain 2, a minimum value $G_{t,ur}$ is considered from the limit strain between both domains ($\gamma_{oct}^{\Delta R} = \gamma_{ur}^\alpha$):

$$G_{t,ur} = G_{t,ur}^{ref} \left(\frac{-p'}{p'_{ref,2}} \right)^{m_2} \tag{13}$$

In the HQH model, when combined with the HS_{MOD} model, the value of $G_{t,ur}^{ref}$ is calculated according to the Expression (14) from $E_{t,ur}^{Iref}$ (a HS_{MOD} model parameter) and $K_t^{Iref} = K_s^{Iref} / (1 - m_1)$, resulting after considering $p^{ini} = 0$:

$$G_{t,ur}^{ref} = \frac{3K_t^{Iref} E_{t,ur}^{Iref}}{9K_t^{Iref} - E_{t,ur}^{Iref}} \tag{14}$$

The fact that γ_{ur}^α coincides with the maximum value of γ_{oct}^H allows applying the expression of G_t^{ap} in domain 1 to deduce the value of $\gamma_{ur}^\alpha = \gamma_{ur}^\alpha (G_{t,ur})$. For that purpose, it is necessary to previously obtain the explicit expression of G_t^{ap} in domain 1, which, unlike what happens with K'_t , is not possible in the general case, but it is under some restrictions in the strain paths within the elastic domain, specifically when $\hat{\mathbf{h}} : \hat{\mathbf{e}} = \hat{\mathbf{h}} : \hat{\mathbf{e}} \approx 1$ and there has been a deviatoric strain rotation of 180° ($\alpha = 180^\circ$) in the previous recent deviatoric strain path. In this case, $G_{s,0}^{ap,\alpha,H,ref} = 0$, $\dot{\gamma}_{oct}^H \approx \dot{\gamma}_{oct}^e$ and $\gamma_{oct}^H \approx \gamma_{oct}^{e,\Delta R}$. Under these assumptions and taking the deviatoric part of the Expression (7) and differentiating the Expression (4), the following expressions are obtained:

$$\dot{\gamma}_{oct} = 2G_s^{ap} \dot{\gamma}_{oct}^e + 2 \frac{\partial G_s^{ap}}{\partial \gamma_{oct}^{e,\Delta R}} \gamma_{oct}^{e,\Delta R} \dot{\gamma}_{oct}^e = 2G_t^{ap} \dot{\gamma}_{oct}^e \approx 2G_t^{ap} \dot{\gamma}_{oct}^H \tag{15}$$

$$G_t^{ap} = G_s^{ap} + \frac{\partial G_s}{\partial \gamma_{oct}^{e,\Delta R}} \gamma_{oct}^{e,\Delta R} \approx G_s^{ap} + \frac{\partial G_s}{\partial \gamma_{oct}^H} \gamma_{oct}^H = \frac{G_{s,0}^{ap,\alpha,H}}{\left(1 + a \left(\frac{\gamma_{oct}^H}{\xi \gamma_{0.7}} \right) \right)^2} \tag{16}$$

Based on the foregoing, the value of γ_{ur}^α is obtained by substituting $G_t^{ap} = G_{t,ur}$ and $\gamma_{oct}^H = \gamma_{ur}^\alpha$ in the Expression (16). Unless stated otherwise, $\xi = 2$ is considered.

$$\gamma_{ur}^\alpha = \frac{\xi \gamma_{0.7}}{a} \left(\sqrt{\frac{G_{s,0}^{ap,\alpha,H,ref}}{G_{t,ur}^{ref}} - 1} \right) \tag{17}$$

3.4 | Poisson's ratio

Drained Poisson's ratio will be variable in both strain domains, since it depends on the value of the stiffness moduli according to $\nu'_s = \nu'_s (K'_s, G_s^{ap})$ in domain 1 and $\nu'_t = \nu'_t (K'_t, G_{t,ur})$ in domain 2.

The value of G_s^{ap} in the range of small strains corresponding to domain 1 can lead to values of ν' too small or even negative and, therefore, physically unreal. To avoid this, it is possible to limit the value of the bulk modulus $K_s^{t,corr}$ through forcing drained Poisson's ratio to be maintained above a threshold value ν'_{min} when deviatoric loadings appear. The same type of correction can be applied in domain 2 to $K_t^{t,corr}$. It is assumed $\nu'_{s,min} \approx \nu'_{t,min} \approx \nu'_{min}$.

$$K_s^{t,corr} = \max \left\{ K'_s, \frac{2G_s^{ap} (1 + \nu'_{min})}{3(1 - 2\nu'_{min})} \right\} \quad (18)$$

$$K_t^{t,corr} = \max \left\{ K'_t, \frac{2G_{t,ur} (1 + \nu'_{min})}{3(1 - 2\nu'_{min})} \right\} \quad (19)$$

3.5 | HQH model state variables

After a reversal and before a later monotonous strain, the soil behavior suggests a gradual adaptation of its internal state, characterized by hidden state variables, until it depends exclusively on the stress tensor and the void ratio,²⁰ state in which proportional strain paths lead to proportional stress paths and, therefore, soil internal state is located within the Swept Out Memory (SOM) region.²¹ This gradual adaptation of soil internal state takes place in domain 1 due to the evolution of internal short-term memory state variables \mathbf{h} and $G_{s,0}^{ap,\alpha,H,ref}$. The internal soil state remains constant in domain 2 (\mathbf{h} and $G_{s,0}^{ap,\alpha,H,ref}$ remain constant) and reversal points information is stored in short-term (\mathbf{e}^R and $\mathbf{e}^{e,R}$) and long-term (\mathbf{H}_{MEM} , \mathbf{E}_{MEM} and \mathbf{E}_{MEM}^e) state variables. The EPHYSS model reaches the SOM region when both all the active strain cycles are closed and the domain 2 is reached, which implies the erasure of the information stored in state variables.

The proposed HQH model uses seven state variables (\mathbf{h} , $G_{s,0}^{ap,\alpha,H,ref}$, \mathbf{e}^R , $\mathbf{e}^{e,R}$, \mathbf{H}_{MEM} , \mathbf{E}_{MEM} and \mathbf{E}_{MEM}^e) to describe the nonlinear reversible, hysteretic and dependent of the recent history soil behavior in Zone II of Jardine, which includes domain 1 and part of domain 2, and one additional state variable ($G_{t,min,\xi=1}^{ap}$) to simulate initial stiffness and stiffness degradation during primary loading when HQH and HS_{MOD} models are combined.

3.5.1 | State variable \mathbf{h}

The \mathbf{h} tensor is a history tensor that stores the value of recent total deviatoric strains, understanding as recent those strains that have not been erased yet by a reversal. The state variable \mathbf{h} acts as a short-term memory variable that can be totally or partially reinitialized after a reversal. The proposed formulation for the history tensor rate $\dot{\mathbf{h}}$ is based on that of the intergranular strain tensor rate δ ,²² although significant modifications are introduced.

$$\dot{\mathbf{h}} = \begin{cases} \left(\mathbb{1} - \hat{\mathbf{h}} \otimes \hat{\mathbf{h}} \rho_\alpha^w \right) : \dot{\mathbf{e}} - \left(\mathbb{1} - \hat{\mathbf{h}} \otimes \hat{\mathbf{e}} \right) : \mathbf{h} & \text{if } \cos(\alpha) > 0 \\ \dot{\mathbf{e}} - \mathbf{h} & \text{if } \cos(\alpha) \leq 0 \end{cases} \quad (20)$$

where $\cos(\alpha) = \hat{\mathbf{h}} : \hat{\mathbf{e}}$, $\rho_\alpha = \gamma_{oct}^H / \gamma_{ur}^\alpha$ and w is a numerical parameter that controls the rate with which \mathbf{h} evolves (values $w \geq 100$ are adopted to have $\dot{\mathbf{h}} \approx \dot{\mathbf{e}}$ in degradation processes after a $90^\circ \leq \alpha \leq 180^\circ$ deviatoric strain rotation, complying $\rho_\alpha^w \rightarrow 0$ if $\rho_\alpha < 1$ and $\rho_\alpha^w \rightarrow 1$ if $\rho_\alpha \approx 1$).

When the closing of an active strain cycle takes place between the active reversal points $s-1$ and s ($s \geq 2$ when a strain cycle exists), which happens when Expression (21) is fulfilled for $N = 1, 2$, the history tensor \mathbf{h} is updated by modifying its modulus but maintaining its previous direction as indicated in Expression (22). This allows recovering the value of the variable $\gamma_{oct}^{H,(n+1)}$ corresponding to the cycle that is immediately superior to the one that is being closed, with a reasonable computational cost.

$$\sqrt[N]{\left(\gamma_{oct}^{\Delta R,(n+1)} \right)^N} > \sqrt{4/3} \sqrt[N]{\left(\left(E_{MEM}^{(n)} \right)_{s(n)} - \left(E_{MEM}^{(n)} \right)_{s(n-1)} \right)^N} \quad (21)$$

$$\mathbf{h}^{(n+1)} = \left(\frac{\beta' \left(H_{MEM}^{(n)} \right)_{s^{(n)}-1}}{\|\mathbf{h}^{(n)}\|} \right) \mathbf{h}^{(n)} \quad (22)$$

3.5.2 | State variable $G_{s,0}^{ap,\alpha,H,ref}$

The variation of maximum stiffness in the HQH model is considered through the state variable $G_{s,0}^{ap,\alpha,H,ref}$, which stores the value of the maximum reference secant shear modulus corresponding to the active degradation curve. The state variable $G_{s,0}^{ap,\alpha,H,ref}$ acts as a short-term memory variable that can be totally or partially reinitialized after a reversal.

$$\dot{G}_{s,0}^{ap,\alpha,H,ref} = \begin{cases} 0 & \text{if } \cos(\alpha^*) < \cos(\alpha) \\ \left(G_{s,0}^{ap,90,H,ref} - G_{s,0}^{ap,\alpha,H,ref} \right) (\cos(\alpha^*) - \cos(\alpha)) & \text{if } 0 < \cos(\alpha) \leq \cos(\alpha^*) \\ \left(G_{s,0}^{ap,90,H,ref} - G_{s,0}^{ap,\alpha,H,ref} \right) + \left(G_{s,0}^{ap,90,H,ref} - G_{s,0}^{ap,180,H,ref} \right) \cos(\alpha) & \text{if } \cos(\alpha) \leq 0 \end{cases} \quad (23)$$

where $\cos(\alpha^*) = (\hat{\mathbf{h}} : \hat{\mathbf{e}})^*$.

The value of the maximum shear modulus after stress reversals in different soils has been measured in many studies.^{23–27} According to these studies it can be concluded that the ratio between the maximum shear modulus after a 180° stress rotation ($G_0^{\theta q/p'=180^\circ}$) and the maximum shear modulus after a 90° stress rotation ($G_0^{\theta q/p'=90^\circ}$) adopts the following values $G_0^{\theta q/p'=90^\circ} / G_0^{\theta q/p'=180^\circ} = 0.30 - 0.69$. But the estimation of the value of maximum shear modulus after a 90° strain reversal $G_{s,0}^{ap,90,H,ref}$ (considering the equivalence $G_{s,0}^{ap,90,H,ref} \approx G_{t,0}^{ap,90,H,ref}$ after a 90° deviatoric strain rotation in the HQH model) is difficult because available data are scarce. However the ratio $G_{t,0}^{ap,90,H,ref} / G_{t,0}^{ap,180,H,ref}$ can be approximated by the the ratio m_T / m_R between the parameters of the hypoplastic model with intergranular strain of Niemunis and Herle²² (both ratios are different from the ratio $G_0^{\theta q/p'=90^\circ} / G_0^{\theta q/p'=180^\circ}$ that considers stress (nor strain) reversals). Nevertheless, in Niemunis and Herle model the reversals depend on the total strain rotations, thus giving place to a coupling between the variation of volumetric strains and the variation of the shear stiffness,^{22,28} but it is possible to show that if $\hat{\mathbf{e}}^{\Delta R} : \hat{\mathbf{e}} = 0$ holds, then $\hat{\mathbf{e}}^{\Delta R} : \hat{\mathbf{e}} = 0$, provided that $\varepsilon_{oct} \dot{\varepsilon}_{oct} = 0$, so, in these cases, for the estimation of $G_{t,0}^{ap,90,H,ref} / G_{t,0}^{ap,180,H,ref}$ from m_T / m_R it will be assumed that the condition $\varepsilon_{oct} \dot{\varepsilon}_{oct} = 0$ is satisfied, that is, the soil does not experience volumetric strains or these strains are small before or immediately after the 90° strain rotation. In Table 1 values of $G_{t,0}^{ap,90,H,ref} / G_{t,0}^{ap,180,H,ref}$ are provided for different soils. The definition of the ratio $G_{t,0}^{ap,90,H,ref} / G_{t,0}^{ap,180,H,ref}$ allows estimating the value of $G_{s,0}^{ap,90,H,ref}$ from that of $G_{s,0}^{ap,180,H,ref}$ by the relation $G_{s,0}^{ap,90,H,ref} = \Lambda G_{s,0}^{ap,180,H,ref}$, taking Λ values of 0.40 – 0.58 for sands and 0.50 for clays.

TABLE 1 Values of $G_{t,0}^{ap,90,H,ref} / G_{t,0}^{ap,180,H,ref}$ for different soils

| Type of soil | $G_{t,0}^{ap,90,H,ref} / G_{t,0}^{ap,180,H,ref}$ |
|---------------------------------|--|
| Hochstetten and Ticino sand (*) | 0.40 ²² |
| Karlsruhe sand | 0.58 ³¹ |
| Toyoura sand | 0.40 ³⁰ |
| | 0.50 ³² |
| Komorany sand | 0.50 ³¹ |
| Firoozkuh no. 161 sand | 0.40 ³¹ |
| Undisturbed London Clay | 0.50 ²⁸ |

(*) Schädlich and Schweiger^{29,30} obtained a value of 0.44 for Hochstetten and Ticino sand in numerical simulations of biaxial compression tests using their multilaminated model.

3.5.3 | State variables e^R and $e^{e,R}$

The state variable e^R , which stores the value of the total deviatoric strain tensor at the last reversal point that conforms the endpoint of the active strain cycle, appears, on the one hand, in the expression $\gamma_{oct}^{\Delta R} = \sqrt{4/3} (\|e\| - \|e^R\|)$, which allows to know if the incremental constitutive equation that must be applied is the one corresponding to domain 1 or domain 2, and, on the other hand, in the expression $e^{\Delta R} = e - e^R$, with which it is possible to calculate the product $\hat{e}^{\Delta R} : \Delta \hat{e}$ that identifies the reversals in which the state variables e^R , $e^{e,R}$, H_{MEM} , E_{MEM} and E_{MEM}^e must be stored. Conversely, the state variable $e^{e,R}$, which stores the value of the elastic deviatoric strain tensor at the last reversal point that conforms the endpoint of the active strain cycle, appears in the deviatoric part of the elastic incremental constitutive equation of domain 1, $\dot{s} = 2G_s^{ap} e^e + 2\dot{G}_s^{ap} (e^e - e^{e,R})$. Both state variables act as short-term memory variables that are totally reinitialized after a reversal, and their update occurs according to the following scheme, where $s^{(n)}$ is the number of reversal points that are active at the beginning of the calculation step ($n \rightarrow n + 1$):

- When $\hat{h}^{(n)} : \Delta \hat{e}^{(n+1)} \leq \cos(\alpha^{*,(n)})$ and $\hat{e}^{\Delta R,(n)} : \Delta \hat{e}^{(n+1)} \leq \cos(\alpha^{*,(n)})$, a deviatoric strain rotation that generates a new reversal point that will conform the endpoint of a new strain cycle occurs:

$$e^{R,(n+1)} = e^{(n)}$$

$$e^{e,R,(n+1)} = e^{e,(n)} \quad (24)$$

- When $\sqrt{N} \sqrt{(\gamma_{oct}^{\Delta R,(n+1)})^N} > \sqrt{4/3} \sqrt{N} \sqrt{((E_{MEM}^{(n)})_{s^{(n)}} - (E_{MEM}^{(n)})_{s^{(n)-1}})^N}$, with $N = 1, 2$, the closing of the strain cycle between the active reversal points $s^{(n)} - 1$ and $s^{(n)}$ ($s^{(n)} > 2$) occurs:

$$e^{R,(n+1)} = \left(\frac{(E_{MEM}^{(n)})_{s^{(n)-2}}}{\|e^{R,(n)}\|} \right) e^{R,(n)}$$

$$e^{e,R,(n+1)} = \left(\frac{(E_{MEM}^{e,(n)})_{s^{(n)-2}}}{\|e^{e,R,(n)}\|} \right) e^{e,R,(n)} \quad (25)$$

when $s^{(n)} = 2$, $e^{R,(n+1)} = 0$ and $e^{e,R,(n+1)} = 0$.

- When neither the deviatoric strain rotation that generates a new reversal point nor the closing of any strain cycle occur:

$$e^{R,(n+1)} = e^{R,(n)}$$

$$e^{e,R,(n+1)} = e^{e,R,(n)} \quad (26)$$

The first cycle to be closed will be the one corresponding to the smallest active strain cycle. The extremes of such cycle correspond to the last two values of $\|h\|$, $\|e\|$ and $\|e^e\|$, memorized, respectively, in the state variables H_{MEM} , E_{MEM} and E_{MEM}^e . Such values are those that have been identified with the $s^{(n)} - 1$ and $s^{(n)}$ components of such variables in the calculation step ($n \rightarrow n + 1$). Moreover, as can be seen, when a cycle closure occurs, the state variables e^R and $e^{e,R}$ are updated by modifying their modulus but maintaining their previous direction. This update allows partially recovering the characteristics of e^R and $e^{e,R}$ corresponding to the cycle that is immediately superior to the one that is being closed, with a reasonable computational cost.

3.5.4 | State variables H_{MEM} , E_{MEM} and E_{MEM}^e

The state variables $\mathbf{H}_{MEM}, \mathbf{E}_{MEM}, \mathbf{E}_{MEM}^e \in \mathbb{R}^{\bar{M}}$ store, respectively, the value of $\|\mathbf{h}\|$, $\|\mathbf{e}^R\|$ and $\|\mathbf{e}^{e,R}\|$ in the reversal points that conform the endpoints of strain cycles, provided that such strain cycles are kept open. The state variables \mathbf{H}_{MEM} , \mathbf{E}_{MEM} and \mathbf{E}_{MEM}^e constitute long-term memory variables capable of storing information of all active historical reversals. In general, all the components of $\mathbf{H}_{MEM}, \mathbf{E}_{MEM}$ and \mathbf{E}_{MEM}^e have an initial value of zero and are updated according to the following scheme, which is similar to that proposed by Hueckel and Nova³³:

- When $\hat{\mathbf{h}}^{(n)} : \Delta \hat{\boldsymbol{\epsilon}}^{(n+1)} \leq \cos(\alpha^{*,(n)})$ and $\hat{\boldsymbol{\epsilon}}^{\Delta R,(n)} : \Delta \hat{\boldsymbol{\epsilon}}^{(n+1)} \leq \cos(\alpha^{*,(n)})$, a deviatoric strain rotation that generates a new reversal point that will conform the endpoint of a new strain cycle occurs (in this case $s^{(n+1)} = s^{(n)} + 1$):

$$\begin{aligned} \left(H_{MEM}^{(n+1)} \right)_{1, \dots, s^{(n+1)}-1} &= \left(H_{MEM}^{(n)} \right)_{1, \dots, s^{(n)}} \\ \left(H_{MEM}^{(n+1)} \right)_{s^{(n+1)}} &= \begin{cases} \min \left\{ \|\mathbf{h}^{(n)}\|, \gamma_{ur}^{\alpha, \xi=1, (n)} \right\} & \text{if } s^{(n+1)} = 1 \\ \|\mathbf{h}^{(n)}\| & \text{if } s^{(n+1)} > 1 \end{cases} \\ \left(H_{MEM}^{(n+1)} \right)_{s^{(n+1)}+1, \dots, \bar{M}} &= 0 \end{aligned} \tag{27}$$

$$\begin{aligned} \left(E_{MEM}^{(n+1)} \right)_{1, \dots, s^{(n+1)}-1} &= \left(E_{MEM}^{(n)} \right)_{1, \dots, s^{(n)}} \\ \left(E_{MEM}^{(n+1)} \right)_{s^{(n+1)}} &= \|\mathbf{e}^{R,(n)}\| \\ \left(E_{MEM}^{(n+1)} \right)_{s^{(n+1)}+1, \dots, \bar{M}} &= 0 \end{aligned} \tag{28}$$

$$\begin{aligned} \left(E_{MEM}^{e,(n+1)} \right)_{1, \dots, s^{(n+1)}-1} &= \left(E_{MEM}^{e,(n)} \right)_{1, \dots, s^{(n)}} \\ \left(E_{MEM}^{e,(n+1)} \right)_{s^{(n+1)}} &= \|\mathbf{e}^{e,R,(n)}\| \\ \left(E_{MEM}^{e,(n+1)} \right)_{s^{(n+1)}+1, \dots, \bar{M}} &= 0 \end{aligned} \tag{29}$$

- When $\sqrt[N]{(\gamma_{oct}^{\Delta R,(n+1)})^N} > \sqrt{4/3} \sqrt[N]{((E_{MEM}^{(n)})_{s^{(n)}} - (E_{MEM}^{(n)})_{s^{(n)}-1})^N}$, with $N = 1, 2$, the closure of the strain cycle between the active reversal points $s^{(n)} - 1$ and $s^{(n)}$ occurs (in this case $s^{(n+1)} = s^{(n)} - 2$ and the $j^{(n)} - th$ components of these variables, that comply $j^{(n)} > s^{(n)} - 1$ and correspond to the reversal points that conform the endpoints of the active strain cycles imbricated in the cycle that is being closed, will be erased):

$$\begin{aligned} \left(H_{MEM}^{(n+1)} \right)_{1, \dots, s^{(n+1)}} &= \left(H_{MEM}^{(n)} \right)_{1, \dots, s^{(n)}-2} \\ \left(H_{MEM}^{(n+1)} \right)_{s^{(n+1)}+1, \dots, \bar{M}} &= 0 \end{aligned} \tag{30}$$

$$\begin{aligned} \left(E_{MEM}^{(n+1)} \right)_{1, \dots, s^{(n+1)}} &= \left(E_{MEM}^{(n)} \right)_{1, \dots, s^{(n)}-2} \\ \left(E_{MEM}^{(n+1)} \right)_{s^{(n+1)}+1, \dots, \bar{M}} &= 0 \end{aligned} \quad (31)$$

$$\begin{aligned} \left(E_{MEM}^{e,(n+1)} \right)_{1, \dots, s^{(n+1)}} &= \left(E_{MEM}^{e,(n)} \right)_{1, \dots, s^{(n)}-2} \\ \left(E_{MEM}^{e,(n+1)} \right)_{s^{(n+1)}+1, \dots, \bar{M}} &= 0 \end{aligned} \quad (32)$$

- When neither the deviatoric strain rotation that generates a new reversal point nor the closure of any strain cycle occur (in this case $s^{(n+1)} = s^{(n)}$):

$$\begin{aligned} \left(H_{MEM}^{(n+1)} \right)_{1, \dots, s^{(n+1)}} &= \left(H_{MEM}^{(n)} \right)_{1, \dots, s^{(n)}} \\ \left(H_{MEM}^{(n+1)} \right)_{s^{(n+1)}+1, \dots, \bar{M}} &= 0 \end{aligned} \quad (33)$$

$$\begin{aligned} \left(E_{MEM}^{(n+1)} \right)_{1, \dots, s^{(n+1)}} &= \left(E_{MEM}^{(n)} \right)_{1, \dots, s^{(n)}} \\ \left(E_{MEM}^{(n+1)} \right)_{s^{(n+1)}+1, \dots, \bar{M}} &= 0 \end{aligned} \quad (34)$$

$$\begin{aligned} \left(E_{MEM}^{e,(n+1)} \right)_{1, \dots, s^{(n+1)}} &= \left(E_{MEM}^{e,(n)} \right)_{1, \dots, s^{(n)}} \\ \left(E_{MEM}^{e,(n+1)} \right)_{s^{(n+1)}+1, \dots, \bar{M}} &= 0 \end{aligned} \quad (35)$$

The condition $s = 0$ is necessary for the soil state to be located within the SOM region.

3.5.5 | State variable $G_{t, \min, \xi=1}^{ap}$

The HQH model does not directly apply the criterion of Hashiguchi¹⁹ for the calculation of G_s^{ap} , despite having an internal structure that allows it. To simulate the initial stiffness of the soil and its degradation in the range of small strains during primary loading, the hardening laws of the plastic model with which the HQH model is combined are modified through the factor $h_i = h_i(G_{t, \min, \xi=1}^{ap})$.

The state variable $G_{t, \min, \xi=1}^{ap}$ is updated as follows in each calculation step:

$$G_{t, \min, \xi=1}^{ap,(n+1)} = \min \left\{ G_{t, \min, \xi=1}^{ap,(n)}, G_{t, \xi=1}^{ap,(n+1)} \approx \frac{\Delta \tau_{oct, \xi=1}^{(n+1)}}{\Delta \gamma_{oct}^{(n+1)}} \right\} \quad (36)$$

- If $\gamma_{oct}^{\Delta R,(n)} \leq \gamma_{ur}^{\alpha,(n)}$ and $\gamma_{oct}^{\Delta R,(n+1)} \leq \gamma_{ur}^{\alpha,(n)}$

$$\frac{\Delta\tau_{oct,\xi=1}^{(n+1)}}{\Delta\gamma_{oct}^{(n+1)}} = \frac{G_{s,\xi=1}^{ap,(n+1)} |\gamma_{oct}^{\Delta R,(n+1)}| - G_{s,\xi=1}^{ap,(n)} |\gamma_{oct}^{\Delta R,(n)}|}{|\gamma_{oct}^{\Delta R,(n+1)}| - |\gamma_{oct}^{\Delta R,(n)}|} \quad (37)$$

- If $\gamma_{oct}^{\Delta R,(n)} \leq \gamma_{ur}^{\alpha,(n)}$ and $\gamma_{oct}^{\Delta R,(n+1)} > \gamma_{ur}^{\alpha,(n)}$

$$\frac{\Delta\tau_{oct,\xi=1}^{(n+1)}}{\Delta\gamma_{oct}^{(n+1)}} = \frac{G_{s,\xi=1}^{ap} \left(\gamma_{ur}^{\alpha,(n)} \gamma_{ur}^{\alpha,(n)} - G_{s,\xi=1}^{ap,(n)} |\gamma_{oct}^{\Delta R,(n)}| + G_{t,ur}^{(n)} \left(|\gamma_{oct}^{\Delta R,(n+1)}| - \gamma_{ur}^{\alpha,(n)} \right) \right)}{|\gamma_{oct}^{\Delta R,(n+1)}| - |\gamma_{oct}^{\Delta R,(n)}|} \quad (38)$$

- If $\gamma_{oct}^{\Delta R,(n)} > \gamma_{ur}^{\alpha,(n)}$ and $\gamma_{oct}^{\Delta R,(n+1)} > \gamma_{ur}^{\alpha,(n)}$

$$\frac{\Delta\tau_{oct,\xi=1}^{(n+1)}}{\Delta\gamma_{oct}^{(n+1)}} = G_{t,ur}^{(n)} \quad (39)$$

3.6 | Hysteretic behavior

The HQH model considers the hysteretic behavior in the deviatoric strain component and not in the volumetric one, because the variation of the bulk modulus between elastic isotropic unloadings and reloadings is negligible.³⁴ This distinguishes the HQH model, provided that $\nu' > \nu'_{\min}$ is met, from several models that consider the dependence $K' = K'(G, \nu')$ or $G = G(K', \nu')$, in which the hysteretic behavior that controls G induces an hysteretic behavior on K' or viceversa.

A model that consider the hysteretic behavior of the soil must define the following concepts: (1) reversal criterion; (2) memory rules; (3) reversal effects on the degradation variables; and (4) reversals effect on the maximum soil stiffness.⁴

3.6.1 | Reversal criterion

The reversal criterion of the HQH model is intrinsic, which means that it arises from the own model equations. It is formulated using strains and the reversals take place in a continuous way with the rotation angle of the recent deviatoric strain path $\hat{\mathbf{h}} : \hat{\mathbf{e}}$.

The HQH model distinguishes between:

- Reversals that affect the value G_s^{ap} through the modification of the state variables $G_{s,0}^{ap,\alpha,H,ref}$ and \mathbf{h} . This occurs when $\|\mathbf{h}^{(n+1)}\| \leq \|\mathbf{h}^{(n)}\|$, which gives the condition $\cos(\alpha) \leq \cos(\alpha^*)$ (Figure 2), where:

$$\cos(\alpha^*) = (\hat{\mathbf{h}} : \hat{\mathbf{e}})^* = \frac{1}{\frac{\|\dot{\mathbf{e}}\|}{\|\mathbf{h}\|} (1 - \rho_\alpha^w) + 1} \quad (40)$$

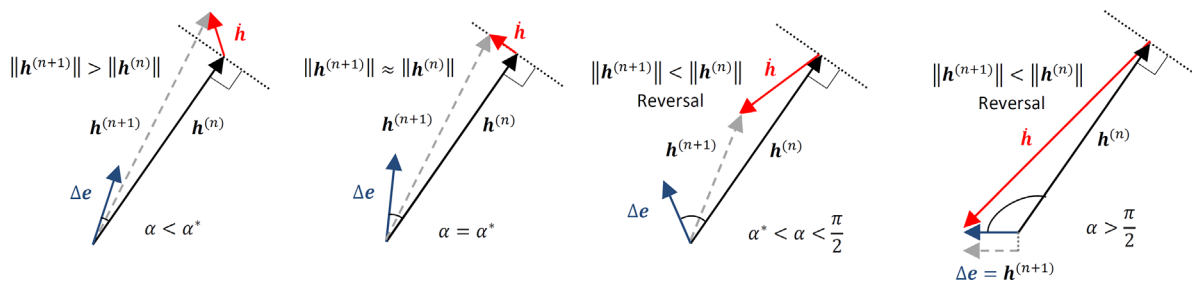


FIGURE 2 Evolution of $\hat{\mathbf{h}}$ according to $\cos(\alpha) = \hat{\mathbf{h}} : \hat{\mathbf{e}}$ and reversal criterion that affects G_s^{ap}

- Reversals that affect the value G_s^{ap} and also give place to a reversal point that defines the endpoint of a new strain cycle. This occurs when the conditions $\cos(\alpha) \leq \cos(\alpha^*)$ and $\hat{e}^{\Delta R} : \hat{e} \leq \cos(\alpha^*)$ are simultaneously met, and implies a modification of the state variables value \mathbf{e}^R , $\mathbf{e}^{e,R}$, \mathbf{H}_{MEM} , \mathbf{E}_{MEM} and \mathbf{E}_{MEM}^e , besides of $G_{s,0}^{ap,\alpha,H,ref}$ and \mathbf{h} .

3.6.2 | Memory rules

HQH model can memorize information in multiple reversal points and, combined with a plastic model, partially satisfies the Generalized Masing Rules¹⁵⁻¹⁶ to reproduce the hysteretic soil behavior.

- **Rule Nr. 1:** To be able to reproduce the initial soil stiffness and its degradation in the small strain range during primary loading branch, the hardening rules of the plastic model with which the HQH model is combined are modified through the factor h_i (see Section 4.3).
- **Rule Nr. 2:** To calculate $\dot{\sigma}$ from $\dot{\epsilon}$ with the constitutive incremental equation in domain 1, $\xi = 2$ is used in the expressions of G_s^{ap} and \dot{G}_s^{ap} .
- **Rule Nr. 3:** When the HQH model is part of an elastoplastic model, the restriction of the stress state over the yield surfaces is considered, forcing the compliance of the Generalized Masing Rule Nr. 3.
- **Rule Nr. 4:** The HQH model partially complies this rule. To avoid the intersection of unloading/reloading branches, an important amount of recent history information must be stored. Apart from the recent history information stored in the history tensor \mathbf{h} , the HQH model can memorize the maximum shear stiffness modulus in the state variable $G_{s,0}^{ap,\alpha,H,ref}$ and all the information of the total and elastic deviatoric strain tensors in the last reversal point that conforms the endpoint of the active strain cycle through the state variables \mathbf{e}^R and $\mathbf{e}^{e,R}$, respectively. As well, HQH is capable to store partial information about the strains in all the reversal points that configure endpoints of active strain cycles through the state variables \mathbf{H}_{MEM} , \mathbf{E}_{MEM} and \mathbf{E}_{MEM}^e .

3.6.3 | Reversals effect on the degradation variable

The reversals effect on the degradation variable $\gamma_{oct}^H(\mathbf{h})$ can be easily deduced from the expression of $\dot{\mathbf{h}}$. When $\cos(\alpha) > \cos(\alpha^*)$, no reversal takes place and, therefore, $\dot{\gamma}_{oct}^H > 0$ and $\gamma_{oct}^H > 0$. Otherwise, when $\cos(\alpha) \leq \cos(\alpha^*)$, a reversal takes place and it will be $\dot{\gamma}_{oct}^H < 0$. Furthermore, in this case, if $0 \leq \cos(\alpha) < \cos(\alpha^*)$ is satisfied after the reversal, then $\gamma_{oct}^H > 0$, and if $-1.0 \leq \cos(\alpha) < 0$ is satisfied after the reversal, then $\gamma_{oct}^H = 0$ (Figure 3).

3.6.4 | Reversals effect on the maximum soil stiffness

The reversals effect on the maximum soil stiffness $G_{s,0}^{ap,\alpha,H,ref}$ can be easily deduced from the expression of $\dot{G}_{s,0}^{ap,\alpha,H,ref}$. When $\cos(\alpha) > \cos(\alpha^*)$, no reversal takes place and, therefore, $\dot{G}_{s,0}^{ap,\alpha,H,ref} = 0$. When $0 < \cos(\alpha) \leq \cos(\alpha^*)$, a reversal takes place and $\dot{G}_{s,0}^{ap,\alpha,H,ref} < 0$ will be complied. Otherwise, when $\cos(\alpha) \leq 0$, a reversal takes place and $\dot{G}_{s,0}^{ap,\alpha,H,ref} > 0$ or $\dot{G}_{s,0}^{ap,\alpha,H,ref} < 0$, depending on the value of $G_{s,0}^{ap,\alpha,H,ref}$ prior to such reversal (Figure 3).

3.7 | Stability criterion

To meet the stability criterion of Hill,³⁵ the following correction is applied to the variable $G_{s,0}^{ap,\alpha,H,ref}$, substituting it with $G_{s,0}^{ap,\alpha,H,ref,CORR}$, so that the value of G_s^{ap} cannot be reduced after a reversal.

$$G_{s,0}^{ap,\alpha,H,ref,CORR,(n+1)} = \begin{cases} G_{s,0}^{ap,\alpha,H,ref,(n+1)} & \text{if } G_s^{ap,(n+1)} > G_s^{ap,(n)} \\ \left(G_s^{ap,(n+1)} \left(1 + a \left(\frac{\gamma_{oct}^{H,(n+1)}}{\xi \gamma_{0.7}} \right) \right) \left(\frac{-p^{(n)}}{p'_{ref,2}} \right)^{-m_2} \right) - G_{s,0}^{ap,\alpha,H,ref,(n)} & \text{if } G_s^{ap,(n+1)} \leq G_s^{ap,(n)} \end{cases} \quad (41)$$

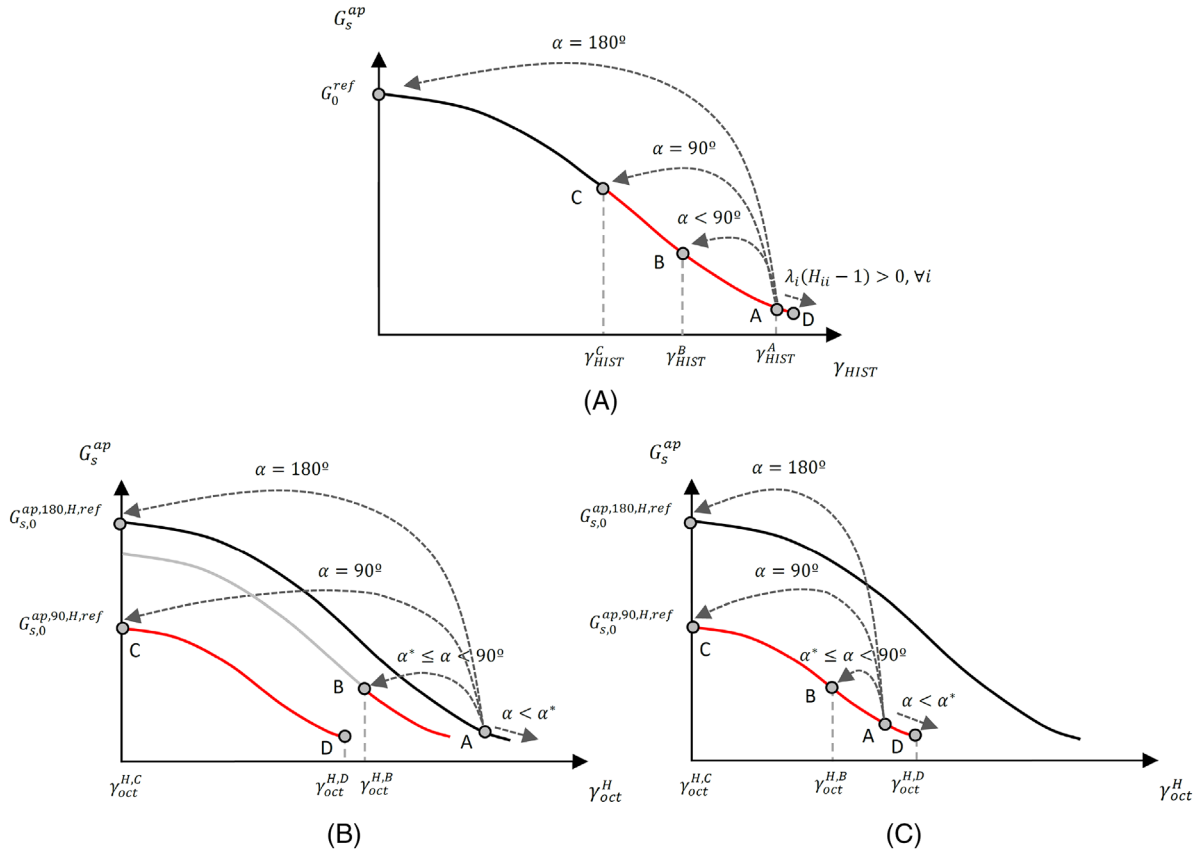


FIGURE 3 Full or partial reversals on (A) SSOM/HS-S/HS-SS models, (B) HQH/EPHYSS models with initial $G_{s,0}^{ap,\alpha,H,ref}$ equal to $G_{s,0}^{ap,180,H,ref}$ and (C) HQH/EPHYSS models with initial $G_{s,0}^{ap,\alpha,H,ref}$ equal to $G_{s,0}^{ap,90,H,ref}$

4 | EPHYSS MODEL AS A COMBINATION OF HQH AND HS_{MOD} MODELS

The EPHYSS model is an advanced elastoplastic model that considers the soil behavior in the range of small strains. Elastoplastic equations are used for the case of $k = 1 \dots q$ yield surfaces: (1) yield surfaces $f_k(\sigma', \chi_k^{pl}) = 0$; (2) plastic potentials $g_k(\sigma', \chi_k^{pl}) = 0$; (3) strain decomposition $\dot{\epsilon} = \dot{\epsilon}^e + \dot{\epsilon}^p$; (4) constitutive equation within yield surfaces $\dot{\sigma}' = G(\epsilon, \sigma', \chi^{el,hist}, \dot{\epsilon})$; (5) plastic strains decomposition $\dot{\epsilon}^p = \sum_{k=1}^q \dot{\epsilon}_k^p$; (6) flow rules $\dot{\epsilon}_k^p = \dot{\lambda}_k \partial g_k(\sigma', \chi_k^{pl}) / \partial \sigma'$; (7) hardening laws $\dot{\chi}_k^{pl} = \dot{\lambda}_k \mathbf{h}_k(\sigma', \chi_k^{pl})$; (8) consistency conditions $\dot{f}_k(\sigma', \chi_k^{pl}) = 0$; and (9) Karush-Kuhn-Tucker conditions $\dot{\lambda}_k \geq 0$, $f_k(\sigma', \chi_k^{pl}) \leq 0$ and $f_k(\sigma', \chi_k^{pl}) \dot{\lambda}_k = 0$.

The elastic part of the EPHYSS model is described with the HQH model, so that:

- In domain 1 ($\gamma_{oct}^{\Delta R} \leq \gamma_{ur}^\alpha$)

$$G(\epsilon, \sigma', \chi^{el,hist}, \dot{\epsilon}) = \mathbf{E}'_s(K'_s, G_s^{ap}) : \dot{\epsilon}^e + \dot{\mathbf{E}}'_s(K'_s, G_s^{ap}) : (-\epsilon_{oct}^e \mathbf{1} + \mathbf{e}^{e,\Delta R}) \quad (42)$$

- In domain 2 ($\gamma_{oct}^{\Delta R} > \gamma_{ur}^\alpha$)

$$G(\epsilon, \sigma', \chi^{el,hist}, \dot{\epsilon}) = \mathbf{E}'_t(K'_t, G_{t,ur}) : \dot{\epsilon}^e \quad (43)$$

On the other hand, the plastic part of the EPHYSS model is described with the HS_{MOD} model, whose theoretical fundament is exposed in this section.

4.1 | Yield surfaces of the EPHYSS model

4.1.1 | Cone yield surface f_s and Mohr-Coulomb limit surface f_{mc}

The EPHYSS model considers a Cone yield surface that controls the plastic strains of the soil under deviatoric loading. Such surface is formulated in terms of axial strain as $f_s = 2\varepsilon_1 - 2\varepsilon_1^e - \gamma^p$, being the plastic state variable $\gamma^p \approx 2\varepsilon_1^p$ under the hypothesis of hard soils in which $\varepsilon_v^p = 3\varepsilon_{oct}^p \approx 0$. To define the Cone yield surface, it is enough to do it in the stress space sectors corresponding to $-\sigma'_j \geq -\sigma'_k \geq -\sigma'_l$ with $\{j, k, l\} \in \{\{1, 2, 3\}, \{1, 3, 2\}, \{2, 1, 3\}\}$:

$$f_{s,jkl} = \frac{2q_a}{E'_i} \frac{(-\sigma'_j - (-\sigma'_l))}{q_a - (-\sigma'_j - (-\sigma'_l))} - \frac{2(-\sigma'_j - (-\sigma'_l))}{E'_{t,ur}} - \gamma^p \quad (44)$$

The EPHYSS model does not explicitly use the E_{50}^{ref} modulus in the formulation of the Cone yield surface, but uses the initial stiffness modulus E_i^{ref} , which is an internal parameter of the model that has to be calculated through an internal algorithm in which it is necessary to introduce the input parameter E_{50}^{ref} (see Section 4.5). The use of E_i^{ref} in the Expression (44) is due to the interaction that exists between the Cone yield surface and the Cap yield surface when both are simultaneously activated.

Furthermore, the stiffness moduli that appear in the model formulation, E'_{50} , $E'_{t,ur}$ and E'_i , vary with the stress level. The parameter p'_{ref} in the Expression (45) refers to a confinement stress ($p'_{ref} = -\sigma'_{3,ref}$).

$$\{E'_{50}, E'_{t,ur}, E'_i\} = \{E_{50}^{ref}, E_{t,ur}^{ref}, E_i^{ref}\} \left(\frac{-\sigma'_3 + c' \cot(\varphi')}{p'_{ref} + c' \cot(\varphi')} \right)^m \quad (45)$$

The yield surface f_s can harden until the plastic state variable γ^p reaches the limit value determined by the resistance criterion of Mohr-Coulomb, which happens when $q = q_f$.

$$q_f = \frac{2 \sin(\varphi')}{1 - \sin(\varphi')} (-\sigma'_3 + c' \cot(\varphi')) \quad (46)$$

Facing the numeric implementation of the EPHYSS model, it is interesting to express the Mohr-Coulomb limit surface f_{mc} in the same stress space sectors used for the Cone yield surface f_s :

$$f_{mc,jkl} = \frac{1}{2} (-\sigma'_j - (-\sigma'_l)) + \frac{1}{2} (-\sigma'_j + (-\sigma'_l)) \sin(\varphi') - c' \cot(\varphi') \quad (47)$$

4.1.2 | Cap yield surface f_c

The EPHYSS model considers a third yield surface denominated Cap yield surface, which allows to close the elastic region in the direction of the hydrostatic axis and reproduce the plastic volumetric soil behavior. In Expression (48) α' is an internal parameter of the model that has to be calculated through an internal algorithm in which it is necessary to introduce the input parameter K_0^{NC} (see Section 4.5) and p_p is a plastic state variable that controls the size of f_c .

$$f_c = \left(\frac{\tilde{q}}{\alpha'} \right)^2 + (-p')^2 - p_p^2 \quad (48)$$

$$\tilde{q} = -\sigma'_1 + \left(\frac{1}{\delta} - 1 \right) (-\sigma'_2) - \frac{1}{\delta} (-\sigma'_3) \quad (49)$$

$$\delta = \frac{3 - \sin(\varphi')}{3 + \sin(\varphi')} \quad (50)$$

4.1.3 | Tension Cut-off yield surface f_t

Finally, the EPHYSS model considers a fourth yield surface, denominated Tension Cut-off yield surface, which considers the soil tensile strength ($-\sigma'_3 = \sigma'_{trac} \geq 0$). To define the Tension Cut-off yield surface, it is sufficient to do it in the principal stress space sectors corresponding to $\{-\sigma'_j \geq -\sigma'_k \geq -\sigma'_l\} \cup \{-\sigma'_k \geq -\sigma'_j \geq -\sigma'_l\}$ with $\{j, k, l\} \in \{\{1, 2, 3\}, \{1, 3, 2\}\}$:

$$f_{t,jkl} = \sigma'_{trac} - (-\sigma'_l) \tag{51}$$

4.2 | Plastic potentials and flow rules

A linear flow rule $-\varepsilon_v^p / \dot{\gamma}^p = \sin(\psi_m)$ is considered on the Cone surface.

The EPHYSS model uses the dilatancy formulation of Li and Dafalias³⁶ $\tan(\psi_m) = (d_0/M)(Me^{\hat{m}\hat{\psi}} - \eta)$ when the soil behavior is contractive ($\psi_m < 0$), and considers the following simplifications: (1) a constant void ratio is assumed when calculating the Been and Jefferies³⁷ state parameter $\hat{\psi}$; (2) $\hat{\psi}\lambda = -1/15$ and $d_0 = M/10$. On the other hand, when the soil behavior is dilatant, the aforementioned simplifications of the Li and Dafalias formulation are not adequate and the original Rowe criterion³⁸ is used, thus avoiding an increase of the number of model parameters.

$$\left\{ \begin{array}{ll} \sin(\psi_m) = \frac{1}{10} \left(-M_{comp} e^{\frac{1}{15} \ln\left(\frac{\eta}{M_{comp}} \frac{\sin(\varphi'_m)(1-\sin(\varphi'_{cv}))}{\sin(\varphi'_{cv})(1-\sin(\varphi'_m))}\right)} + \eta \right) & \text{if } \sin(\varphi'_m) \leq \sin(\varphi'_{cv}) \\ \sin(\psi_m) = \min\left(\frac{\sin(\varphi'_m) - \sin(\varphi'_{cv})}{1 - \sin(\varphi'_m)\sin(\varphi'_{cv})}, \sin(\psi) \right) & \text{if } \sin(\varphi'_m) > \sin(\varphi'_{cv}) \text{ and } \psi > 0 \\ \sin(\psi_m) = \sin(\psi) & \text{if } \sin(\varphi'_m) \geq \sin(\varphi'_{cv}) \text{ and } \psi \leq 0 \\ \sin(\psi_m) = 0 & \text{if } \sin(\varphi') = 0 \end{array} \right. \tag{52}$$

$$M_{comp} = \frac{6 \sin(\varphi'_{cv})}{3 - \sin(\varphi'_{cv})} \tag{53}$$

$$\sin(\varphi'_m) = \max\left(\frac{-\sigma'_1 - (-\sigma'_3)}{-\sigma'_1 + (-\sigma'_3) + 2c' \cot(\varphi')}, \frac{-\sigma'_1(1 - K_0^{NC})}{-\sigma'_1(1 + K_0^{NC}) + 2c' \cot(\varphi')}\right) \tag{54}$$

$$\eta = \max\left\{\frac{q}{p'}, \frac{(1 - K_0^{NC})}{1/3(1 + 2K_0^{NC})}\right\} \tag{55}$$

Dilatancy in critical state models is zero when the soil reaches the critical state. EPHYSS model is not a critical state model but can approximate critical state phenomenon by using a ‘‘Dilatancy cut-off’’ criterion that consists in forcing the dilatancy to be zero when the void ratio reaches a maximum value (that is, $\psi_m = 0$ when $e = e_{max}$). This criterion adds a new parameter e_{max} to the model. In the model version presented in this paper, the ‘‘Dilatancy Cut-Off’’ criterion has not been considered.

The definition of the flow rule for the Cone yield surface and the Mohr-Coulomb yield surface is carried out through the following expressions of the plastic potentials in the principal stress space sectors corresponding to $-\sigma'_j \geq -\sigma'_k \geq -\sigma'_l$ with $\{j, k, l\} \in \{\{1, 2, 3\}, \{1, 3, 2\}, \{2, 1, 3\}\}$.

$$g_{s,jkl} = \frac{1}{2} \left(-\sigma'_j - (-\sigma'_l) \right) - \frac{1}{2} \left(-\sigma'_j + (-\sigma'_l) \right) \sin(\psi_m) \tag{56}$$

$$g_{mc,jkl} = \frac{1}{2} \left(-\sigma'_j - (-\sigma'_l) \right) - \frac{1}{2} \left(-\sigma'_j + (-\sigma'_l) \right) \sin(\psi) \tag{57}$$

Finally, regarding to the Cap yield surface and the Tension Cut-off yield surface, associated plasticity is assumed, considering, therefore, $g_c = f_c$ and $g_{t,jkl} = f_{t,jkl}$.

4.3 | Hardening laws

The EPHYSS model uses two hardening variables: (1) the plastic deviatoric strain γ^p that controls the size of the Cone yield surface f_s ; and (2) the preconsolidation stress p_p that controls the size of the Cap yield surface f_c . The hardening laws of the EPHYSS model are the following:

$$\dot{\gamma}^p = (\dot{\lambda}_s h_s) h_i = \dot{\lambda}_s h_i \quad (58)$$

$$\dot{p}_p = (\dot{\lambda}_c h_c) h_i = \dot{\lambda}_c 2H (-p') \left(\frac{p_p + c' \cot(\varphi')}{p'_{ref} + c' \cot(\varphi')} \right)^m h_i \quad (59)$$

$$H = \frac{K_t'^{ref}}{\frac{K_{t,ur}'}{K_c'} - 1} \quad (60)$$

$$h_i = \left(\frac{G_{t,min,\xi=1}^{ap}}{G_{t,ur}} \right)^{1 + \frac{E_{t,ur}'^{ref}}{E_i'^{ref}}} \quad (61)$$

The parameter p'_{ref} in the Expression (59) refers to a confinement stress ($p'_{ref} = -\sigma'_{3,ref}$). The effect of the factor h_i is maximum when $G_{t,min,\xi=1}^{ap} = G_{s,0}^{ap,180,H}$ and vanishes when $G_{t,min,\xi=1}^{ap} = G_{t,ur}$ (see Section 3.5.5). The evolution of $G_{t,min,\xi=1}^{ap}$ follows the degradation curve corresponding to the primary loading branch, whose values are lower than that of the elastic unloading or reloading branches. For that, in the calculation of h_i the value $\xi = 1$ is used following the Hashiguchi criterion.¹⁹ Moreover, the plastic modulus H depends on $K_t'^{ref} = K_s'^{ref} / (1 - m_1)$ according to the Expression (60), where $K_s'^{ref}$ is an input parameter of the HQH model, and $K_{t,ur}'/K_c'$ is an internal parameter that has to be calculated through an internal algorithm in which it is necessary to introduce the input parameter $E_{oed}'^{ref}$ (see Section 4.5).

4.4 | EPHYSS model parameter identification

The parameters of the EPHYSS model are listed and described in Table 2.

The identification of the parameters $K_s'^{ref}$, $p'_{ref,1}$ and m_1 can be obtained from unloadings and reloadings in the isotropic consolidation phase of triaxial tests, while the identification of the parameters $G_{s,0}^{ap,180,H,ref}$, $\gamma_{0.7}$, $p'_{ref,2}$, m_2 and ν'_{min} can be obtained from resonant column and triaxial tests with internal strain measurement ($G_{s,0}^{ap,180,H,ref}$ can be obtained, as well, from seismic in situ tests). Furthermore, the identification of $G_{s,0}^{ap,90,H,ref}$ can be obtained from the results of tests with internal strain measurement in which it is possible to control the rotation of the deviatoric strains, such as, for example, biaxial, true triaxial or hollow cylinder with torsion tests (since these tests are very rare in the professional practice, it has been proposed the following expression $G_{s,0}^{ap,90,H,ref} = \Lambda G_{s,0}^{ap,180,H,ref}$ to estimate $G_{s,0}^{ap,90,H,ref}$, where Λ takes values of 0.40 – 0.58 for sands and 0.50 for clays, as indicated in Section 3.5.2). The identification of the parameters associated with the HS_{MOD} model is widely known.^{39,40}

TABLE 2 EPHYSS parameters

| EPHYSS elastic part (HQB model) | | |
|---|----------------------|---|
| K_s^{Iref} | (kN/m ²) | Drained secant elastic bulk modulus for $-p' = p'_{ref,1}$. |
| $G_{s,0}^{ap,180,H,ref}$ | (kN/m ²) | Maximum secant shear modulus of the degradation curve corresponding to a 180° deviatoric strain rotation and $-p' = p'_{ref,2}$. |
| $G_{s,0}^{ap,90,H,ref}$ | (kN/m ²) | Maximum secant shear modulus of the degradation curve corresponding to a 90° deviatoric strain rotation and $-p' = p'_{ref,2}$. |
| $\gamma_{0.7}$ | (-) | Value of γ_{oct}^H for which $G_s^{ap} = 0.722G_{s,0}^{ap,\alpha,H}$. |
| m_1 | (-) | Factor that controls the dependency level of K'_s with $-p'$ and adopts values between 0.00 and 1.00. |
| m_2 | (-) | Factor that controls the dependency level of G_s^{ap} and $G_{t,ur}$ with $-p'$ and usually takes values between 0.40 and 0.60 for sands and between 0.50 and 1.00 for clays. |
| $p'_{ref,1}$ | (kN/m ²) | Reference effective mean stress in the expression of K'_s . |
| $p'_{ref,2}$ | (kN/m ²) | Reference effective mean stress in the expression of G_s^{ap} and $G_{t,ur}$. |
| ν'_{min} | (-) | Minimum value of Poisson's ratio. |
| EPHYSS plastic part (HS _{MOD} model) | | |
| E_{50}^{Iref} | (kN/m ²) | Secant longitudinal stiffness modulus for a mobilization of the 50% of q_f in a drained triaxial test for $-\sigma'_3 = p'_{ref}$. |
| E_{oed}^{Iref} | (kN/m ²) | Reference oedometric tangent modulus in noval loading for $-\sigma'_3 = p'_{ref}$. |
| $E_{t,ur}^{Iref}$ | (kN/m ²) | Reference longitudinal stiffness tangent modulus in elastic unloadings and reloadings for $-\sigma'_3 = p'_{ref}$. |
| m | (-) | Coefficient that controls the dependence level of E_{50} , E_{oed} , $E_{t,ur}$ and E'_i with the stress. |
| p'_{ref} | (kN/m ²) | Reference effective confinement stress ($p'_{ref} = -\sigma'_{3,ref} = 100kPa$ by default). |
| c' | (kN/m ²) | Effective cohesion. |
| φ' | (deg) | Maximum effective friction angle. |
| ψ | (deg) | Maximum dilatancy angle. |
| K_0^{NC} | (-) | Coefficient of lateral earth stress for a normally consolidated stress state ($K_0^{NC} = 1 - \sin(\varphi')$ by default). |
| R_f | (-) | Ratio q_f/q_a ($R_f = 0.9$ by default). |
| σ'_{trac} | (kN/m ²) | Tension limit value ($\sigma'_{trac} = 0$ kN/m ² by default). |

4.5 | EPHYSS model internal parameters

The EPHYSS model considers three internal parameters E_i^{Iref} , α' and $K'_{t,ur}/K'_c$ that explicitly appear in the model formulation. These internal parameters are calculated from the three model input parameters E_{50}^{Iref} , K_0^{NC} and E_{oed}^{Iref} using an internal algorithm. The initial stiffness modulus E_i^{Iref} is related with the value of E_{50}^{Iref} . The coefficient that controls the shape of the Cap yield surface α' is related with the value of K_0^{NC} . And the ratio between the elastic volumetric modulus and the secant volumetric modulus for the primary isotropic compression $K'_{t,ur}/K'_c$ is related with the value of E_{oed}^{Iref} . The parameter p'_{ref} in the Expression (62) refers to a confinement stress ($p'_{ref} = -\sigma'_{3,ref}$).

$$E'_{oed} = E_{oed}^{Iref} \left(\frac{-\sigma'_1 + c' \cot(\varphi')}{p'_{ref} + c' \cot(\varphi')} \right)^m = E_{oed}^{Iref} \left(\frac{-\sigma'_3/K_0^{NC} + c' \cot(\varphi')}{p'_{ref} + c' \cot(\varphi')} \right)^m \quad (62)$$

The algorithm that has been implemented to calculate such internal parameters^{4,41} considers two numerical tests: first, a drained triaxial test is reproduced to obtain the value of E_i^{Iref} ; and, subsequently, an oedometric test is reproduced to obtain the value of α' and $K'_{t,ur}/K'_c$.

5 | LOCAL INTEGRATION OF THE CONSTITUTIVE EQUATIONS

The standard calculation strategy in elastoplastic models is used for the local integration of the constitutive equations of the EPHYSS model. This strategy uses the trial stress $\sigma^{(tr)}$ (63), which assumes that the soil behavior is totally elastic. The

Expression (63) will be the one used when $\gamma_{oct}^{\Delta R,(n)} > \gamma_{ur}^{\alpha,(n)}$, that is, in domain 2. However, such expression will be modified when $\gamma_{oct}^{\Delta R,(n)} \leq \gamma_{ur}^{\alpha,(n)}$, that is, in domain 1, where $\sigma'^{(tr,NL)}$ is used (64).

$$\sigma'^{(tr)} = \sigma'^{(n)} + \mathbf{E}'_t{}^{(n+1)} : \Delta \varepsilon^{(n+1)} \quad (63)$$

$$\sigma'^{(tr,NL)} = \sigma'^{(n)} + \mathbf{E}'_s{}^{(n+1)} : \Delta \varepsilon^{(n+1)} + \Delta \mathbf{E}'_s{}^{(n+1)} : \left(-\varepsilon_{oct}^{e,(n+1)} \mathbf{1} + \mathbf{e}^{e,\Delta R,(n+1)} \right) \quad (64)$$

After calculating the trial stress $\sigma'^{(tr)}$ or $\sigma'^{(tr,NL)}$ according to the case, and defining the elastic domain as $\mathcal{D}_e = \{\sigma' | f_k(\sigma', \chi_k^{pl}) < 0, k = 1 \dots q\}$, the procedure is as follows:

- If $\sigma'^{(tr)} \in \mathcal{D}_e$ or $\sigma'^{(tr,NL)} \in \mathcal{D}_e$ according to the case, the following variables will be updated: (1) the stress tensor $\sigma'^{(n+1)} = \sigma'^{(tr,NL)}$ or $\sigma'^{(n+1)} = \sigma'^{(tr)}$ according to the case; (2) the plastic state variables according to $\chi_k^{pl,(n+1)} = \chi_k^{pl,(n)}$; and (3) the elastic state variables $\chi^{el,hist,(n+1)}$.
- If $\sigma'^{(tr)} \notin \mathcal{D}_e$ or $\sigma'^{(tr,NL)} \notin \mathcal{D}_e$ according to the case, it will be necessary to apply the numerical scheme of the Return Mapping. In this case the tensors $\Delta \mathbf{E}'_{s,[i]}{}^{(n+1)} = \mathbf{E}'_s(\Delta K'_{s,[i]}{}^{(n+1)}, \Delta G_{s,[i]}{}^{ap,(n+1)})$ and $\varepsilon_{oct,[i]}^{e,(n+1)} \mathbf{1} + \mathbf{e}_{[i]}^{e,\Delta R,(n+1)}$ should be calculated implicitly, iterating over the value of the elastic strain tensor increment $\Delta \varepsilon_{[i]}^{e,(n+1)}$. When convergence is reached ($\varepsilon_{abs}^{e,(n+1)} \leq \text{TOL}_{\varepsilon_{abs}^e}$ and $\varepsilon_{rel}^{e,(n+1)} \leq \text{TOL}_{\varepsilon_{rel}^e}$), the value $\Delta \varepsilon_{[i]}^{e,(n+1)} = \Delta \varepsilon_{[i+1]}^{e,(n+1)}$ will be adopted and the following variables will be updated: (1) the stress tensor $\sigma'^{(n+1)}$, according to Expression (67) or Expression (68) as appropriate; (2) the plastic state variables $\chi_k^{pl,(n+1)}$; and (3) the elastic state variables $\chi^{el,hist,(n+1)}$.

$$\varepsilon_{abs}^{e,(n+1)} = \|\Delta \varepsilon_{[i+1]}^{e,(n+1)} - \Delta \varepsilon_{[i]}^{e,(n+1)}\| \quad (65)$$

$$\varepsilon_{rel}^{e,(n+1)} = \frac{\varepsilon_{abs}^{e,(n+1)}}{\|\Delta \varepsilon_{[i]}^{e,(n+1)}\|} \quad (66)$$

$$\sigma'_{[i]}{}^{(n+1)} = \sigma'_{[i]}{}^{(tr,NL)} - \sum_{k=1}^q \lambda_{k,[i]}^{(n+1)} \mathbf{E}'_s{}^{(n+1)} : \partial g_k(\sigma'_{[i]}{}^{(n+1)}, \chi_{k,[i]}^{pl,(n+1)}) / \partial \sigma' \quad (67)$$

$$\sigma'^{(n+1)} = \sigma'^{(tr)} - \sum_{k=1}^q \lambda_k^{(n+1)} \mathbf{E}'_t{}^{(n+1)} : \partial g_k(\sigma'^{(n+1)}, \chi_k^{pl,(n+1)}) / \partial \sigma' \quad (68)$$

The so-called Implicit Closest Point Projection Algorithm has been used for the local integration of the equations. This algorithm uses a Backward Euler Elastic Predictor/Return Mapping type integration scheme within the methods of radial return, and belongs to the algorithms class denominated Generalized Midpoint Algorithms within the linear multistep methods.^{3,42–44} Furthermore, for the return on the intersection of 2 or 3 yield surfaces, Koiter's Rules have been adopted.⁴⁵ As well, iterative algorithms within the elastic part have been incorporated to the general algorithm.

A major problem in multisurface elastoplastic calculations is to establish a strategy to determinate on which surface or surfaces must be the Return Mapping done, especially when the stress state is next to an intersection zone between several yield surfaces. The strategy for the surface selection considered in the EPHYSS model is based on the proposal of Bonnier.⁴⁶

6 | DIFFERENCES AND COMMON ASSUMPTIONS BETWEEN EPHYSS AND HS-SS MODELS

Differences and common assumptions between EPHYSS and HS-SS models are discussed in Castellón⁴ and Castellón and Ledesma,² and will be summarized in this section.

The HS-SS model implemented in Plaxis is one of the few models widely used in professional practice that considers soil behavior in the range of small strains and uses known and relatively easy to obtain/estimate parameters. The HS-SS model is based on the Hardening Soil Small (HS-S) model³ which adds, to the elastic formulation of the Small Strain Overlay Model (SSOM),³ the plastic formulation of the Hardening Soil (HS) model^{47,48} adding two modifications: (1) it replaces the dilatancy criterion of Rowe³⁸ with that of Li and Dafalias³⁶ to describe the contractive behavior of the soil; and (2) modifies the hardening laws by introducing the factor h_i . The HS-S model significantly improves the approach to soil behavior provided by the HS model, although it has certain limitations.³ Some applications can be found in Foster et al.,⁴⁹ Ramos et al.⁵⁰ and Ledesma and Alonso.⁵¹

The HS-SS model presents some small differences with respect to the HS-S model.² These differences appear in the expressions that both models use to calculate the dilatancy angle and in the expression of the Cap-surface hardening law that each model uses, in which \dot{p}_p depends on the confinement in the HS-S model and on the state variable p_p itself in the HS-SS model.

The elastic part of HS-SS and EPHYSS models (SSOM and HQH models respectively): (1) are based on the apparent secant shear modulus G_s^{ap} degradation curve provided by the Dos Santos and Correia model,¹⁸ which is limited by a minimum value derived from the minimum tangent shear modulus $G_{t,ur}$; (2) consider the recent history of deviatoric strains; (3) use history tensors that act as Simpson brick models⁵²; (4) consider similar thermodynamic-type corrections; and (5) can be combined with multiple plastic models leading to incrementally multilinear advanced elastoplastic models. When both models are used by themselves, they use the Hashiguchi¹⁹ criterion to differentiate primary load from unloadings/reloadings. However, since the intention is to compare the EPHYSS and HS-SS models, while minimizing the differences caused by their respective plastic formulations, it has been adopted, in the EPHYSS model, the same strategy used in the HS-SS model, which consists of considering, on the one hand, a factor $\xi = 2$ in the expression of the apparent secant shear modulus G_s^{ap} and, on the other hand, the factor h_i that modifies the hardening laws to avoid overlapping the mechanisms of SSOM and HQH models and the mechanisms of plastic models with which they are combined, that try to explain the reduction of soil stiffness during the primary loading.

Despite its great advantages, the elastic part of HS-SS model (SSOM model) presents some limitations that the elastic part of the EPHYSS model (HQH model) solves, such as: (1) the use of an intrinsic reversal criterion which means that it arises from the own model equations (and not an arbitrary extrinsic one like in the SSOM model, where the reversals depend on the product sign of the eigenvalues of $\dot{\mathbf{e}}$ with the components of $\mathbf{H} - \mathbf{1}$ in the same direction); (2) the ability to recover the stiffness in a continuous way with the rotation angle of deviatoric strain recent paths $\hat{\mathbf{h}} : \hat{\mathbf{e}}$, through the use of a history tensor \mathbf{h} inspired by the intergranular strain tensor δ of the Niemunis and Herle model²² (and not in a discontinuous way like in the SSOM model which uses a triple Simpson brick model⁵²); (3) the consideration of infinite degradation curves of the shear modulus thanks to the state variable $G_{s,0}^{ap,\alpha,H,ref}$ (Figures 1B and 3B,C), which provides the model with versatility and great adaptability to experimental results (and not just a single degradation curve like the SSOM model as shown in Figures 1A and 3A); (4) the consideration of a variable Poisson's ratio $\nu' \geq \nu'_{min}$ that does not limit the values of the bulk modulus (and not of a constant Poisson's ratio like in the SSOM model, that forces the proportionality $K' \propto G$); (5) the consideration of multiple state variables that define different short and long-term memory levels in a similar way to how the Hueckel and Nova model³³ does, which endows the HQH model with robustness to reproduce the hysteretic behavior of the soil; (6) the consideration of the strain-induced anisotropy; or (7) a higher level of compliance with the Generalized Masing Rules, especially with Rule No. 4, thanks to the greater amount of information that the HQH model stores at the reversal points if compared with the SSOM.

Regarding the plastic part of the EPHYSS model, the same formulation as the plastic part of the HS-SS model is used to keep the original formulation of the HS model. However, a generalization of the HS model to include a mean effective stress dependency of the elastic moduli is straightforward. The goal of the EPHYSS model is to improve the elastic part of the HS-SS model and not its plastic part. Most of the EPHYSS model limitations are purely inherited from its plastic part (HS_{MOD}) which is based on the well-known HS model.^{47,48} Some of these limitations are the following: (1) the use of the Mohr-Coulomb strength criterion does not lead to accurate results for intermediate extension-compression stress states; (2) EPHYSS model considers a void ratio independent formulation that does not include the concept of critical void ratio, so the evolution of plastic volumetric strain at intermediate or large strains is not properly described; (3) the

model is not suited for modeling materials at different void ratios with a single set of parameters; (4) kinematic hardening is not considered; and (5) the cone yield surface is formulated under the hypothesis of hard soils ($\epsilon_v^p \approx 0$) and, therefore, EPHYSS is not appropriate for reproducing deviatoric stress paths in soft soils if plasticity is predominant.

The elastic part of HS-SS and EPHYSS models (SSOM and HQH models respectively) requires the same or equivalent few and simple parameters, except for an additional parameter required by the HQH model, which is the maximum shear modulus after a reversal of the deviatoric strains of 90° ($G_{s,0}^{ap,90,H,ref}$), which can be obtained from biaxial, true triaxial or hollow cylinder with torsion tests with internal strain measures. It is possible to estimate the value of the HQH parameters K_s^{ref} , $p'_{ref,1}$, m_1 , $G_{s,0}^{ap,180,H,ref}$, $G_{s,0}^{ap,90,H,ref}$, $\gamma_{0.7}$, $p'_{ref,2}$, m_2 and ν'_{min} from the value of the HS-SS parameters G_0^{ref} , $\gamma_{0.7}$, $E'_{t,ur}$, ν'_{ur} , m and p'_{ref} as follows: $K_s^{ref} \approx (1/3)E'_{t,ur}(1 - m_1)/(1 - 2\nu'_{ur})$, $p'_{ref,1} \approx p'_{ref,2} \approx p'_{ref}$ (however, the parameter p'_{ref} of the SSOM model refers to a confinement stress while parameters $p'_{ref,1}$ and $p'_{ref,2}$ of the HQH models refers to mean stresses), $m_1 \approx m_2 \approx m$, $\nu'_{min} \approx \nu'_{ur}$, $G_{s,0}^{ap,180,H,ref} \approx G_0^{ref}$ and $G_{s,0}^{ap,90,H,ref} = \Lambda G_0^{ref}$, taking Λ values of 0.40 – 0.58 for sands and of 0.50 for clays.² These approximations are considered enough, in general, to reproduce soil stiffness in numerical simulations in the absence of more data. However, the fact that K_s^{ref} and G_s^{ap} vary, respectively, with $(-p')^{m_1}$ and $(-p')^{m_2}$ in the EPHYSS model, while $E'_{t,ur}$ and G_0 do it so with $(-\sigma'_3 + c' \cot(\varphi'))^m$ in the HS-SS model, leads to formulate a set of transformations based on the proposals by Obrzud and Truty⁴⁰ for boundary value problems.

In relation to the minimum reference shear modulus ($G_{t,ur}^{ref}$), in the HS-SS model it is calculated from the reference elastic tangent modulus ($E'_{t,ur}$) and from Poisson's ratio (ν'_{ur}), which are assumed to be constant, while in the EPHYSS model it is calculated according to the Expression (14).

Finally, regarding the parameters corresponding to the plastic part of the EPHYSS model, both internal and external are the same than those used in the HS-SS model. In addition to that, in EPHYSS, HS, HS-S or HS-SS models, the plastic modulus H depends on $K_t^{ref} = K_s^{ref} / (1 - m_1)$, where K_s^{ref} is an input parameter of the EPHYSS model but it has to be calculated from the elastic relation $K_s^{ref} = K_s^{ref} (E'_{t,ur}, \nu'_{ur})$ in the HS, HS-S or HS-SS models.

7 | TESTS FOR THE VALIDATION AND VERIFICATION OF THE EPHYSS MODEL AND ITS COMPARISON WITH THE HS-SS MODEL

Different triaxial, oedometric and biaxial tests, compiled from diverse thesis and papers, have been simulated to carry out a partial verification of the EPHYSS model, as well as a validation and a comparison with the HS-SS model. The simulations have been run with PLAXIS 2D 2015. Table 3 shows EPHYSS and HS-SS parameters for the different soils used in the simulations. The parameters of the EPHYSS model for each material have been obtained from the HS-SS model parameters, that were extracted from the indicated references, using the expressions in Section 6.

7.1 | Triaxial tests

Numerical simulations of drained and undrained triaxial tests on loose and dense Hostun sand with different confinement stresses have been conducted, as well as drained triaxial tests on reconstituted kaolinite clay with different confinement stresses (Figure 4–7) and triaxial tests with stress rotations in the deviatoric plane on London clay (Figure 8).

In general, the approximation of both models to the experimental measurements of the triaxial tests is quite good. However, the dilatant behavior of the dense sand with $-\sigma'_3 = 100$ kPa (Figure 4C) is not correctly reproduced, and the volumetric stiffness in both loose and dense sands are bigger than those obtained in the tests (Figures 4B and 5B), which is due to the dependence of K' with G and ν' (either in the entire range of strains in the HS-SS model, or when $\nu' \leq \nu'_{min}$ in the EPHYSS model). EPHYSS model can improve the volumetric stiffness approximation to the experimental curves by reducing ν'_{min} , although this would lead to important errors in the prediction of horizontal displacements in boundary value problems with significant deviatoric loadings and, therefore, it is not recommended.

In standard triaxial tests shown in Figures 4–7 no strain rotations are applied and, therefore, EPHYSS and HS-SS models predict similar soil behavior as both: (1) use the same value of the maximum shear stiffness ($G_0^{ref} = G_{s,0}^{ap,180,H,ref}$); (2) use the same shear stiffness degradation curve formulation; and (3) have a similar evolution of the variable that controls shear stiffness degradation. However, there are still some differences between the results obtained with both models, which are explained as follows: (1) the elastic stiffness moduli of the EPHYSS model depend on $-p'$ ($-\Delta p' = 1/3 \Delta q$ during triaxial

TABLE 3 Parameters of the EPHYSS and HS-SS models for different soils^{3,22,23,29,53,54}

| ELASTIC BEHAVIOR | Parameters | Loose | | Dense | | Hochstetten sand | Ticino sand | Reconstituted | | Units | |
|------------------|------------------|--------------------------|-------------|-------------|-------------|------------------|-------------|----------------|---------|----------------------|----------------------|
| | | Hostun sand | Hostun sand | Hostun sand | London clay | | | Kaolinite clay | | | |
| ELASTIC BEHAVIOR | HS-SS & EPHYSS | $\gamma_{0.7}$ | 0.0001 | 0.0002 | 0.000055 | 0.00013 | 0.00055 | 0.0002 | 0.00055 | (-) | |
| | HS-SS | G_0^{ref} | 70000 | 112500 | 68000 | 100000 | 33333 | 26000 | 33333 | 26000 | (kN/m ²) |
| | | ν'_{ur} | 0.25 | 0.25 | 0.20 | 0.20 | 0.20 | 0.20 | 0.20 | 0.20 | (-) |
| | EPHYSS | K_s^{ref} | 8300 | 22500 | 5000 | 13335 | 1277 | 2333 | 1277 | 2333 | (kN/m ²) |
| | | m_1 | 0.75 | 0.55 | 0.50 | 0.50 | 0.80 | 0.80 | 0.80 | 0.80 | (-) |
| | | $P'_{ref,1}$ | 100 | 100 | 100 | 100 | 100 | 100 | 100 | 100 | (kN/m ²) |
| | | $G_{s,0}^{ap,180,H,ref}$ | 70000 | 112500 | 68000 | 100000 | 33333 | 26000 | 33333 | 26000 | (kN/m ²) |
| | | $G_{s,0}^{ap,90,H,ref}$ | 28000 | 45000 | 27000 | 40000 | 16666 | 13000 | 16666 | 13000 | (kN/m ²) |
| | | m_2 | 0.75 | 0.55 | 0.50 | 0.50 | 0.80 | 0.80 | 0.80 | 0.80 | (-) |
| | | $P'_{ref,2}$ | 100 | 100 | 100 | 100 | 100 | 100 | 100 | 100 | (kN/m ²) |
| | ν'_{min} | 0.20 | 0.20 | 0.20 | 0.20 | 0.20 | 0.20 | 0.20 | 0.20 | (-) | |
| PLASTIC BEHAVIOR | HS-SS & EPHYSS | E_0^{ref} | 12000 | 30000 | 6000 | 16000 | 2150 | 7000 | 2150 | 7000 | (kN/m ²) |
| | | $E_{t,ur}^{ref}$ | 60000 | 90000 | 18000 | 48000 | 11500 | 21000 | 11500 | 21000 | (kN/m ²) |
| | | E_{oed}^{ref} | 16000 | 30000 | 6000 | 16000 | 1050 | 7000 | 1050 | 7000 | (kN/m ²) |
| | | c' | 0.0 | 0.0 | 0.0 | 0.0 | 0.0 | 0.0 | 0.0 | 0.0 | (kN/m ²) |
| | | ϕ' | 34 | 42 | 33 | 33 | 20 | 20 | 20 | 20 | (deg) |
| | | ψ | 0 | 16 | 0 | 0 | 0 | 0 | 0 | 0 | (deg) |
| | | P'_{ref} | 100 | 100 | 100 | 100 | 100 | 100 | 100 | 100 | (kN/m ²) |
| | | m | 0.75 | 0.55 | 0.50 | 0.50 | 0.80 | 0.80 | 0.80 | 0.80 | (-) |
| | | K_0^{NC} | 0.44 | 0.40 | 0.45 | 0.50 | 0.50 | 0.66 | 0.50 | 0.66 | (-) |
| | | R_f | 0.90 | 0.90 | 0.90 | 0.90 | 0.90 | 0.90 | 0.90 | 0.90 | (-) |
| | σ'_{trac} | 0.0 | 0.0 | 0.0 | 0.0 | 0.0 | 0.0 | 0.0 | 0.0 | (kN/m ²) | |

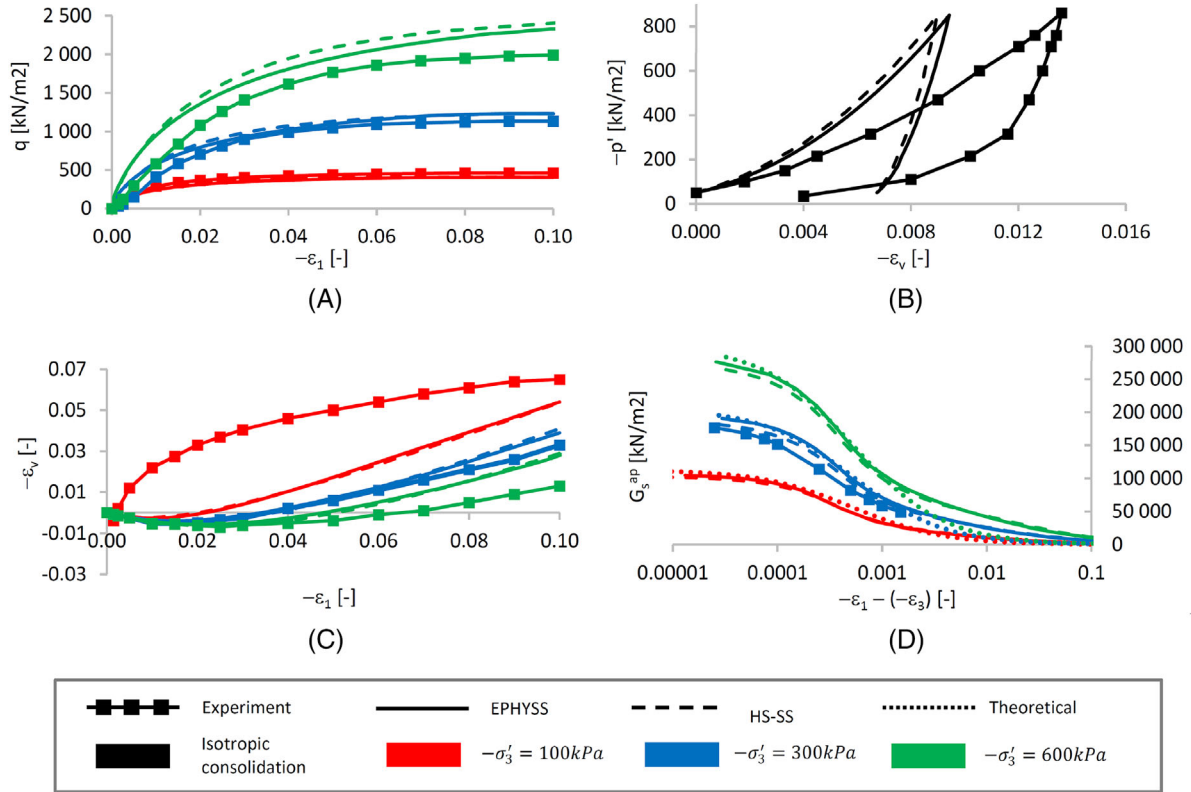


FIGURE 4 Drained triaxial tests on dense Hostun sand^{3,53,54} and simulations with the EPHYSS and HS-SS models

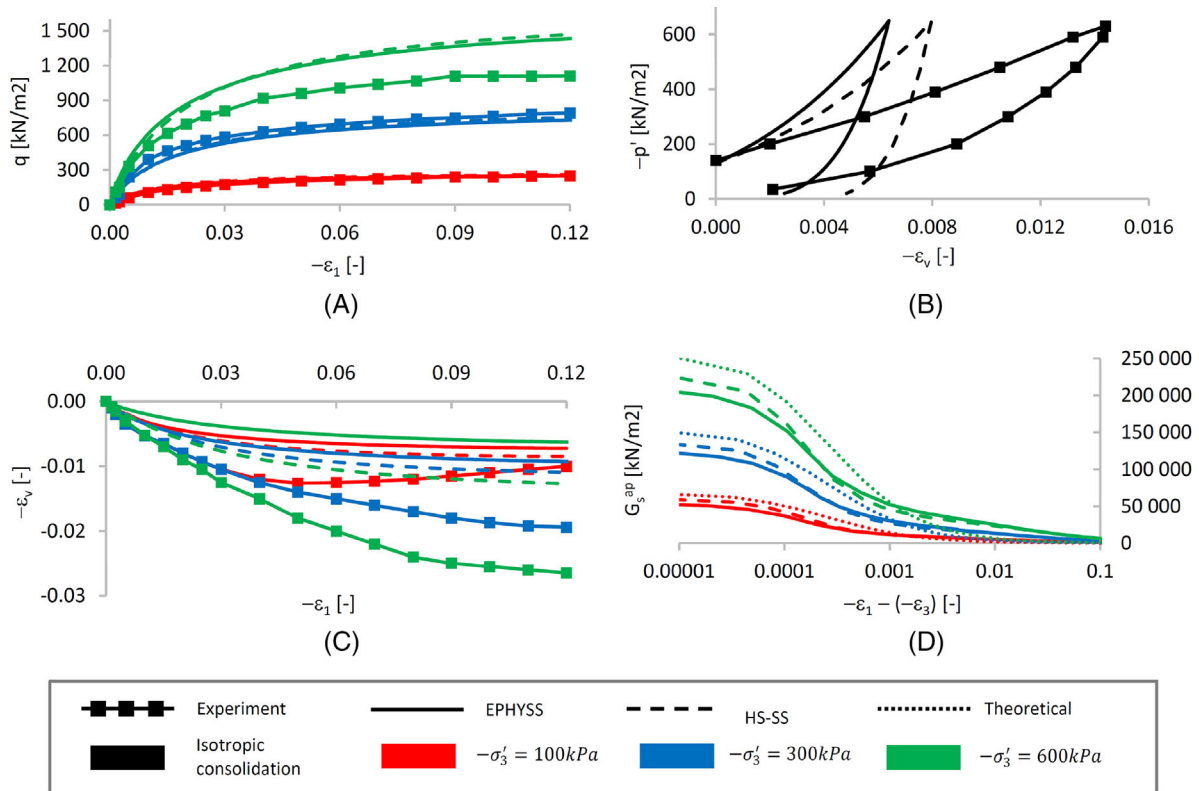


FIGURE 5 Drained triaxial tests on loose Hostun sand^{3,53,54} and simulations with the EPHYSS and HS-SS models

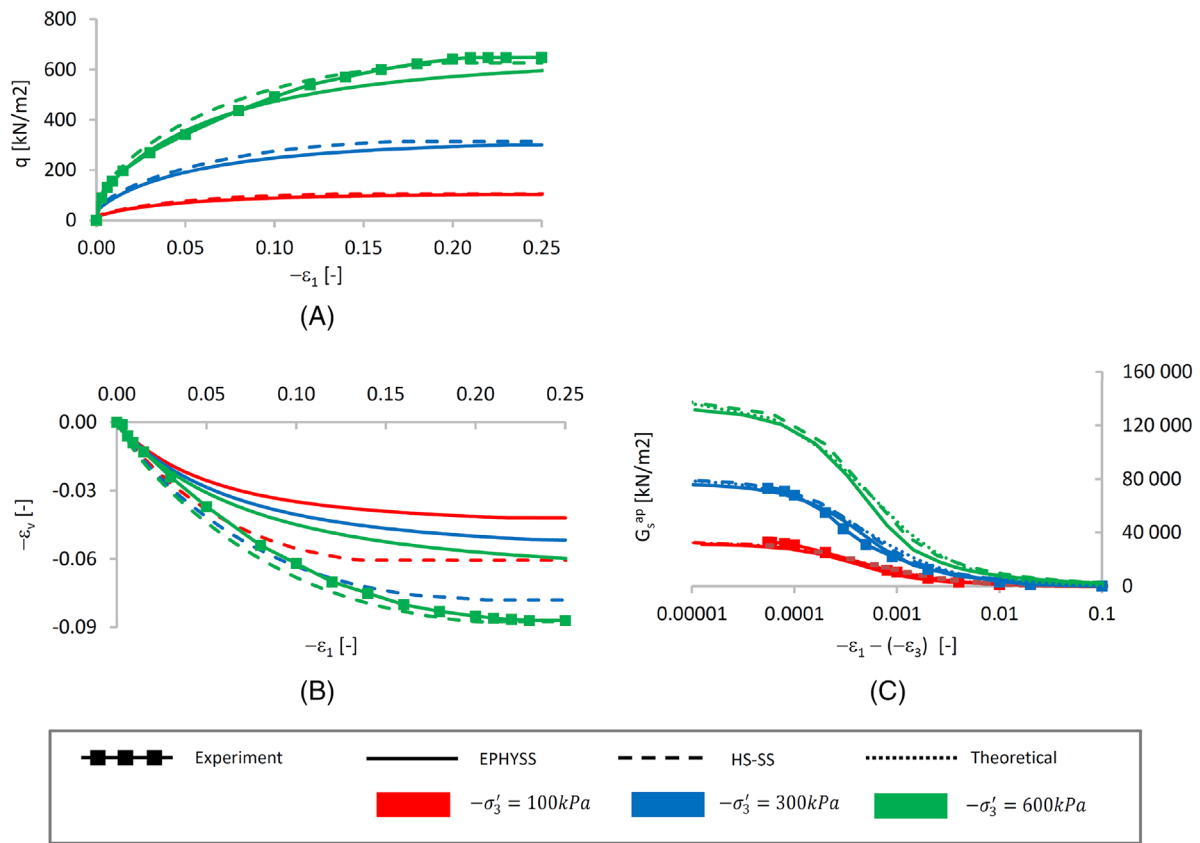


FIGURE 6 Drained triaxial tests on reconstituted kaolinite clay^{3,23} and simulations with the EPHYSS and HS-SS models

test), while the elastic stiffness moduli of the HS-SS model depend on $-\sigma'_3 + c' \cot(\varphi')$ ($-\Delta\sigma'_3 = 0 \text{ kN/m}^2$ during triaxial test); (2) the previous point implies that both models consider different values of the internal parameters E_i^{ref} , α' and $K'_{t,ur}/K'_c$, which affects the plastic behavior; (3) the different values of the internal parameter E_i^{ref} give place to different values of the factor h_i ; (4) EPHYSS model considers independent K' and G values whenever $\nu' > \nu'_{min}$ is complied, while in HS-SS model the linear dependence $K' = (2/3)G(1 + \nu')/(1 - 2\nu')$ is considered; (5) the small differences in the dilatancy rules between both models; and (6) EPHYSS model considers strain-induced anisotropy within domain 1.

In addition to that, in Figures 4–6 certain differences are observed between the degradation curves of G_s^{ap} provided by the EPHYSS model and the theoretical curve G_s^{ap} according to the Expression (4). These differences are due to: (1) the effect that the factor h_i introduces on the degradation curves in presence of plastic strains; and (2) the fact that the value of G_s^{ap} is affected by the condition $G_t^{ap} = G_{t,ur}$ in both models when $\gamma_{oct}^H \geq \gamma_{ur}^\alpha$ or $\gamma_{HIST} \geq \gamma_c$, respectively, which is not considered in the Expression (4).

In Figure 7, both the EPHYSS and the HS-SS models present some limitations in the approximation of the experimental curves $q - (-\varepsilon_1)$ of undrained triaxial tests on dense Hostun sand. This is because the adopted dilatation formulation in both models does not consider the void ratio of the material as a state variable.

In Figure 8 four samples of reconstituted London clay are consolidated to point A and subsequently taken to point O ($OCR = 2$). Once at point O, a stress path is applied to each of the samples following different angles $\theta_{q/p'}$ in $q - (-p')$ space. It is necessary to remember that in this type of tests the deviatoric strain path rotation angle is $\alpha = 180^\circ$ in all paths, except in the BOX one, where $\alpha = 0^\circ$. Therefore, the results predicted by EPHYSS and HS-SS models are very similar, which is logical since the only active degradation curve in the EPHYSS model is the one corresponding to the maximum shear stiffness ($G_{s,0}^{ap,180,H,ref}$), which is the same (and the only one) considered in the HS-SS model (G_0^{ref}).

7.2 | Oedometric tests

Simulations of oedometric tests have been conducted on dense and loose Hostun sand with four load cycles (Figure 9). The approximation of both models results to experimental measurements is good. All the reversals in these tests have a

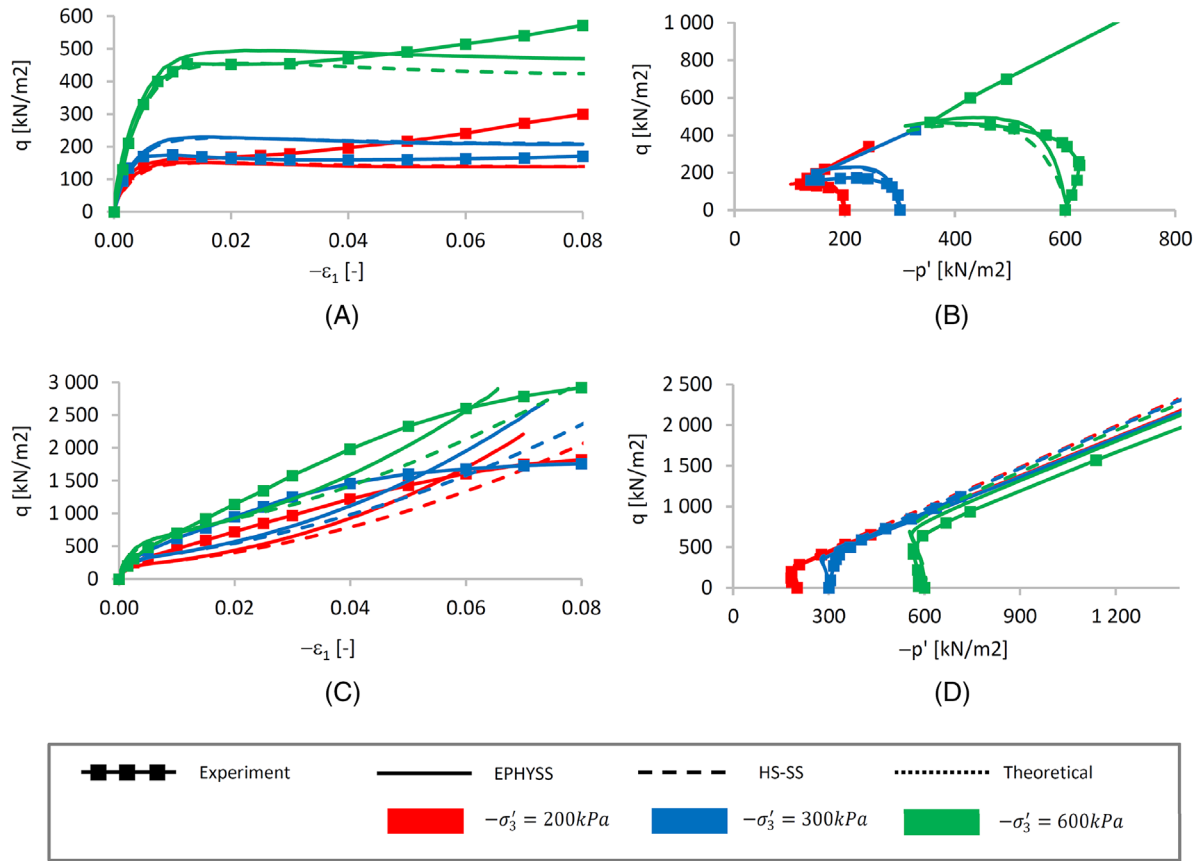


FIGURE 7 Undrained triaxial tests on dense (A and B) and loose (C and D) Hostun sand^{3,53,54} and simulations with the EPHYSS and HS-SS models

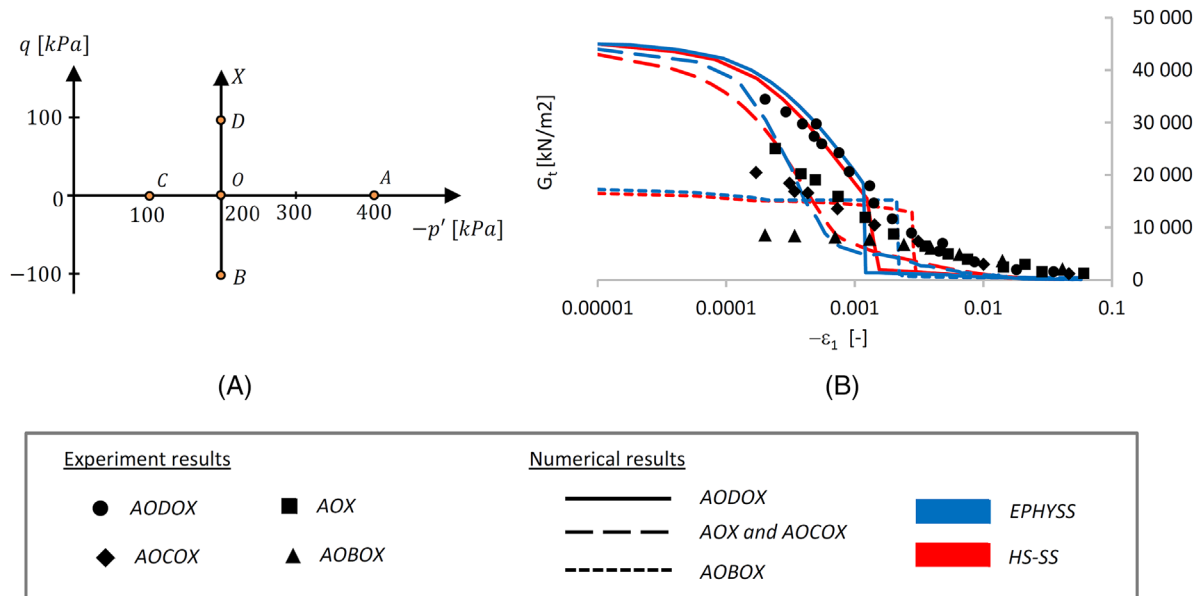


FIGURE 8 (A) Triaxial tests paths on reconstituted London clay.^{3,23} (B) Experimental data and simulations with the EPHYSS and HS-SS models

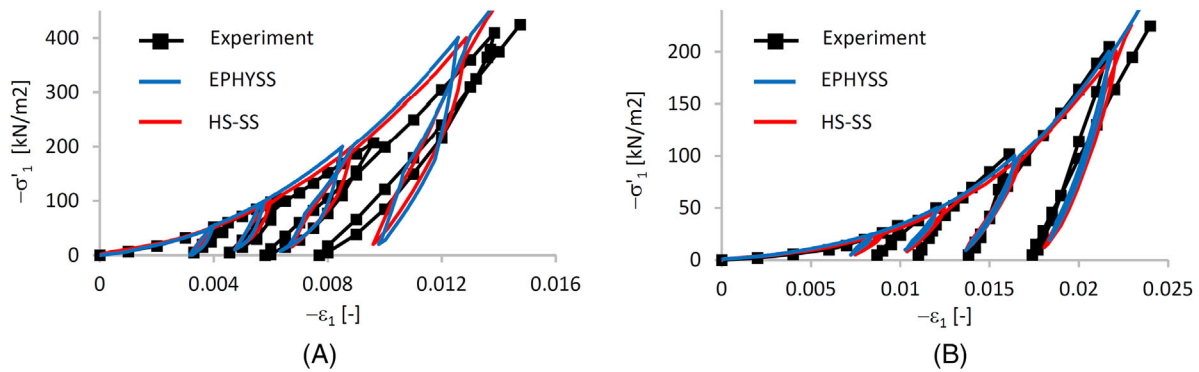


FIGURE 9 Oedometric test on (A) dense and (B) loose Hostun sand^{3,53,54} and simulations with the EPHYSS and HS-SS models

deviatoric strain path with $\alpha = 180^\circ$, therefore the only active degradation curve in the EPHYSS model is the one corresponding to the maximum shear stiffness, which is the same considered in the HS-SS model, so very similar results are obtained with EPHYSS and HS-SS models.

7.3 | Biaxial tests

Numerical simulations of drained biaxial tests on loose and dense Hostun sand with different confinement stresses have been conducted (Figure 10). The approximation of both model results to the experimental measurements is good, except in the range of strains in which a process of localization and shear band formation appears. Since no strain rotations take place in these tests, the EPHYSS and HS-SS model predict similar results. The slight differences between them are the same that have been explained in Section 7.1 for triaxial tests.

Furthermore, numerical simulations of biaxial tests with rotations in the recent strain path have been performed on Hochstetten and Ticino sand (Figure 11). Following the scheme of Figure 11A, first, a biaxial loading (OA) with identical strain increments is made in both directions, until reaching values of $-\sigma'_{xx} = -\sigma'_{yy} = 150 \text{ kN/m}^2$. Subsequently, a biaxial unloading (AO') is made with identical decrements of strain in both directions. And then a biaxial loading ($O'B$) with identical strain increments in both directions is made again, reaching a value of $-\sigma'_{xx} = -\sigma'_{yy} = 100 \text{ kN/m}^2$ in B with an increase of strain from O' of $-\Delta\varepsilon_{xx} = -\Delta\varepsilon_{yy} = 0.0005$. Finally, rotations of $\beta = 0^\circ$, $\beta = 90^\circ$ and $\beta = 180^\circ$ are applied in the total strain paths. It is shown that $\alpha = \beta$ for angles of $\beta = 0^\circ$, $\beta = 90^\circ$ and $\beta = 180^\circ$. Figure 11B shows the degradation curves of the apparent tangent shear modulus G_t^{ap} in the simulations conducted with the following models on Hochstetten sand: (1) hypoplastic with intergranular strain according to Benz^{3,22}; (2) HS-SS; and (3) EPHYSS. Moreover, the theoretical degradation curves of G_t^{ap} according to the EPHYSS model are added as verification thereof.

The three models are able to reproduce the shear stiffening of the soil induced by strain rotations, although some differences appear in the results obtained with each one of them. The maximum values of G_t^{ap} after a $\alpha = 90^\circ$ strain rotation in the EPHYSS model and in the hypoplastic model with intergranular strain are similar, while such value is different in the HS-SS model (Figure 11B). This is due to the fact that the value of the parameter corresponding to the maximum shear modulus for strain rotations of 90° is common in both models, but this parameter does not exist in the HS-SS model, which reproduces the increase of the stiffness corresponding to such rotation only by the reduction of the state variable γ_{HIST} . As well, the jump that can be seen in EPHYSS results for $\alpha = \beta = 90^\circ$ is due to the fact that belonging to one domain or another is evaluated by the strain $\gamma_{oct}^{\Delta R}$, while the stiffness depends on the state variable γ_{oct}^H .

Finally, a biaxial test with strain reversal on Ticino sand has been carried out (Figure 11), following the same methodology used in the tests with Hochstetten sand. In this case, the values $-\varepsilon_{xx} = -\varepsilon_{yy} = 0.0165$ are adopted in A , $-\varepsilon_{xx} = -\varepsilon_{yy} = 0.01425$ in O' and $\Pi = 0.01\%$, $\Pi = 0.02\%$, $\Pi = 0.04\%$, $\Pi = 0.06\%$, $\Pi = 0.10\%$ and $\Pi = 0.20\%$ in B , where Π is the accumulated strain in $O'B$. Furthermore, rotations of $\beta = 0^\circ$, $\beta = 22.5^\circ$, $\beta = 45^\circ$, $\beta = 67.5^\circ$, $\beta = 90^\circ$, $\beta = 112.5^\circ$, $\beta = 135^\circ$, $\beta = 157.5^\circ$ and $\beta = 180^\circ$ are applied in the total strain paths in B . Figure 11 shows the curves $G_t^{ap}/G_{t,ur} - \beta$ for different values of Π in the following models: (1) hypoplastic with intergranular strain (Figure 11C)²²; (2) multilaminated for small strains (Figure 11D)²⁹; (3) HS-SS (Figure 11E); and (4) EPHYSS (Figure 11F).

As can be seen, when $\Pi \geq 0.10\%$ the HS-SS model provides values of $G_t^{ap}/G_{t,ur}$ for any angle β (except $\beta = 180^\circ$) much lower than those obtained with the rest of the models, which implies that strain rotations in the HS-SS model do not

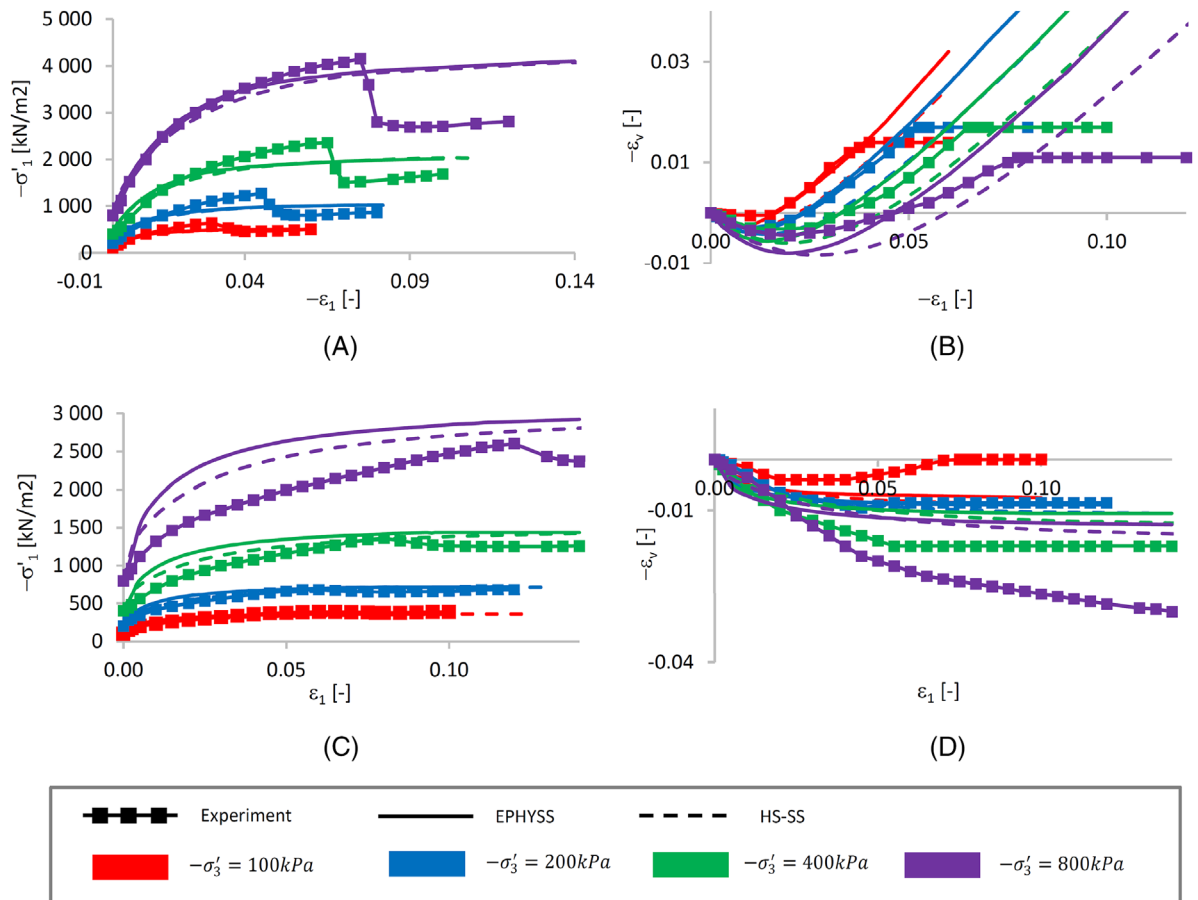


FIGURE 10 Drained biaxial tests on dense (A and B) and loose (C and D) Hostun sand^{3,53,54} and simulations with the EPHYSS and HS-SS models

produce the same soil stiffness recovery that appears in the other three models. This is due to the high value of the strain $-\varepsilon_{xx} = -\varepsilon_{yy} = \Pi$ before the strain rotation is produced, which, in turn, gives place to high levels of the HS-SS history tensor components H_{ij} before the reversal and, therefore, $\gamma_{HIST} \gg \gamma_c$. In these cases, after the strain rotation, the H_{yy} component of the \mathbf{H} tensor is reinitialized, but not the H_{xx} component, which keeps the previous value of such rotation and is high enough to provide values of γ_{HIST} which still are superior than γ_c , therefore, small or no stiffness recovery is produced. The latter does not occur in any of the other three models (hypoplastic with intergranular strain, multilaminated for small strains or EPHYSS), in which the elastic stiffness recovery is less dependent on the value of the accumulated strain Π due to the consideration of more complex history tensors or other state variables (\mathbf{H}_{MEM} , \mathbf{E}_{MEM} and \mathbf{E}_{MEM}^c in the case of the EPHYSS model) that allows memorizing more information of the recent history apart from that stored in the history tensor. And additional advantage of the EPHYSS model is the use of very similar parameters to those of the HS-SS model, which facilitates its use in the geotechnical professional practice.

8 | CORRECTION OF THE HS-SS MODEL INCONSISTENCIES WITH EPHYSS MODEL

8.1 | Numerical tests

A group of numerical simulations of oedometric (Figure 12) and triaxial (Figure 13) tests have been conducted with the aim of demonstrating that the formulation of the EPHYSS model allows to correct the inconsistencies detected in the HS-SS model.⁴⁻⁷ These simulations have been run with both PLAXIS 2D 2015 and PLAXIS 2D 2018. Parameters corresponding to Hostun loose sand (Table 3) have been used in all tests, incorporating values of the permeability coefficients $k_{horizontal} = k_{vertical} = 1m/day$.

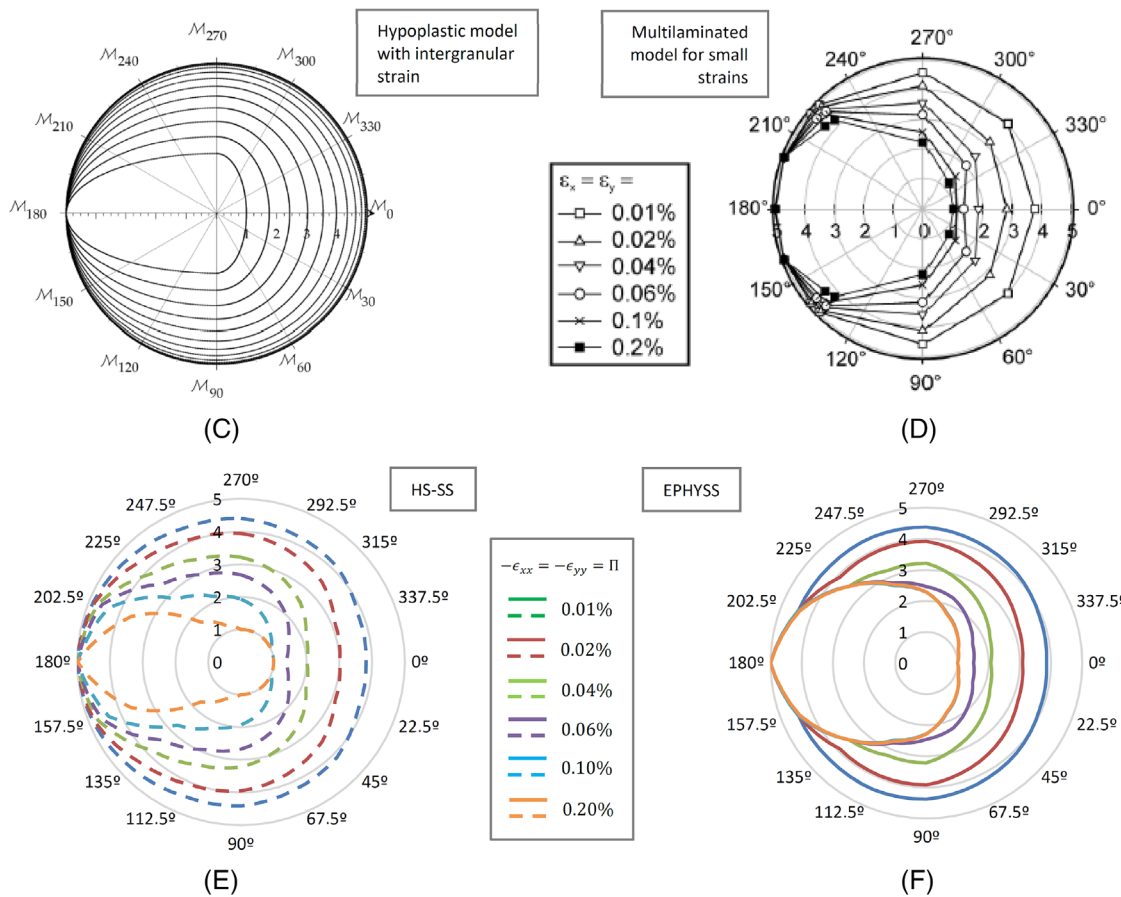
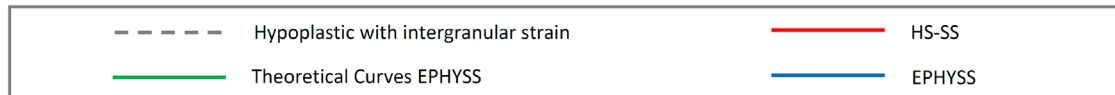
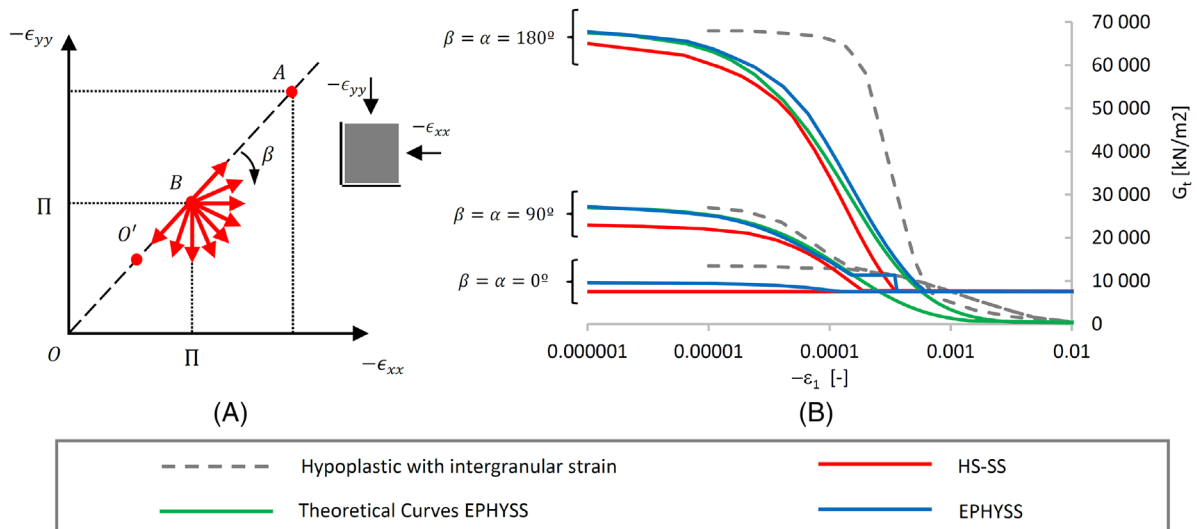


FIGURE 11 (A) Strain paths in the simulations of the biaxial tests, (B) degradation curves of G_t^{ap} on Hochstetten sand with rotations of $\beta = 0^\circ$, $\beta = 90^\circ$, and $\beta = 180^\circ$ in the hypoplastic model of Niemunis and Herle,²² in HS-SS model and in EPHYSS model, (C) $G_t^{ap}/G_{t,ur} - \beta$ curves on Ticino sand in the model of Niemunis and Herle for values of $L(\sigma', e) = 1$, $N(\sigma', e) = 0$, $m_R = 5$, $m_T = 2$ and values of $\chi = 2.0$ (from Benz³), (D) $G_t^{ap}/G_{t,ur} - \beta$ curves for different values of Π on Ticino sand in the multilaminated model of Schädlich and Schweiger (from Schädlich and Schweiger²⁹), (E) $G_t^{ap}/G_{t,ur} - \beta$ curves for different values of Π on Ticino sand in the HS-SS model, (F) $G_t^{ap}/G_{t,ur} - \beta$ curves for different values of Ticino sand in the EPHYSS model

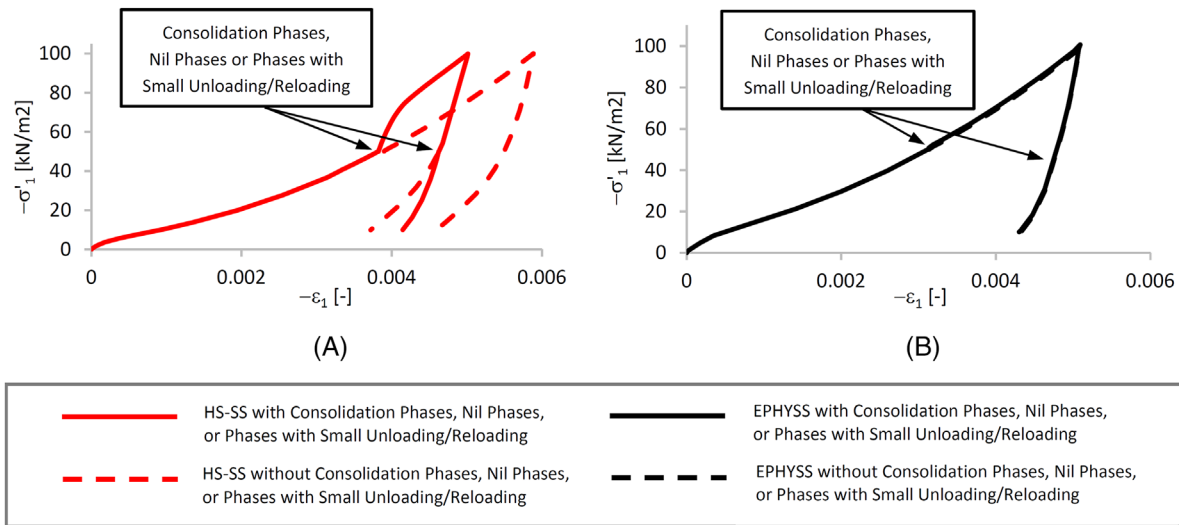


FIGURE 12 Oedometric numerical tests with HS-SS and EPHYSS models

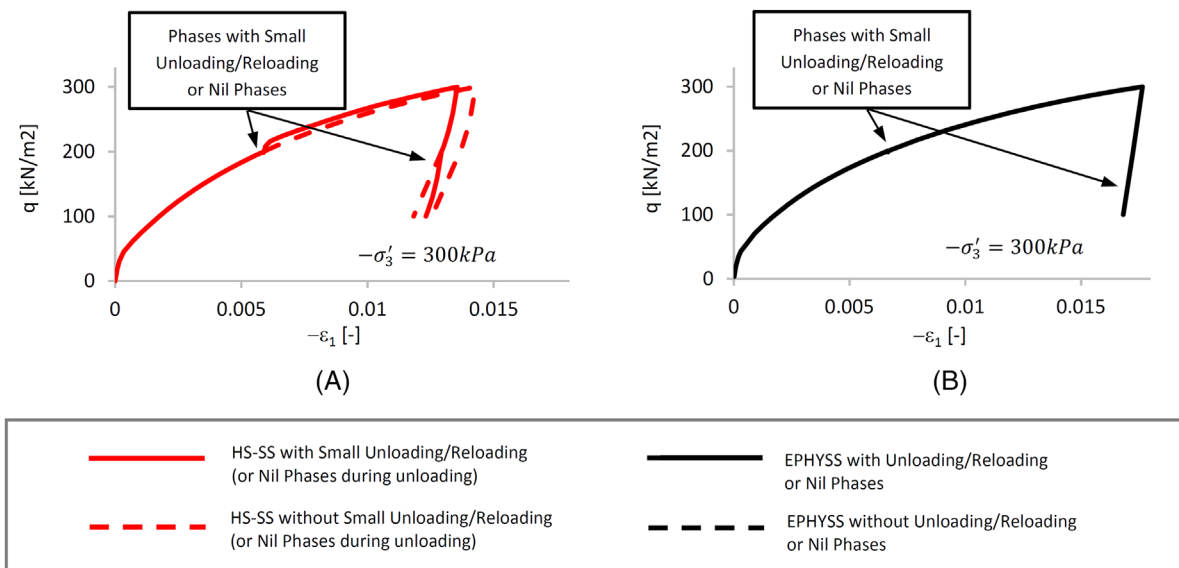









FIGURE 13 Triaxial numerical tests with HS-SS and EPHYSS models, $-\sigma'_3 = 300kPa$

In oedometric tests, the HS-SS model shows the same inconsistencies related to variations in stiffness during consolidation phases, nil phases and phases with small unloading/reloading, which give place to deviations in the oedometric curves, both in the elastoplastic and in the elastic branch (Figure 12A). In all these cases, the reinitialization of all the components of the history tensor \mathbf{H} has been detected. These effects can have a very relevant influence on the results of numerical simulations, since they are cumulative.

Regarding to the deviatoric phases of the numeric triaxial tests conducted using the HS-SS model, no stiffness variations are observed when nil phases are introduced during the primary loading (Figure 13A). Stiffness variations are observed, due to the reinitialization of all the components of the history tensor \mathbf{H} , when a nil phase is introduced during the unloading branch (Figure 13A) and when a small unloading/reloading is introduced both in the primary loading and in the unloading branch (Figure 13A).

Furthermore, in the EPHYSS model no variations of the stiffness that give place to the deviation of the oedometric or triaxial curves are observed (Figures 12B and 13B). This is because EPHYSS model, despite experiencing reversals similar to those observed in the HS-SS model, is capable of correcting its effect in the subsequent calculation phases thanks to the introduction of the state variables \mathbf{H}_{MEM} , \mathbf{E}_{MEM} and \mathbf{E}_{MEM}^e which accumulate enough information from the recent history

TABLE 4 Geotechnical units^{53,54}

| Unit | Description | Code | Color |
|----------------|---|---------|---|
| Fill | Anthropic fill | Ra |  |
| Quaternary | Red clays and yellow carbonated silts | Qa1-Qa2 |  |
| | Gravels and sands | Qa3 |  |
| Pliocuaternary | Sands and gravels | PQ1 |  |
| | Clays and silts | PQ2 |  |
| Pliocene | Sands with intercalated clay, silt and greenish marl layers | Pl1 |  |
| | Blue-gray marly clays | Pl2 |  |

of the soil to recover the historical stiffness corresponding to a specific branch of previous loading/unloading/reloading, despite the possible cycles embedded in it. This implies an improvement of the compliance level of the Generalized Masing Rules Nr. 3 and Nr. 4.

8.2 | Study of a large urban excavation in Barcelona

An example of application involving a large excavation in an urban environment is presented. It refers to the future railway station of La Sagrera in Barcelona, which will constitute an important intermodal hub in the local, national and European public transport network. The construction of the station involved an excavation 650 m long, 35 to 80 m wide and 20 m deep.

The geology of the area was described in the construction project.⁵⁵ Additional geotechnical site investigations were carried out when defining the groundwater drainage of the excavation.⁵⁶ The site is located in the Barcelona plain, which consist of Quaternary formations that overlie a substrate mainly formed by Paleozoic and Pliocene series. Table 4 shows the geotechnical units considered from the available information from top to bottom.

For the hydrogeological characterization of the subsoil of the future station, the transmissivities of the different layers of the soil were calibrated from: (1) the information available in the historical records; (2) the information of the different geotechnical site investigations carried out during and after the project phase; and (3) the results obtained in the analysis of the pumping tests performed in March 2011.⁵⁶ Given the nature of the soil concerned, anisotropy of permeability (k) has been considered by adopting values of $k_{vertical} = 0.1k_{horizontal}$ in all materials.

The magnitude of the excavation has required a large site investigation. Multiple field and laboratory tests were conducted, including: soil identification, pressuremeter tests, SPT, pumping tests, CD, CU and UU triaxial tests, direct shear tests, oedometric tests and chemical analysis of the soil and the groundwater. Furthermore, within this investigation 4 high-quality block samples were taken from the excavation bottom in order to conduct resonant column tests using different confinement stresses (100 kPa, 200 kPa and 300 kPa) to determine soil parameters in the range of small strains.⁴ One of the 4 block samples is located in the Qa1-Qa2 unit and the remaining three in the PQ2 unit. A total of 20 cylindrical samples were obtained from the 4 block samples, 13 of them vertically and 7 horizontally. The tests conducted provided isotropic values $G_0^{ref} = 103 \text{ MPa}$ and $\gamma_{0.7} = 1.20 \cdot 10^{-4}$ in the unit Qa1-Qa2 and $G_0^{ref} = 100 \text{ MPa}$ and $\gamma_{0.7} = 2.00 \cdot 10^{-4}$ in the PQ2 unit. No tests are available for the direct determination of the values of the parameters G_0^{ref} and $\gamma_{0.7}$ of the materials corresponding to the geotechnical units Ra, Qa3, PQ1, Pl1 and Pl2, and, therefore, these have been estimated from correlations with the results of other tests. The expression of Hardin and Black⁵⁷ has been used considering the function $f(e)$ given by Hardin and Richart⁵⁸ with $\hat{B} = 2.97$, resulting the relation $G_0 = 33((2.97 - e)^2 / (1 + e))(-p' / p'_{ref})^{0.50}$. The value of e can be obtained from the relation $e = (w^* \gamma_s) / (S_r \gamma_w)$, where it is usual to consider $\gamma_s / \gamma_w \approx 2.65$. Likewise, for materials located below the water table, $S_r \approx 1.0$ can be considered, and in the case of unit Qa3, $S_r \approx 0.75$ has been assumed. Otherwise, empirical correlations of type $G_0 = A'(N_{60})^{B'}$ have been used, specifically those proposed by Hara et al.⁵⁹ for Tertiary soils and the expressions of Ohsaki and Iwasaki⁶⁰ for all types of soils, cohesive soils and granular soils. It has been found that the expression from Ohsaki and Iwasaki for cohesive soils provides values of $G_0 = 105 \text{ MPa}$ for the materials corresponding to the geotechnical unit Qa1-Qa2 and $G_0 = 115 \text{ MPa}$ for those corresponding to the geotechnical unit PQ2, which are very close to the values obtained with the resonant column tests. To estimate the value of $\gamma_{0.7}$, two correlations have been used: (1) the empirical chart of Vucetic and Dobry⁶¹ that relates $PI - \gamma - G_0$ has been used in the case of cohesive soils; and (2) the expression of Dos Santos and Correia¹⁸ for normally consolidated soils, which results

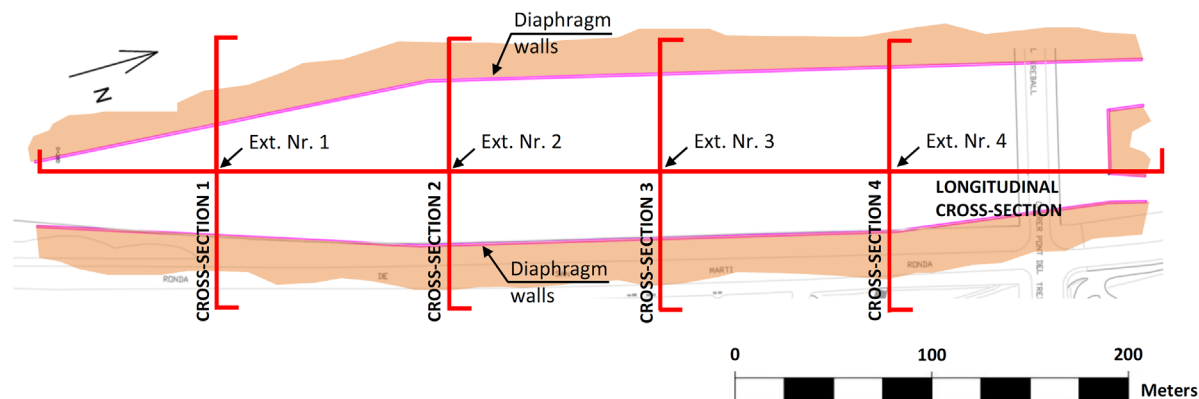


FIGURE 14 Plant with transversal cross-sections and longitudinal cross-section

from combining the expression $\gamma_{0.7} = \alpha\tau_{\max}/G_0$ with the Mohr-Coulomb strength criterion, has been used in the case of granular soils.

Table 5 provides soils specific weight, permeabilities and parameter values of the EPHYSS and HS-SS models for each of the geotechnical units. All the materials are normally consolidated, so that $OCR = 1$.

As indicated in Section 6, it is important to highlight the fact that K'_s and G_s^{ap} vary, respectively, with $(-p')^{m_1}$ and $(-p')^{m_2}$ in the EPHYSS model, while $E'_{t,ur}$ and G_0 do it so with $(-\sigma'_3 + c' \cot(\varphi'))^m$ in the HS-SS model. That leads to formulate a set of transformations based on the proposals by Obrzud and Truty,⁴⁰ which let obtain EPHYSS model parameters $G_{s,0}^{ap,180,H,ref}$ and K_s^{Iref} from HS-SS parameters. The effect that the difference between $G_{s,0}^{ap,180,H,ref}$ (EPHYSS) and G_0^{ref} (HS-SS) generates in the $G_t^{ap}/G_{t,ur}$ graphs should be taken into account, as well as the difference between $G_{t,ur}^{ref} = G_{t,ur}^{ref}(E_{t,ur}^{ref}, K_s^{ref}, m_1)$ (EPHYSS) and $G_{t,ur}^{ref} = G_{t,ur}^{ref}(E_{t,ur}^{ref}, \nu_{ur}^I)$ (HS-SS), both due to the adjustment aforementioned.

In addition to the conventional monitoring, 4 extensometers of 60 m depth below the excavation bottom were installed. With these extensometers it was possible to measure the vertical uplift of the ground during the excavation process. Likewise, the measurements of the extensometers have been taken simultaneously with the surface surveying of the transversal profiles of the excavation in which each of these extensometers is located.⁶² Considering the high number of measurements made, it was decided to choose those corresponding to the most relevant excavation phases: Phase 0 (initial state); Phase A (03/03/2011); Phase B (06/05/2011); Phase C (06/30/2011); and Phase D (04/02/2012). Figure 14 shows in the work plant the situation of the transversal cross-sections that contain each of the extensometers and the longitudinal cross-section that includes all of them.

Based on the geometry of the excavation and the selected phases, a total of five 2D numerical models have been made, corresponding, respectively, to the four transversal cross-sections and the longitudinal one, which refer to the profiles shown in Figure 14. The geometry of the models analyzed, in each of the calculation phases, is shown in Figures 15 and 16. Earth heaps during the work have been simulated as equivalent loadings. The water table is at the reference level + 2,5 m, and it was not reached in any of the analyzed excavation phases.

Two types of analysis have been performed: (1) drained analysis which considers drained conditions for materials corresponding to all geotechnical units; (2) undrained-consolidated analysis which considers: (a) in the materials corresponding to the less permeable geotechnical units (Ra, Qa1-Qa2, PQ2 and Pl2) and in each excavation phase, a first subphase with undrained conditions, followed by a second consolidation subphase, whose duration corresponds to the period between the respective phases of excavation in which water pressures have been almost dissipated (after the application of the undrained loading in Phase D, no subsequent consolidation phase is applied); and (b) in the materials corresponding to the most permeable geotechnical units (Qa3, PQ1 and Pl1), drained conditions have been considered in the two subphases of each calculation phase described in point (a). In the undrained loading subphases it has been considered $S_r \approx 1$ and a maximum allowed suction of $T = 100 \text{ kN/m}^2$ in the materials located under the water table and $S_r \approx 0$ in materials located above the water table in order to simplify the problem. It should be noted that these two types of analysis will generally provide different ground deformation profiles because different effective stress paths are followed in each of them. However, in the range of small strain, the state of the soil is far from yield surfaces and the resulting profiles in both analyses will be closer as differences will only come from elastic non-linearities, which are similar in both models if no big reversals take place. Deformation profiles would be identical if linear elasticity was considered within yield surfaces.

TABLE 5 Soils specific weight, permeabilities and parameters of the EPHYSS and HS-SS models for each of the geotechnical units^{53,54}

| | Ra | Qa1-Qa2 | Qa3 | PQ1 | PQ2 | PI1 | PI2 | Units |
|------------------|-------------------------------|-----------------------|-----------------------|-----------------------|-----------------------|-----------------------|-----------------------|----------------------|
| Specific weight | 18/20 | 19/21 | 19.5/21.5 | 19/21 | 19/21 | 18.5/20.5 | 18.5/20.5 | (kN/m ³) |
| Permeability | $\gamma_{sat}/\gamma_{unsat}$ | 2.0×10^{-4} | II | 17 | 1.0×10^{-1} | 1.40 | 8.0×10^{-3} | (m/day) |
| | $k_{horizontal}$ | 2.0×10^{-5} | 1.1 | 1.7 | 1.0×10^{-2} | 0.14 | 8.0×10^{-4} | (m/day) |
| | $k_{vertical}$ | 2.0×10^{-5} | 1.1 | 1.7 | 1.0×10^{-2} | 0.14 | 8.0×10^{-4} | (m/day) |
| ELASTIC BEHAVIOR | HS-SS & EPHYSS | 1.50×10^{-4} | 1.58×10^{-4} | 2.76×10^{-4} | 2.00×10^{-4} | 4.00×10^{-5} | 2.20×10^{-4} | (-) |
| | $\gamma_{0.7}$ | 41.9 | 168.7 | 205.4 | 100.0 | 182.1 | 188.4 | (MN/m ²) |
| | G_0^{ref} | 0.20 | 0.20 | 0.20 | 0.20 | 0.20 | 0.20 | (-) |
| | ν_{ur}^{ref} | 14.6 | 156.8 | 17.0 | 8.9 | 20.4 | 9.5 | (MN/m ²) |
| | K_s^{ref} | 0.50 | 0.50 | 0.50 | 0.65 | 0.50 | 0.70 | (-) |
| | m_1 | 100 | 100 | 100 | 100 | 100 | 100 | (kN/m ²) |
| | $p'_{ref,1}$ | 38.5 | 141.6 | 167.5 | 76.4 | 143.5 | 115.6 | (MN/m ²) |
| | $G_{s,0}^{ap,180,H,ref}$ | 16.9 | 62.3 | 73.7 | 38.2 | 63.2 | 57.8 | (MN/m ²) |
| | $G_{s,0}^{ap,90,H,ref}$ | 0.50 | 0.50 | 0.50 | 0.65 | 0.50 | 0.70 | (-) |
| | m_2 | 100 | 100 | 100 | 100 | 100 | 100 | (kN/m ²) |
| | $p'_{ref,2}$ | 0.20 | 0.20 | 0.20 | 0.20 | 0.20 | 0.20 | (-) |
| | ν'_{min} | 0.20 | 0.20 | 0.20 | 0.20 | 0.20 | 0.20 | (-) |
| PLASTIC BEHAVIOR | HS-SS & EPHYSS | 19.0 | 24.0 | 25.0 | 20.0 | 31.0 | 31.0 | (MN/m ²) |
| | E_{50}^{ref} | 57.0 | 72.0 | 75.0 | 60.0 | 93.0 | 93.0 | (MN/m ²) |
| | $E_{t,ur}^{ref}$ | 15.2 | 19.2 | 20.0 | 16.0 | 24.8 | 24.8 | (MN/m ²) |
| | E_{oed}^{ref} | 5 | 1 | 1 | 30 | 20 | 70 | (kN/m ²) |
| | c' | 28 | 34 | 38 | 29 | 35 | 25 | (°) |
| | ϕ' | 0 | 0 | 0 | 0 | 0 | 0 | (°) |
| | ψ | 100 | 100 | 100 | 100 | 100 | 100 | (kN/m ²) |
| | p'_{ref} | 0.50 | 0.50 | 0.50 | 0.65 | 0.50 | 0.70 | (-) |
| | m | 0.53 | 0.44 | 0.40 | 0.52 | 0.43 | 0.56 | (-) |
| | K_0^{NC} | 0.90 | 0.90 | 0.90 | 0.90 | 0.90 | 0.90 | (-) |
| | R_f | 0 | 0 | 0 | 0 | 0 | 0 | (kN/m ²) |
| | σ'_{trac} | 0 | 0 | 0 | 0 | 0 | 0 | (kN/m ²) |

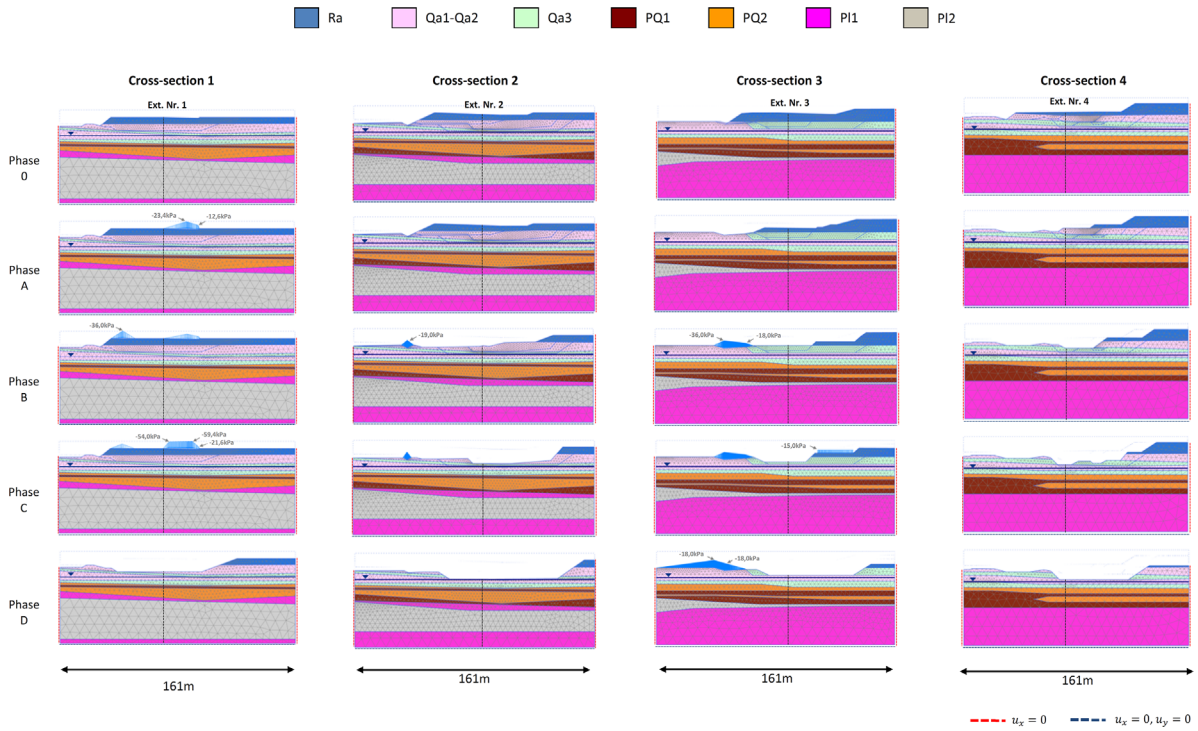


FIGURE 15 Transversal cross-sections with phases 0, A, B, C and D

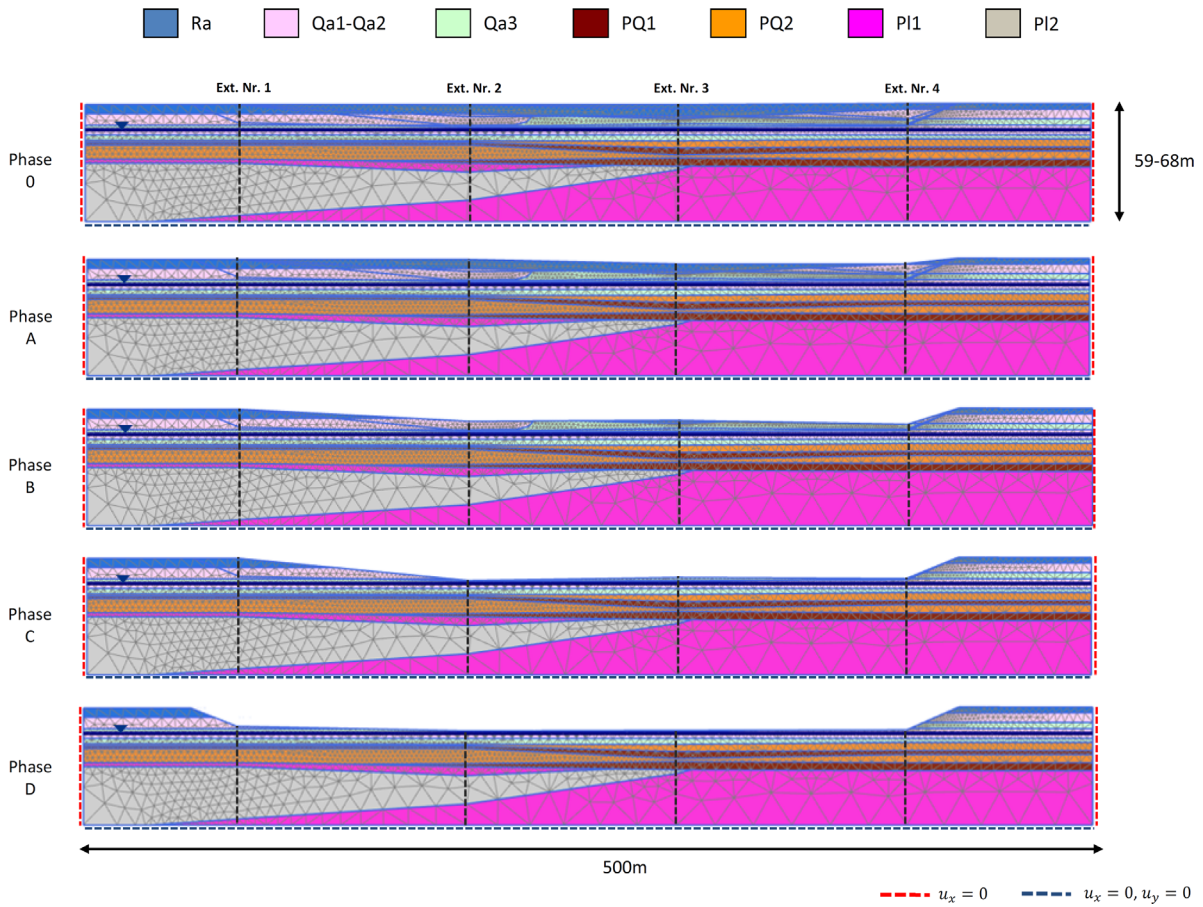


FIGURE 16 Longitudinal cross-section with phases 0, A, B, C and D

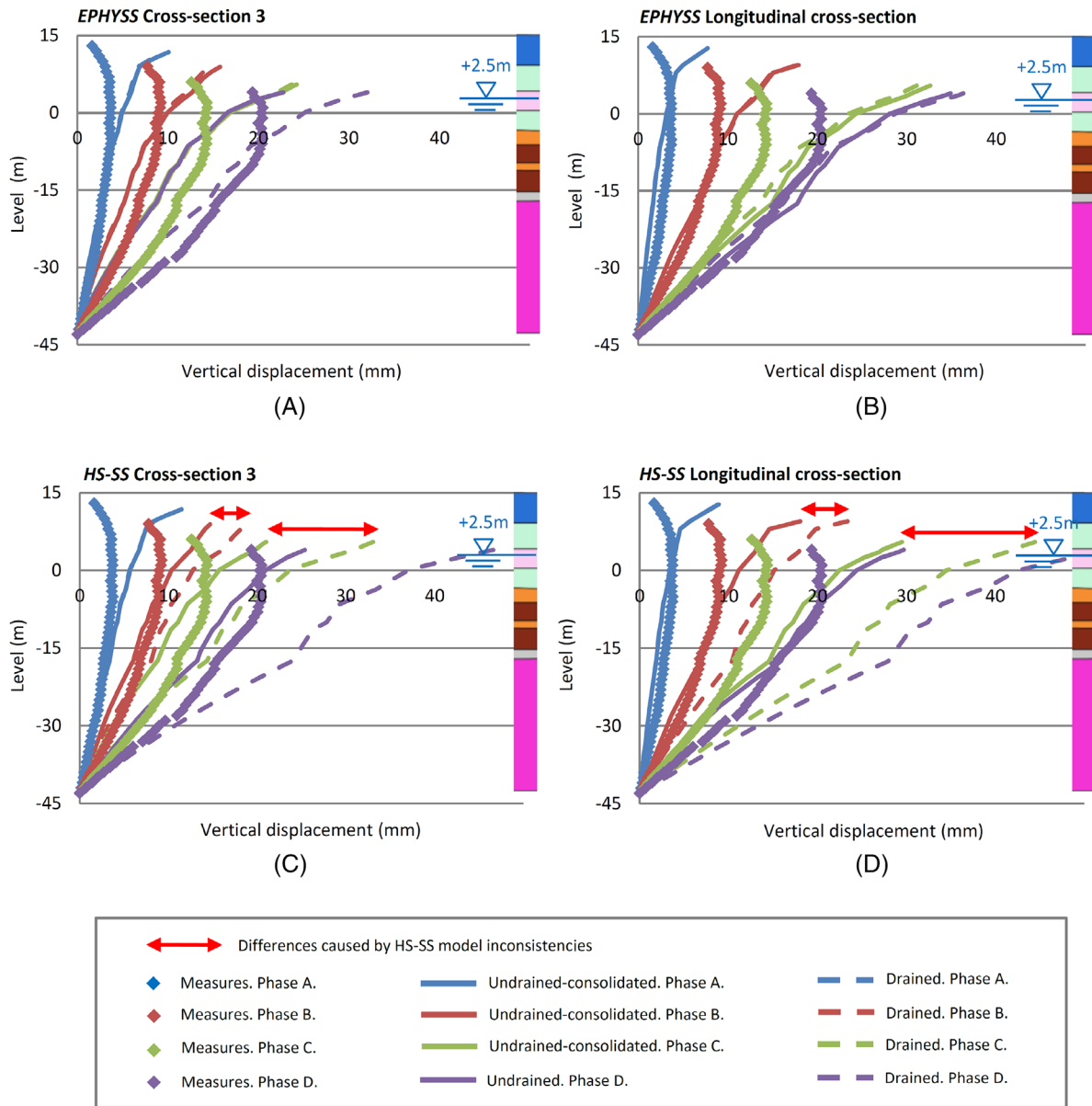


FIGURE 17 Numerical results and field measurements of the extensometer Nr. 3.⁶² Cross-section 3 with (A) EPHYSS model and (C) HS-SS model. Longitudinal cross-section with (B) EPHYSS model and (D) HS-SS model

In addition to that, after the calculation phase in which in situ field stresses are determined, both soil strain history and soil displacements have been reinitialized.

Numerical results and field measurements of the extensometer Nr. 3 are shown in Figure 17 (other simulations results can be found in Castellón⁴). As it can be seen, the simulations conducted with the EPHYSS or HS-SS models are not able to reproduce the upper part of the displacement profiles measured with the extensometers, in which a remarkable reduction in vertical soil displacements is appreciated. This behavior can be explained by the progressive drying of the soil near the water table as the excavation progresses, which generates gradual increases in suction in the unsaturated zone of the soil and, therefore, a shrinkage of it.⁶ According to the simulations performed with the Barcelona Basic Model (BBM),⁶³ the value of these displacements caused by shrinkage can be of the order of 5 mm,⁶ thus approaching the observations. In any case, the use of the EPHYSS model allows to improve the approximation to the measures taken with the extensometers with respect to the values calculated with the HS-SS model. In Figure 17 the results of the simulations with the EPHYSS model approximate quite well the measurements of the extensometer Nr. 3 in the different calculation phases, especially in the transversal cross-section of the drained analysis. Furthermore, simulations with the HS-SS model approximate these measures better or worse depending on whether, in a certain calculation phase, the results of the transversal or

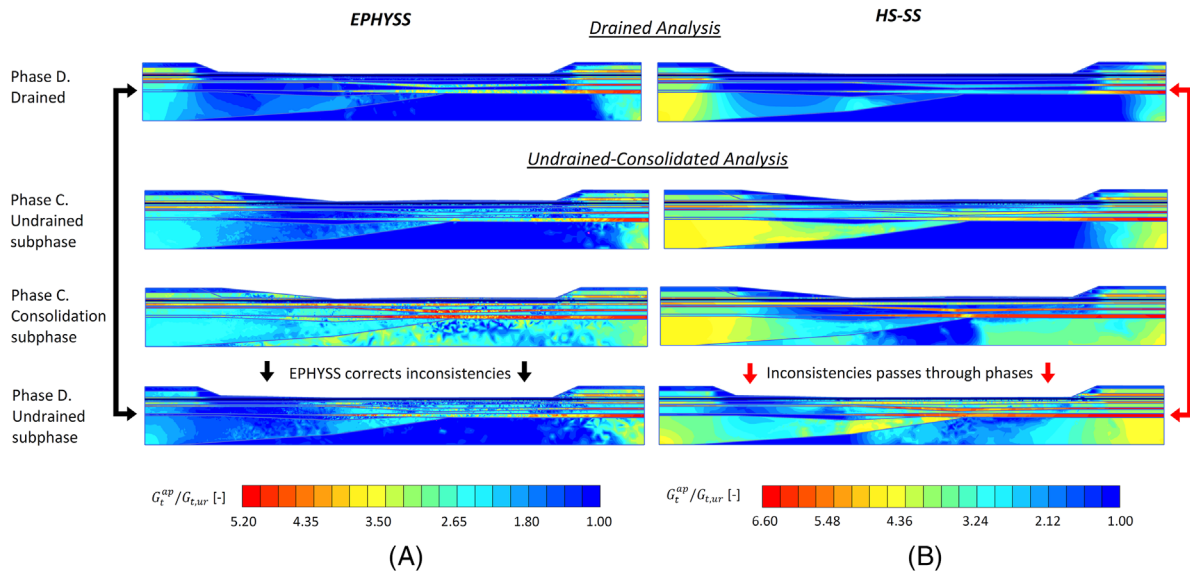


FIGURE 18 Effect of the inconsistencies in HS-SS model and inconsistencies correction in the EPHYSS model. Simulation with the longitudinal cross-section in (A) EPHYSS model and (B) HS-SS model

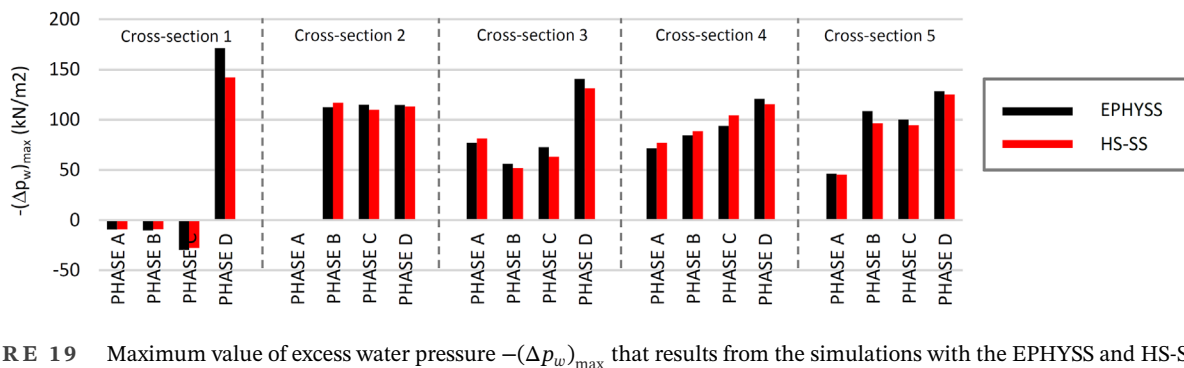


FIGURE 19 Maximum value of excess water pressure $-(\Delta p_w)_{\max}$ that results from the simulations with the EPHYSS and HS-SS models

longitudinal cross-section of the drained or undrained-consolidated analysis are considered. In general, measurements are better simulated with EPHYSS model.

It is important to point out the effect of the inconsistencies generated by the consolidation phases in the undrained-consolidated analysis with HS-SS model that can be observed in Figure 17. They are due to the reinitialization of the components of the HS-SS model history tensor (\mathbf{H}), giving place to markedly lower displacements than those obtained in the corresponding drained phases. Equivalent reinitialization of the components of EPHYSS model history tensor (\mathbf{h}) happens, however, this problem is solved in EPHYSS by defining new state variables (\mathbf{H}_{MEM} , \mathbf{E}_{MEM} and \mathbf{E}_{MEM}^e). The effect of such inconsistencies in the HS-SS model is especially evident in the results of phases B and C. On the other hand, note that part of the difference between the displacement profile of the drained and undrained-consolidated analysis corresponding to phase D, both in the HS-SS model and in the EPHYSS model, is because no consolidation has been considered in such phase after the application of the corresponding undrained loading.

Inconsistencies in the simulations with the HS-SS model can be easily detected in the graphs $G_t^{ap} / G_{t,ur}$ corresponding to the consolidation subphase of the undrained-consolidated analysis, when compared with the same graphs corresponding to the respective undrained loading subphases of the undrained-consolidated analysis, which are shown in Figure 18 for the longitudinal cross-section. It can be clearly seen how both the EPHYSS and the HS-SS models have numerical reversals during the consolidation subphase that give place to a soil stiffening. Nevertheless, unlike the HS-SS model (Figure 18B), in which these reinitializations influence the subsequent soil history, in the EPHYSS model (Figure 18A) this effect is corrected and does not accumulate, having no influence in following phases.

In Figures 19 and 20 it can be seen, respectively, how the maximum value of the excess water pressure generated during the undrained loading subphases of the undrained-consolidated analysis and the distributions of such excesses are very

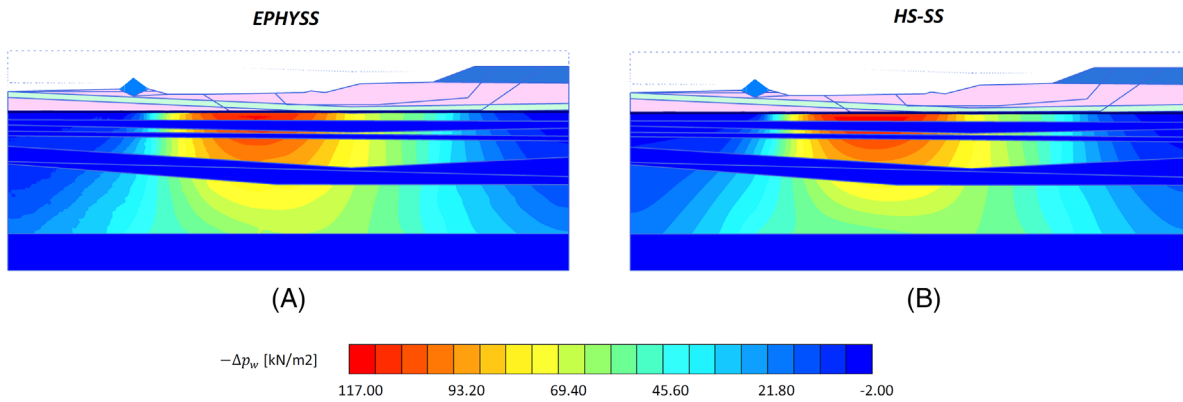


FIGURE 20 Water pressures in (A) EPHYSS and (B) HS-SS simulations after undrained subphase corresponding to Phase B in transversal cross-section of Extensometer Nr. 2

similar in the simulations performed with both models. The small existing differences can be attributed to the nonlinear behavior of K'_s with $-p'$.

Finally, it must be pointed out that the calculation time when solving boundary value problems with EPHYSS, using conventional processor, falls within the reasonable values for a commercial geotechnical software.

9 | CONCLUSIONS

The behavior of the soil in the range of small strains should be always considered in the analysis of geotechnical problems when sensitive constructions are affected, which is very common in urban environments. The EPHYSS model described in this paper, which is composed by the HQH model and the Cap-Cone HS_{MOD} model, is capable to reproduce the quasi-static behavior of the soil in Zones I, II, III and IV of Jardine.¹ Zones I and II, where soil behavior is nonlinear reversible, hysteretic and dependent on the recent history, are described by the HQH model, which also considers the strain-induced anisotropy, while Zones III and IV of Jardine are described by the HS_{MOD} model. EPHYSS model inherits some important limitations from the HS_{MOD} model that makes it unsuitable in numerical analyses of geotechnical works in which intermediate or large strains play a significant role. However, in many geotechnical works in urban areas, under safe conditions and far from failure, small strains dominate and therefore EPHYSS model is appropriate.

The reversible part of the EPHYSS model considers two strain domains. The elastic bulk modulus is common in both domains. A degradation law of the shear modulus is considered in domain 1 until it reaches a minimum value in domain 2. Poisson's ratio is variable in both domains, and always greater than ν'_{\min} . Furthermore, the EPHYSS model considers 10 state variables: 8 of these variables correspond to the reversible part of it (HQH model) and 2 to its plastic part (HS_{MOD} model). These HQH model state variables define different short and long-term memory levels that provide the EPHYSS model with robustness for the reproduction of soil hysteretic behavior in quasi-static problems, using in some of them a layer structure similar to that proposed by Hueckel and Nova.³³ As well, EPHYSS model state variables allow to consider soil strain-induced anisotropy and let the model complies with the Generalized Masing Rules^{15,16} Nr. 1, Nr. 2, Nr. 3 and partially the Nr. 4. Additionally, the EPHYSS model meets the stability criterion of Hill.³⁵

All EPHYSS parameters can be obtained from well-known tests and are common or related to HS-SS model parameters, except for $G_{s,0}^{ap,90,H,ref}$ that must be obtained from biaxial, true triaxial or hollow cylinder with torsion tests with internal strain measures. However, since these tests are very rare in the professional practice, it has been proposed the following expression for $G_{s,0}^{ap,90,H,ref}$ estimation: $G_{s,0}^{ap,90,H,ref} \approx \Lambda G_{s,0}^{ap,180,H,ref}$, where Λ takes values of 0.40 – 0.58 for sands and 0.50 for clays.

Different oedometric, triaxial and biaxial tests compiled from various thesis and papers have been simulated to carry out a partial verification of EPHYSS model, as well as a validation and a comparative analysis with the HS-SS model. Both models provide a very good approximation to the experimental data. When no strain rotations take place or when reversals are total ($\alpha = 180^\circ$), EPHYSS model provides similar results to those of the HS-SS model, except for some differences related to stiffness stress dependency, stiffness moduli dependencies, dilatancy formulation and the consideration of strain induced anisotropy. However, there are some significant differences between both models when the reversals are

partial ($\alpha < 180^\circ$). From the numerical biaxial tests in which the results of the simulations with the EPHYSS model are compared with those of the HS-SS model, the hypoplastic model with intergranular strain of Niemunis and Herle²² and the multilaminated model of Schädlich and Schweiger,²⁹ it is concluded that the HS-SS model is not capable of reproducing stiffness recovery when the cumulated strain value prior to the rotation is high. The latter does not occur in any of the other three advanced models, where the soil elastic recovery is less dependent on the value of the previous accumulated strain. This represents an added advantage of the EPHYSS model, as it is a model easy to use in the professional practice.

Finally, it is concluded from simulations of numerical oedometric and triaxial tests in which consolidation phases, nil phases or phases with small unloading/reloading have been introduced, that the EPHYSS model is capable to correct the effect of the inconsistencies detected in the HS-SS model,⁴⁻⁷ which are cumulative and can have very important effects on the results of boundary value problems. The effect of the correction of HS-SS inconsistencies is also shown in a large urban excavation that has been studied, which corresponds to the works of the future intermodal station of La Sagrera, in Barcelona. The soil parameters have been obtained from the tests carried out during the project phase of the station, from empirical correlations and from 20 resonant column tests conducted in cylindrical samples obtained from high-quality block samples. Four extensometers were installed, reaching 60 m depth below the excavation bottom to measure soil uplift. Numerical simulations of the excavation have been conducted in four transversal cross-sections that contain, each of them one extensometer, and in a longitudinal cross-section that contains all of them. The EPHYSS and HS-SS models have been used and the results obtained with them have been compared. In the study conducted, two types of analysis were performed, a drained analysis and an undrained-consolidated analysis. From the results of the simulations with the EPHYSS and HS-SS models it is concluded that none of them can reproduce the upper part of the displacement profiles measured with the extensometers, in which an evident reduction in the vertical displacements is observed. This behavior can be explained by the progressive drying of the soil near the water table as the excavation progresses, which generates gradual increments in suction in the unsaturated area of the soil and, therefore, a shrinkage of it.⁶ In any case, it is concluded that simulations with the EPHYSS model significantly improve the approximation to the measurements of the extensometers in the different calculation phases if compared with the results of the simulations obtained with the HS-SS model, both in the transversal and in the longitudinal cross-sections. In the results of the simulations with the HS-SS model, the effect of the inconsistencies generated by the consolidation subphases in the undrained-consolidated analysis can be clearly seen, which leads to displacements markedly lower than those obtained in the corresponding drained phases. The EPHYSS model is able to correct the effect of these inconsistencies thanks to the model state variables. Finally, it can be seen that both, the distributions of excess water pressure and the maximum value of such excess, are very similar in both models.

It is concluded that, in general, the EPHYSS model significantly improves the approximation to the experimental measures with respect to the HS-SS model, especially in those boundary value problems that present partial reversals in the deviatoric strains or high cumulated strain values prior to reversals; resolves the inconsistencies of the latter with a reasonable computational cost; and requires simple parameters, most of them common to those of the HS-SS model. All this makes EPHYSS a model that can be used for analysis and design in geotechnical professional practice.

LIST OF SYMBOLS AND ABBREVIATIONS

- a Parameter of the shear modulus expression according to the model of Dos Santos and Correia¹⁸ whose value is $a = 0.385$ and which is used in the SSOM, HS-S, HS-SS, HQH and EPHYSS models.
- A' Soil parameter in the expression of Hara et al.¹⁹ that correlates G_0 with N_{60} .
- B' Soil parameter in the expression of Hara et al.¹⁹ that correlates G_0 with N_{60} .
- \hat{B} Soil parameter in the expression of Hardin and Richart¹⁸ to obtain the value of G_0 .
- c' Effective cohesion.
- d_0 Soil parameter in the Li and Dafalias dilatancy formulation³⁶.
- e Void ratio.
- $(e_{cv})_a$ Void ratio at point “a” on the critical state line (constant volume).
- \mathbf{e} $= \epsilon - \epsilon_{oct} \mathbf{1}$.
- \mathbf{e}^e $= \epsilon^e - \epsilon_{oct}^e \mathbf{1}$.
- $\mathbf{e}^{e,R}$ State variable that stores the elastic deviatoric strain tensor value (\mathbf{e}^e) at the last reversal point R that forms the endpoint of the active strain cycle in the HQH and EPHYSS models.
- $\mathbf{e}^{e,\Delta R}$ $= \mathbf{e}^e - \mathbf{e}^{e,R}$.

| | |
|---|---|
| \mathbf{e}^R | State variable that stores the total deviatoric strain tensor value (\mathbf{e}) at the last reversal point R that conforms the endpoint of the active strain cycle in the HQH and EPHYSS models. |
| $\mathbf{e}^{e,\Delta R}$ | $= \mathbf{e} - \mathbf{e}^R$. |
| E_{oed}^{ref} | Reference oedometric tangent modulus in primary loading for $-\sigma'_3 = p'_{ref}$ in the HS, HS-S, HS-SS and EPHYSS models. |
| E_i^{ref} | Internal parameter related to E_{50}^{ref} that represents the reference initial drained stiffness tangent modulus for $-\sigma'_3 = p'_{ref}$ in the HS-S, HS-SS and EPHYSS models. |
| $E_{t,ur}^{ref}$ | Reference stiffness tangent modulus in elastic unloadings and reloadings for $-\sigma'_3 = p'_{ref}$ in the HS, HS-S, HS-SS and EPHYSS models. |
| E_{50}^{ref} | Secant stiffness modulus for a mobilization of the 50% of q_f in a drained triaxial test for $-\sigma'_3 = p'_{ref}$ in the HS, HS-S, HS-SS and EPHYSS models. |
| \mathbf{E}_{MEM} | State variable formed by a vector with the values $\ \mathbf{e}\ $ in the reversal points R_i that conforms the endpoints of the active strain cycles defined by the conditions $\cos(\alpha) \leq \cos(\alpha^*)$ and $\hat{\mathbf{e}}^{\Delta R_{i-1}} : \hat{\mathbf{e}} \leq \cos(\alpha^*)$ in the HQH and EPHYSS models. |
| \mathbf{E}_{MEM}^e | State variable formed by a vector with the values $\ \mathbf{e}^e\ $ in the reversal points R_i that conforms the endpoints of the active strain cycles defined by the conditions $\cos(\alpha) \leq \cos(\alpha^*)$ and $\hat{\mathbf{e}}^{\Delta R_{i-1}} : \hat{\mathbf{e}} \leq \cos(\alpha^*)$ in the HQH and EPHYSS models. |
| \mathbf{E}'_s | Secant stiffness tensor. |
| \mathbf{E}'_t | Tangent stiffness tensor. |
| G | Shear modulus. |
| G_0 | Maximum shear modulus. |
| G_0^{ref} | Maximum apparent shear modulus for $-\sigma'_3 = p'_{ref}$ in the SSOM, HS-S and HS-SS models. |
| $G^{\theta_{q/p'}}$ | Maximum shear stiffness after a $\theta_{q/p'}$ stress rotation in $q - p'$ space. |
| $G_{s,0}^{ap,\alpha,H,ref}$ | State variable that represents the maximum secant shear modulus of the degradation curve corresponding to a α deviatoric strain rotation and $-p' = p'_{ref,2}$ in the HQH and EPHYSS models. |
| $G_{s,0}^{ap,180,H,ref}$ | Soil parameter that represents the maximum secant shear modulus of the degradation curve corresponding to a 180° deviatoric strain rotation and $-p' = p'_{ref,2}$ in the HQH and EPHYSS models. |
| $G_{s,0}^{ap,90,H,ref}$ | Soil parameter that represents the maximum secant shear modulus of the degradation curve corresponding to a 90° deviatoric strain rotation and $-p' = p'_{ref,2}$ in the HQH and EPHYSS models. |
| $G_{s,\xi=1}^{ap}$ | Secant apparent shear modulus G_s^{ap} with $\xi = 1$ in the SSOM, HS-S, HS-SS, HQH and EPHYSS models. |
| $G_{t,ur}^{ref}$ | Reference elastic shear modulus for $-\sigma'_3 = p'_{ref}$ in the SSOM, HS-S and HS-SS models and for $-p' = p'_{ref,2}$ in the HQH and EPHYSS models. |
| $G_{t,\min,\xi=1}^{ap}$ | Minimum apparent tangent shear modulus for primary loading ($\xi = 1$) in the SSOM, HS-S, HS-SS, HQH and EPHYSS models. |
| h_c | Plastic hardening modulus associated to the Cap yield surface. |
| h_s | Plastic hardening modulus associated to the Cone yield surface. |
| $(\hat{\mathbf{h}} : \hat{\mathbf{e}})^*$ | Cosine of the rotation angle in the recent total deviatoric strain path from which reversals appear in the HQH and EPHYSS models. |
| \mathbf{h} | State variable (history tensor) that stores the recent total deviatoric strain history in the HQH and EPHYSS models. |
| \mathbf{h}_k | Generalized plastic modulus associated to the yield surface f_k . |
| \mathbf{H} | State variable (history tensor) that stores the recent total deviatoric strain history in the SSOM, HS-S and HS-SS models. |
| \mathbf{H}_{MEM} | State variable formed by a vector with the values $\ \mathbf{h}\ $ in the reversal points R_i that conform the endpoints of active strain cycles defined by the conditions $\cos(\alpha) \leq \cos(\alpha^*)$ and $\hat{\mathbf{e}}^{\Delta R_{i-1}} : \hat{\mathbf{e}} \leq \cos(\alpha^*)$ in the HQH and EPHYSS models. |
| k | Permeability. |
| $k_{horizontal}$ | Horizontal permeability. |
| $k_{vertical}$ | Vertical permeability. |
| K' | Bulk modulus. |

- K_s^{ref} Reference secant bulk modulus for $-p' = p'_{ref,1}$.
- K_t^{ref} = $K_s^{ref} / (1 - m_1)$ is the reference tangent bulk modulus for $-p' = p'_{ref,1}$.
- $K'_{t,ur} / K'_c$ Internal parameter in the HS-S, HS-SS and EPHYSS models related with the value of E_{oed}^{ref} that represent the ratio between the elastic bulk modulus and the secant bulk modulus for the primary isotropic compression.
- K_0^{NC} Coefficient of lateral earth stress for a normally consolidated stress state ($K_0^{NC} = 1 - \sin(\varphi')$ by default).
- $L(\sigma', e)$ Fourth-order linear tensor in a hypoplastic model that introduces void ratio as a state variable.²²
- m Coefficient that controls the dependence level of E'_{50} , E'_{oed} , $E'_{t,ur}$ and E'_i with the stress in the HS-S, HS-SS and EPHYSS models.
- m_R Soil parameter that controls stiffness value before a rotation of the strain path of 180° in the model of Niemunis and Herle.²²
- m_T Soil parameter that controls stiffness value before a rotation of the strain path of 90° in the model of Niemunis and Herle.²²
- m_1 Soil parameter that controls the dependence of K'_s on $-p'$ in the HQH and EPHYSS models.
- m_2 Soil parameter that controls the dependence of G_s^{ap} and $G_{t,ur}$ on $-p'$ in the HQH and EPHYSS models.
- \hat{m} Soil parameter in the Li and Dafalias dilatancy formulation.³⁶
- M Critical stress ratio.
- \bar{M} Internal parameter that determines the maximum number of reversal points in which is possible to memorize $\|\mathbf{h}\|$, $\|\mathbf{e}^R\|$ and $\|\mathbf{e}^{e,R}\|$ in the HQH and EPHYSS models.
- $N(\sigma', e)$ Second-order tensor in a hypoplastic model that introduces void ratio as a state variable.²²
- N_{60} Result of the SPT.
- OCR = $\sigma'_{v,max} / \sigma'_v$.
- p' = $\sigma'_{oct} = 1/3\sigma'_{ii}$.
- p'^{ini} = $1/3\sigma'^{ini}_{ii}$ is the value of the initial mean stress p' .
- p_a Atmospheric pressure.
- p'_{ref} Reference confinement stress ($p'_{ref} = \sigma'_{3,ref} = 100kPa$ by default).
- $p'_{ref,1}$ Reference mean stress in the expression of K'_s in the HQH and EPHYSS models.
- $p'_{ref,2}$ Reference mean stress in the expressions of G_s^{ap} and $G_{t,ur}$ in the HQH and EPHYSS models.
- PI Plasticity Index.
- q = $-\sigma'_1 - (-\sigma'_3)$.
- q_a = q_f / R_f is the asymptotic deviatoric soil stress.
- q_f Deviatoric soil strength given by the Mohr-Coulomb criterion.
- \hat{R} Parameter with the maximum value of $\|\delta\|$ in the model of Niemunis and Herle.²²
- R_f Soil parameter that represents the ratio q_f / q_a ($R_f = 0.9$ by default).
- s Active reversal points in the HQH and EPHYSS models.
- $\mathbf{s}^{\Delta R}$ = $\mathbf{s} - \mathbf{s}^R$.
- \mathbf{s} = $\sigma' - \sigma'_{oct}\mathbf{1}$.
- \mathbf{s}^R Deviatoric strain tensor in the last reversal point R that conforms the endpoint of the active strain cycle in the HQH and EPHYSS models.
- S_r Soil saturation degree.
- T Water cavitation stress.
- $TOL_{\epsilon_{abs}^e}$ ϵ_{abs}^e admitted tolerance.
- $TOL_{\epsilon_{rel}^e}$ ϵ_{rel}^e admitted tolerance.
- u_x Imposed displacement in the global x-direction.
- u_y Imposed displacement in the global y-direction.
- w^* Water content.
- w Numerical parameter in the HQH and EPHYSS models that controls the speed with which $\hat{\mathbf{h}}$ evolves.
- α = $\arccos(\hat{\mathbf{h}} : \hat{\mathbf{e}})$.
- α^* = $\arccos(\hat{\mathbf{h}} : \hat{\mathbf{e}})^*$ is the rotation angle in the recent total deviatoric strain path from which reversals appear in the HQH and EPHYSS models.
- β Rotation angle of the incremental total strain.

- β' Factor in the HQH and EPHYSS models that adopts values of $\beta' = 2$ if $s = 2$, and $\beta' = 1$ if $s > 2$.
- $\gamma_c = (\xi\gamma_{0.7}/a)(\sqrt{G_0^{ref}/G_{t,ur}^{ref}} - 1)$ is the limit shear strain from which $G_t^{ap} = G_{t,ur}$ in the SSOM, HS-S and HS-SS models.
- $\gamma_{HIST} = \sqrt{4/3}\|\mathbf{H}\dot{\mathbf{e}}\|/\|\dot{\mathbf{e}}\|$ is a history variable of the SSOM, HS-S and HS-SS models.
- $\gamma_{oct} = \sqrt{4/3}\|\mathbf{e}\|$.
- $\gamma_{oct}^e = \sqrt{4/3}\|\mathbf{e}^e\|$.
- $\gamma_{oct}^{e,R} = \sqrt{4/3}\|\mathbf{e}^{e,R}\|$.
- $\gamma_{oct}^{e,\Delta R} = \gamma_{oct}^e - \gamma_{oct}^{e,R}$.
- $\gamma_{oct}^H = \sqrt{4/3}\|\mathbf{h}\|$ is a history variable of the HQH and EPHYSS models.
- γ^p Plastic shear strain that is used as plastic state variable in the HS, HS-S, HS-SS and EPHYSS models.
- $\gamma_{oct}^R = \sqrt{4/3}\|\mathbf{e}^R\|$.
- $\gamma_{oct}^{\Delta R} = \gamma_{oct} - \gamma_{oct}^R$.
- γ_{sat} Saturated soil specific weight.
- γ_{unsat} Unsaturated soil specific weight.
- $\gamma_{ur}^\alpha = (\xi\gamma_{0.7}/a)(\sqrt{G_{s,0}^{ap,\alpha,H,ref}/G_{t,ur}^{ref}} - 1)$ is the limit shear strain between domain 1 and domain 2 for the active degradation curve α from which $G_t^{ap} = G_{t,ur}$ in the HQH and EPHYSS models.
- $\gamma_{ur}^{\alpha,\xi=1} = (\gamma_{0.7}/a)(\sqrt{G_{s,0}^{ap,\alpha,H,ref}/G_{t,ur}^{ref}} - 1)$.
- $\gamma_{0.7}$ Shear strain value in the shear modulus expression according to the model of Dos Santos and Correia¹⁸ for which $G_s^{ap}(\gamma_{0.7}) = 0.722G_0$.
- δ Intergranular strain tensor in the model of Niemunis and Herle.²²
- $\epsilon_{oct} = 1/3\epsilon_{ii}$.
- $\epsilon_{oct}^e = 1/3\epsilon_{ij}^e$.
- $\epsilon_{oct}^p = 1/3\epsilon_{ij}^p$.
- ϵ Total strain tensor.
- ϵ^e Elastic strain tensor.
- ϵ^p Plastic strain tensor.
- ϵ_k^p Plastic strain tensor associated to the yield surface f_k .
- $\epsilon^R = \epsilon_{oct}\mathbf{1} + \mathbf{e}^R$.
- $\epsilon^{\Delta R} = \epsilon - \epsilon^R$.
- $\eta = q/p'$.
- $\theta_{q/p'}$ Stress rotation in $q - p'$ space.
- λ Slope of the critical state line.
- λ_i $i - th$ eigenvalue of $\dot{\mathbf{e}}$.
- λ_k Plastic multiplier associated to the yield surface f_k .
- ν' Drained Poisson's ratio of a specific material.
- ν'_{min} Minimum drained Poisson's ratio.
- ν'_s Secant drained Poisson's ratio.
- ν'_t Tangent drained Poisson's ratio.
- ν'_{ur} Drained Poisson's ratio in reversible unloading/reloading processes.
- ξ Scale factor that controls the shape of the degradation curve of G_s^{ap} , and can adopt the values $\xi = 1$ and $\xi = 2$.
- $\rho_\alpha = \gamma_{oct}^H/\gamma_{ur}^\alpha$.
- $\sigma'_{oct} = 1/3\sigma'_{ii}$.
- σ'_v Effective vertical stress.
- $\sigma'_{v,max}$ Maximum historic effective vertical stress.
- σ'_{trac} Soil tensile strength.
- $\boldsymbol{\sigma}'$ Effective stress tensor.
- $\boldsymbol{\sigma}'^{ini}$ Initial effective stress tensor.
- $\tau_{max} = (a/4)(2c'(1 + \cos(2\varphi')) + (-\sigma'_1)(1 + K_0^{NC})\sin(2\varphi'))$.
- $\tau_{oct} = \sqrt{1/3}\|\mathbf{s}\|$.
- φ' Maximum effective friction angle.

| | |
|---------------------------------|---|
| φ'_{cv} | Effective constant volume friction angle, $\sin(\varphi'_{cv}) = (\sin(\varphi') - \sin(\psi))/(1 - \sin(\varphi') \sin(\psi))$. |
| φ_z | Rotation around z-axis. |
| χ | Parameter of the model of Niemunis and Herle ²² for interpolation between $\ \delta\ /\tilde{R} = 0$ and $\ \delta\ /\tilde{R} = 1$. |
| $\chi^{el,hist}$ | $= (\mathbf{h}, G_{s,0}^{ap,\alpha,H,ref}, \mathbf{e}^R, \mathbf{e}^{e,R}, \mathbf{H}_{MEM}, \mathbf{E}_{MEM}, \mathbf{E}_{MEM}^e)$ elastic state variables in the HQH and EPHYSS models. |
| χ_k^{pl} | plastic state variables associated to the yield surface f_k in HS, SSOM, HS-S, HS-SS, HQH and EPHYSS models. |
| ψ_m | Mobilized dilatancy angle. |
| ψ | Maximum dilatancy angle. |
| $\hat{\psi}$ | $= e - (e_{cv})_a + \lambda(-p'/p_a)$ Been and Jefferies state parameter. ³⁷ |
| $\mathbf{1}$ | $(1)_{ij} = \delta_{ij}$. |
| $\mathbb{1}$ | $(\mathbb{1})_{ijkl} = 1/2(\delta_{ik}\delta_{jl} + \delta_{il}\delta_{jk})$. |
| \mathbb{R} | Real numbers. |
| $\ \mathbf{A}\ $ | $= \sqrt{A_{ij}A_{ij}}$. |
| $ a $ | $ a = a$ if $a > 0$ and $ a = -a$ if $a < 0$, $a \in \mathbb{R}$. |
| $a^{(n)}$ | The superscript (n) indicates that a is evaluated at the beginning of the calculation step $(n) \rightarrow (n + 1)$. |
| $a_{[i]}$ | The subscript $[i]$ indicates that a is evaluated in the $i - th$ iteration. |
| $A_{ij\dots k}$ | $ij \dots k - th$ component of \mathbf{A} . |
| $\dot{\mathbf{A}}$ | Infinitesimal rate of \mathbf{A} . |
| $\Delta\mathbf{A}$ | Finite rate in \mathbf{A} . |
| $\hat{\mathbf{A}}$ | $\hat{\mathbf{A}} = \mathbf{A}/\ \mathbf{A}\ $ if $\ \mathbf{A}\ \neq 0$ and $\hat{\mathbf{A}} = 0$ if $\ \mathbf{A}\ = 0$. |
| $\mathbf{A} \otimes \mathbf{B}$ | $(\mathbf{A} \otimes \mathbf{B})_{ijkl} = A_{ij}B_{kl}$. |
| $\mathbf{A} : \mathbf{B}$ | $= A_{ij}B_{ij}$. |
| EPHYSS | Elastoplastic Hysteretic Small Strain model. ⁴ |
| SOM | Swept Out Memory region. ²¹ |
| SSOM | Small Strain Overlay Model. ³ |
| HQH | Hysteretic Quasi-Hypoelastic model. ⁴ |
| HS | Hardening Soil model. ^{47,48} |
| HS-S | Hardening Soil Small model. ³ |
| HS-SS | Hardening Soil with Small Strain Stiffness model of Plaxis (based on HS-S). |
| HS _{MOD} | Hardening Soil Modified model ⁴ (based on plastic part of HS-S). |

ACKNOWLEDGEMENTS

The authors acknowledge the partners involved in the construction of La Sagrera station, in particular ADIF (Administration), INECO (Construction Management), Audingintraesa-Ayesa-Cicsa (Technical Assistance), Dragados-Acciona-Comsa-Acsa (Construction companies) and Geocisa (Monitoring company) for their support and for providing field measurements and field and laboratory data required in the analyses. The authors also acknowledge the support from Christian Hoffmann in charge of the Resonant Column Tests. Finally, the collaboration from Lilia Maria Grover Pimienta in the final edition the manuscript is gratefully acknowledged.

DATA AVAILABILITY STATEMENT

Data available on request from the authors.

ORCID

Javier Castellón  <https://orcid.org/0000-0002-7022-9316>

Alberto Ledesma  <https://orcid.org/0000-0003-3321-3849>

REFERENCES

- Jardine RJ. Some observations on the kinematic nature of soil stiffness. *Soil Found.* 1992;32(2):111-124.
- Castellón J, Ledesma A. Small strains in soil constitutive modeling. *Arch Comput Meth Eng.* Submitted for publication; 2021. <https://doi.org/10.1007/s11831-021-09697-1>
- Benz T. *Small-Strain Stiffness of Soils and its Numerical Consequences.* PhD Thesis. Stuttgart, Germany: Institut für Geotechnik der Universität Stuttgart; 2007.

4. Castellón J. *Estudio del comportamiento del suelo en el rango de las pequeñas deformaciones y desarrollo del modelo constitutivo EPHYSS*. PhD Thesis. Barcelona, Spain: Universitat Politècnica de Catalunya; 2019.
5. Brinkgreve RBJ, Broere W, Waterman D. *Plaxis 2D, version 9.0, Material Models Manuals*. Plaxis BV, Delft; 2008.
6. Castellón J. *Análisis teórico, numérico y experimental del comportamiento de suelos en el rango de las pequeñas deformaciones*. Master Thesis. Barcelona, Spain: Universitat Politècnica de Catalunya; 2013.
7. Niemunis A, Cudny M. Discussion on “Dynamic soil structure interaction: a three-dimensional numerical approach and its application to the Lotung case study”. Poor performance of the HSS model. *Comput Geotech*. 2018;98:243-245. <https://doi.org/10.1016/j.compgeo.2018.02.003>
8. Darve F. *Une formulation incrémentale nonlineaire de lois rhéologiques; application aux sols*. PhD Thesis. Grenoble, France: Université Scientifique et Médicale de Grenoble; 1978.
9. Darve F, Labanieh S. Incremental constitutive law for sands and clays, simulations of monotonic and cyclic tests. *Int J Numer Anal Methods Geomech* 1982;6(2):243-275. <https://doi.org/10.1002/nag.1610060209>
10. Darve F. The expression of rheological laws in incremental form and the main classes of constitutive equations. In: Darve F, ed. *Geomaterials: Constitutive Equations and Modelling*. London, England: Elsevier; 1990. <https://doi.org/10.1201/9781482296532>
11. Nelson I, Baron ML. Application of variable moduli models to soil behavior. *Int J Solids Struct*. 1971;7(4):399-417. [https://doi.org/10.1016/0020-7683\(71\)90111-9](https://doi.org/10.1016/0020-7683(71)90111-9)
12. Sandler IS. The cap model for static and dynamic problems. In: *The Seventeenth U.S. Symposium on Rock Mechanics*. Utah, USA, 25–27 August. American Rock Mechanics Association, 1A2-1, 1976.
13. Nelson I. Constitutive Models for use in Numerical Computations. In: Proceedings of the Plastic and Long Term Effect, DMSR. 1977. Karlsruhe, Germany. Rotterdam, Netherlands: A. A. Balkema. 1977; 2, 45-97.
14. Sandler IS, Baron ML. Recent development in the constitutive modeling of geological materials. *3rd International Conference on Numerical Methods in Geomechanics*. Aachen, Germany. 1979, 363-376.
15. Masing G. Residual stress and hardening the brass. In: Meissner, E. (ed.) *Second International Congress of Applied Mechanics*. 12–17 September 1926. Zurich, Switzerland, 1926, 12-17.
16. Pyke RM. Nonlinear soil models for irregular cyclic loadings. *J Geotechn Eng Div*. 1979;105(6):715-726.
17. Duncan JM, Byrne P, Wong KS, Mabry P. *Strength, Stress-Strain and Bulk Modulus Parameters for Finite Element Analyses of Stresses and Movements in Soil Masses*. Report No. UCB/GT/80-01. Berkeley, California, USA: Office of Research Services, University of California; 1980, 20-49.
18. Dos Santos JA, Correia AG. Reference threshold shear strain of soil. Its application to obtain an unique strain-dependent shear modulus curve for soil. In: *Proceedings of the Fifteenth International Conference on Soil Mechanics and Geotechnical Engineering*. Istanbul, Turkey, 2001, 27–31 August. Rotterdam, Netherlands: A. A. Balkema.
19. Hashiguchi K. Fundamental requirements and formulations of elastoplastic constitutive equations with tangential plasticity. *Int J Plast*. 1993;9(5):525-549. [https://doi.org/10.1016/0749-6419\(93\)90018-L](https://doi.org/10.1016/0749-6419(93)90018-L)
20. Gudehus G. *Physical Soil Mechanics*. Heidelberg, Germany: Springer-Verlag Berlin Heidelberg; 2011.
21. Gudehus G, Goldscheider M, Winter H. Mechanical properties of sand and clay and numerical integration methods: some sources of errors and bounds of accuracy. In: Gudehus G, ed. *Finite Elements in Geomechanics*. Chichester, England: John Wiley & Sons, 1977, 121-150.
22. Niemunis A, Herle I. Hypoplastic model for cohesionless soils with elastic strain range. *Mech Cohes Frict Mater*. 1997;2(4):279-299. [https://doi.org/10.1002/\(SICI\)1099-1484\(199710\)2:4<3C279::AID-CFM29%3E3.0.CO;2-8](https://doi.org/10.1002/(SICI)1099-1484(199710)2:4<3C279::AID-CFM29%3E3.0.CO;2-8)
23. Richardson D. *Investigations of Threshold Effects in Soil Deformations*. Unpublished Doctoral Thesis. London, England: City University London; 1988.
24. Atkinson JH, Richardson D, Stallebrass SE. Effect of recent stress history on the stiffness of overconsolidated soil. *Géotechnique*. 1990;40(4):531-540. <https://doi.org/10.1680/geot.1990.40.4.531>
25. Smith PR, Jardine RJ, Hight DW. The yield of Bothkennar clay. *Géotechnique*. 1992;42(2):257-274. <https://doi.org/10.1680/geot.1992.42.2.257>
26. Stallebrass SE, Taylor RN. The development and evaluation of a constitutive model for the prediction of ground movements in overconsolidated clay. *Géotechnique*. 1997;47(2):235-253. <https://doi.org/10.1680/geot.1997.47.2.235>
27. Jovicic V. *The Measurement and Interpretation of Small Strain Stiffness of Soils*. Unpublished Doctoral Thesis. London, England: City University London; 1997.
28. Masín D. Clay hypoplasticity model including stiffness anisotropy. *Géotechnique*. 2014;64(3):232-238. <https://doi.org/10.1680/geot.13.P.065>
29. Schädlich B, Schweiger HF. A multilaminar constitutive model accounting for anisotropic small strain stiffness. *Int J Numer Anal Methods Geomech*. 2012;37(10):1337-1362. <https://doi.org/10.1002/nag.2089>
30. Benz T, Vermeer PA, Schwab R. A small-strain overlay model. *Int J Numer Anal Methods Geomech*. 2009;33(1):25-44.
31. Mohammadi-Haji B, Ardakani A. Calibration of a hypoplastic constitutive model with elastic strain range for firoozkuh sand. *Geotech Geol Eng*. 2020;38:5279-5293. <https://doi.org/10.1007/s10706-020-01363-w>
32. Ng CWW, Boonyarak T, Masin D. Three-dimensional centrifuge and numerical modeling of the interaction between perpendicularly crossing tunnels. *Can Geotech J*. 2013;50(9):935-946
33. Hueckel T, Nova R. Some hysteresis effects of behaviour of geologic media. *Int J Solids Struct*. 1979;15(8):625-642. [https://doi.org/10.1016/0020-7683\(79\)90076-3](https://doi.org/10.1016/0020-7683(79)90076-3)
34. Lade PV, Abelev AV. Characterization of cross-anisotropic soil deposits from isotropic compression test. *Soils Found*. 2005;45(5):89-102. https://doi.org/10.3208/sandf.45.5_89

35. Hill R. A general theory of uniqueness and stability in elastic-plastic solids. *J Mech Phys Solids*. 1958;6(3):236-249. [https://doi.org/10.1016/0022-5096\(58\)90029-2](https://doi.org/10.1016/0022-5096(58)90029-2)
36. Li XS, Dafalias YF. Dilatancy for cohesionless soils. *Géotechnique*. 2000;50(4):449-460. <https://doi.org/10.1680/geot.2000.50.4.449>
37. Been K, Jefferies MG. A state parameter for sands. *Géotechnique*. 1985;35(2):99-112. <https://doi.org/10.1680/geot.1985.35.2.99>
38. Rowe PW. The stress-dilatancy relation for static equilibrium of an assembly of particles in contact. *Proc R Soc A*. 1962;269(1339):500-527. <https://doi.org/10.1098/rspa.1962.0193>
39. Surarak C, Likitlersuang S, Wanatowski D, Balasubramaniam A, Oh E, Guan H. Stiffness and strength parameters for hardening soil model of soft and stiff Bangkok clays. *Soils Found*. 2012;52(4):682-697. <https://doi.org/10.1016/j.sandf.2012.07.009>
40. Obrzud R, Truty A. The Hardening Soil Model – A Practical Guidebook. *ZSoil.PC 100701 Report*. Switzerland: Zace Services Ltd; 2018.
41. De Santos C. *Backanalysis Methodology Based on Multiple Optimization Techniques for Geotechnical Problems*. PhD Thesis. Barcelona, Catalonia, Spain: Universitat Politècnica de Catalunya; 2015.
42. Simo JC. Numerical analysis of classical plasticity. In: Ciarlet PG, Lions JJ, eds. *Handbook for Numerical Analysis, Volume 4*. Amsterdam, Netherlands: Elsevier; 1998.
43. Simo JC, Hughes TJR. *Computational Inelasticity*. New York, USA: Springer; 1998.
44. Jeremic B, Sture S. Implicit integration in elastoplastic geotechnics. *Mech Cohes Frict Mater*. 1997;2(2):165-183. [https://doi.org/10.1002/\(SICI\)1099-1484\(199704\)2](https://doi.org/10.1002/(SICI)1099-1484(199704)2)
45. Koiter WT. General theorems for elastic-plastic solids. In: Sneddon IN, Hill R, eds. *Progress in Solid Mechanics, Volume 1*. Amsterdam, Netherlands: North-Holland Publishing Co.; 1960; 165-221.
46. Bonnier PG. Implementation aspects of constitutive modeling. *Soft Clay Modelling for Engineering Practice Workshop*, 1. Trondheim, Norway: Norwegian University of Science and Technology; 2000.
47. Schanz T. *Zur Modellierung des mechanischen Verhaltens von Reibungsmaterialien*. Habilitation Thesis. Communication 45 of the Institute of Geotechnical Engineering. Stuttgart, Germany: Universität Stuttgart; 1998.
48. Schanz T, Vermeer PA, Bonnier PG. The hardening soil model: formulation and verification. In: Brinkgreve RBJ, ed. *Beyond 2000 in Computational Geotechnics - 10 Years of PLAXIS*. Rotterdam, Neetherlands: A.A. Balkema; 1999; 281-296.
49. Foster J, Paraskevopoulou C, Miller R. Investigation of the interaction of the construction of building S1 on underlying Thameslink. *Geomech Geoeng*, 2021;16(1):20-43. <https://doi.org/10.1080/17486025.2019.1643502>
50. Ramos G, Garcia-Fontanet A, Ledesma A, Raveendra R, Polo T. Toronto-York Spadina subway extensión tunnelling under Schulich building. *Can J Civ Eng*. 2019;46(2):87-103. <https://doi.org/10.1139/cjce-2017-0062>
51. Ledesma A, Alonso EE. Protecting sensitive constructions from tunnelling: the case of World Heritage buildings in Barcelona. *Géotechnique*. 2017;67(10):914-925. <http://doi.org/10.1680/jgeot.SiP17.P.155>
52. Simpson B. Retaining structures: displacement and design. *Géotechnique*. 1992;42(4):541-576. <https://doi.org/10.1680/geot.1992.42.4.541>
53. Biarez J, Hicher P-Y. *Elementary Mechanics of Soil Behaviour: Saturated Remoulded Soils*. Rotterdam, Netherlands: A. A. Balkema; 1994.
54. Desrues J, Vermeer PA, Zweschper B. Database for test on Hostun RF Sand. *Institutsbericht 13*. Stuttgart, Germany: Universität Stuttgart; 2000.
55. Adif. *Proyecto de construcción de la Estructura de la Estación de La Sagrera. Línea de Alta Velocidad Madrid-Zaragoza-Barcelona-Frontera Francesa*. Barcelona, Spain: Administrador de Infraestructuras Ferroviarias – Barcelona Sagrera Alta Velocitat (GPO, Sener); 2009.
56. Vázquez-Suñé E, Pujades E, Escorcía J, Jurado A. *Informe técnico: Evaluación de efecto barrera, efecto dren y caudales de drenaje durante la excavación del recinto de la estación de La Sagrera*. Barcelona, Spain: Grup de Hidrologia Subterrànea, IDÆA (CSIC)-UPC; 2011.
57. Hardin BO, Black WL. Vibration modulus of normally consolidated clays. *J Soil Mech Found Div*. 1968;94(2):353-370.
58. Hardin BO, Richart Jr., FE. Elastic wave velocities in granular soils. *J Soil Mech Found Div*. 1963;89(1):33-66.
59. Hara A, Ohta T, Niwa M, Tanaka S, Banno T. Shear modulus and shear strength of cohesive soils. *Soils Found*. 1974;14(3):1-12. https://doi.org/10.3208/sandf1972.14.3_1
60. Ohsaki Y, Iwasaki R. On dynamic shear moduli and Poisson's ratio of soil deposits. *Soils Found*. 1973;13(4):61-73. https://doi.org/10.3208/sandf1972.13.4_61
61. Vucetic M, Dobry R. Effect of soil plasticity on cyclic response. *J Geotechn Eng*. 1991;177(1):89-107. [https://doi.org/10.1061/\(ASCE\)0733-9410\(1991\)117:1\(89\)](https://doi.org/10.1061/(ASCE)0733-9410(1991)117:1(89))
62. Adif. *Campaña de investigación geotécnica complementaria. Extensómetros*. Internal Report OT-016. Barcelona, Spain: UTE Estructura Sagrera AVE (Acciona, Dragados, Comsa, Acsa); 2010.
63. Alonso EE, Gens A, Josa A. A constitutive model for partially saturated soils. *Géotechnique*. 1990;40(3):405-430. <https://doi.org/10.1680/geot.1990.40.3.405>

How to cite this article: Castellón J, Ledesma A. Development of a new advanced elastoplastic constitutive model that considers soil behavior at small strains. The EPHYSS model. *Int J Numer Anal Methods Geomech*. 2022;46:1991–2032. <https://doi.org/10.1002/nag.3360>